De-risking of faults associated with picking strategies: Implications for assessing fault growth and reactivation potential for CO_2 storage in the Northern Horda Platform

Viktor Styrmo Hansen

Master Thesis in Geosciences
Structural Geology and Tectonics
60 credits

Department of Geosciences
Faculty of Mathematics and Natural Sciences

UNIVERSITY OF OSLO

August 2022

De-risking of faults associated with picking strategies: Implications for assessing fault growth and reactivation potential for CO_2 storage in the Northern Horda Platform

Supervisors: Sian Lianne Evans, Emma Michie Haines, Alvar Braaten, Elin Skurtveit, Mark Mulrooney.

http://www.duo.uio.no/

Printed: Reprosentralen, Universitetet i Oslo

Acknowledgements

First, I want to express my gratitude to my main supervisors Emma Michie Haines and Sian Lianne Evans. Emma helped me start the process of writing this thesis, helped define the study outline and thought me software skills in T7. Even after she left the university for maternity leave, she has always answered all my questions fast and with enthusiasm. In the process of finalizing the thesis Sian has given valuable feedback at very short notices. Thank you.

A thank you to my fellow students at the Geoscience M.Sc. program at UiO for all the good times we have had over the last couple of years.

Finally, I would like to thank my son, William, who was born three months before the submission of this thesis. Thank you for giving me motivation to keep on. Last but not least, I want to thank my partner Lene who has taken care of our little family while I have worked on the thesis.

Viktor Styrmo Hansen

Bergen, Norway, August 1, 2022

Preface

This master's thesis (ECT 60) is submitted to the Department of Geosciences, University of Oslo (UiO), in the candidacy of the Master of Science program Structural Geology and Tectonics (ECTS 120). The Main supervisors are Post doc. Emma Michie Haines and Post doc. Sian Lianne Evans.

This thesis is a contribution to the University of Oslo and the Norwegian CCS Research Center (NCCS),and the associated spinnoff project FRISK (NGI, NORCE, UiO, UiB).

Software is the curtesy of Badleys Geoscience (T7). Seismic data is the curtesy of Equinor ASA and Gasnova SF.

Abstract

Structural de-risking of Carbon Capture and Storage (CCS) prospects are highly dependent on the effects of faults. Seismic scale faults will dictate how injected CO_2 migrate within the subsurface. Depending on fault characteristics (e.g., strike, dip, and throw) faults can act either as conduits to CO_2 migration or as baffles/ barriers. Locally increased pressure might also cause a fault to reactivate, making new migration pathways. To make any meaningful prediction on CO_2 behavior after injection the quality of structural models are essential.

The results from this study show that the strategy used (sampling interval and surface generating algorithms) when picking faults and fault cut-off lines impact the results of fault characteristics. Throw-Distance profiles, which is widely used in fault growth analysis failed to identify areas of possible linkage when faults were picked at coarser intervals. Near fault tips, coarser sampling intervals lead to missed data and fault surfaces that were considerable shorter than when picked at finer intervals.

Increased sampling intervals also leads to an increase in the average fault stability, missing small areas of high reactivation potential. However, due to the nature of human error when picking faults from segment to segment, sampling intervals close to the seismic resolution resulted in fault surfaces being overly rugous, not honoring the seismic data.

Picking faults at 100 m intervals identified all fault segments also identified at 25 m intervals. Considering time invested vs. details found, this study recommends 100 m intervals when picking the main body of the fault, for the creation of Throw-Distance profiles. To capture the whole length of faults sampling intervals close to the vertical resolution of the survey is recommended approaching fault tips.

Assessing fault reactivation potential, interpreters are advised to be aware of how human error and triangulation methods influence surface rugosity and hence also geomechanical results. Optimum picking strategy will be a balance between smoothing over human error while still maintaining as much geological details as possible.

Table of contents

1.0 Introduction

This study provides an assessment of how picking strategy influences structural de-risking of potential CO_2 storage sites. Emphasis is given on fault segmentation analysis through fault attributes such as throw and strike, and on the potential for fault reactivation through geomechanical analysis. Up until recently, no standardized picking strategies have been documented (Tao & Alves, 2019), and this study contributes to further understanding of uncertainties related to seismic interpretation investigating fault growth models and reactivation analysis. This chapter introduces previous research, the aims, and objectives of the study as well as the motivation.

1.1 Motivation

Following ratification of the Paris agreement in 2015, Norway committed to cutting climate emissions by 50% by the year of 2050 (U.N, 2015). To achieve the goal of reducing climate emissions the Norwegian Ministry of Petroleum and Energy has made “a plan of action” (handlingsplan) for CO_2 (Ministry of Petroleum and Energy, 2014). In 2018 The European commission outlined an ambitious plan for net zero emissions by 2050. Both the plan of action by the Norwegian Ministry of Petroleum and Energy and the European Commission describes Carbon Capture and Storage (CCS) as an important and necessary technology to meet the ambitious goals (Ministry of Petroleum and Energy, 2014) (E.U. Commission, 2018).

Being a frontrunner of CCS technology, Norway has been employing CCS for more than 25 years at two facilities where CO_2 is stored in the subsurface. The Snøhvit storage project in the Barents Sea and the Sleipner sequestration project in the North Sea (fig. 1). Both these facilities are saline aquifers that annually store 0,7Mt and 1Mt of CO_2 respectively. (Hansen et al., 2013) (Furre, et al., 2017).

To achieve the goals of the Paris agreement, a part of a possible solution is more CCS facilities on a larger scale. However, the Norwegian government and the European Commission are clear in the fact that full-scale CO_2 storage is not economically justifiable, and further research and development in technology is needed to achieve this (Ministry of Petroleum and Energy, 2014) (E.U. Commission, 2018).

In CCS, CO_2 is captured at industry point sources or directly from the air and transported eighter by ships or pipelines to suitable injection sites before being injected into geological trapping structures subsurface e.g., saline aquifers, depleted hydrocarbon reservoirs or organic rich shale (US Department of Energy, 2020).

To demonstrate the technology and stimulate further development of CCS Norway is planning a full-scale CCS operation by 2024. This project called Longship will capture CO_2 first at the Norcem AS cement factory in Breivik and at a later stage possibly at Fortum Oslo Varme. Then the CO_2 is transported by ship to Naturgassparken in Øygarden (western Norway). The storage part of the project is called Northern Lights and is a collaboration between Equinor ASA, A/S Norske Shell and Total E&P Norge AS. They aim to pump CO_2 from Naturgassparken through pipelines and inject it into saline aquifers in the North Sea. In 2019 the Northern Lights project was awarded the first license (EL001) to store CO_2 on the Norwegian continental shelf (Ministry of Petroleum and Energy, 2019). EL001 is corresponding to the Aurora exploitation license (Figure 1.2) (Holden 2021).

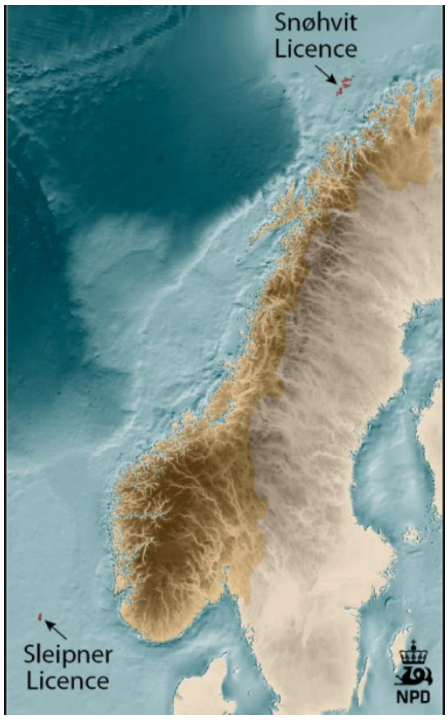

Figure 1.1 is showing the location of present Carbon Capture and Storage (CCS) sites on the Norwegian continental shelf. (The Norwegian Petroleum Directorate, 2014)

On April 5th, 2022, the Ministry of Petroleum and Energy announced that Equinor was awarded the operatorship of the CO_2 licenses for Smeaheia storage site in the North Sea and the Polaris site in the Barents Sea. The Smeaheia CO_2 storage site is the location for this study. Center for Environment-friendly Energy Research, called the Norwegian CCS research center (NCCS) was launched by the Research Council of Norway to contribute to research on CCS in Norway (NCCS, 2019)

This study is part of a spin-off project from NCCS called FRISK, researching methods for de-risking faults for CO_2 storage. FRISK is a collaboration between research partners Norwegian Geotechnical Institute (NGI), Norwegian Research Centre (NORCE), the University of Oslo (UiO) and the University of Bergen (UiB).

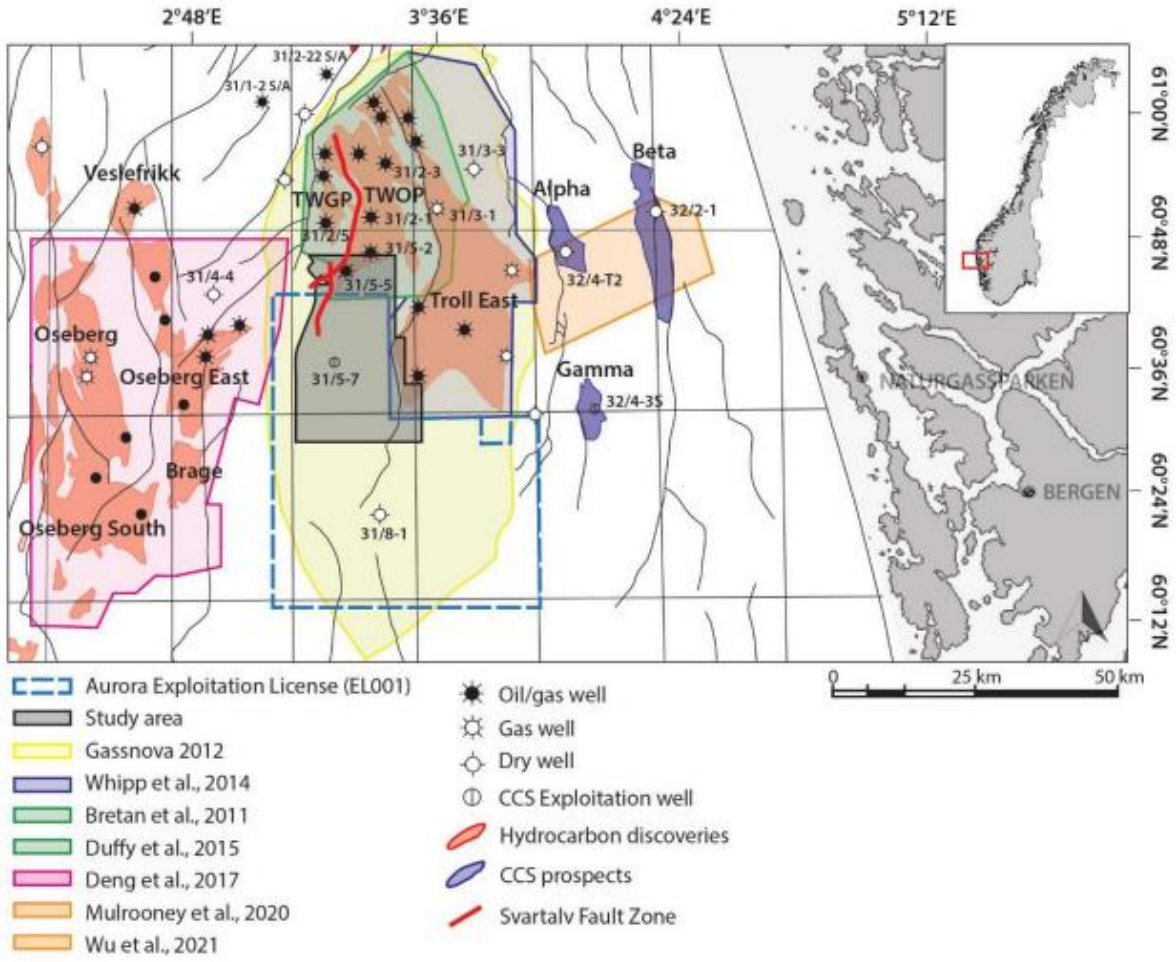

Figure 1.2 presents the study area. The three CO2 storing prospects at Smeaheia are outlined in purple. Studies investigating different areas in the proximity to the Smeaheia fault block are showed in different colors. The GN1101 3D seismic survey utilized in this study is orange. This area was investigated by Mulrooney et al., 2020 and by Wu er al., 2021. Figure modified from Holden (2021)

1.2 Study Area and Research Background

The study area of this project is the Smeaheia fault block within the Horda platform (figure 1.2) it is located approximately 20 km east of the Troll A platform and 40 km northwest of Naturgassparken located in Øygarden municipality near Bergen (Mulrooney et al., 2020). The Smeaheia fault block is an eastward tilting half graben, bounded in the west by the Vette Fault

Zone and in the east by Øygarden Fault Complex. In the 90's and 00's the prospect of oil and gas led to the drilling of wells 32/4-1 and 32/2-1 but they were found to be dry. Today Smeaheia is the location of three possible CO_2 prospects, called Alpha, Beta and Gamma (figure 1.2) (Mulrooney et al., 2020). The primary storage unit, a saline aquifer is called the Sognefjord Formation, consisting good reservoir quality sandstone approximately 1250 m below the seabed. The Sognefjord Formation is overlain by the Draupne Formation acting as a cap rock.

The proximity to the Troll field ensures that the area around Smeaheia has been the subject of numerous studies (e.g., (Bolle, 1992; Faleide et al., 2015; Whipp et al., 2014)). The Smeaheia Fault Block itself has also been the subject of studies the last couple of years investigating the possibility of CO_2 storage (e.g., (Mulrooney et al., 2020; Wu et al., 2021)). The Smeaheia Fault Block, structural setting and storage units are being further presented in chapter 2, geological setting.

De-risking of the potential hazards of CO_2 migrating out of an intended storing site is essential. Faults that intersect the storage and sealing unit, may alter how CO_2 migrate, depending on fault orientation and fault properties. Faults can work both as conduits to fluid flow or as baffles/barriers (e.g.,(Mulrooney et al., 2020)). The added pore pressure from injected CO2 may also cause faults to reactivate leading to up section fluid flow (e.g., (Michie et al., 2021)). When planning an injection strategy for a storage site all risks regarding CO2 migration and pore pressure variations need to be understood. Theory on how fault properties alter fluid flow, and the reactivation potential of faults are presented further in chapter 3.

How fault interpretation in the subsurface is performed have been outlined by several studies (e.g., (Badley, 1985; Boult & Freeman, 2007; Yielding & Freeman, 2016). However, there has been few studies regarding the precise picking strategy (sampling interval) for improved accuracy that should be used when interpreting both fault segments and fault cutoff lines (Michie et al., 2021; Tao & Alves, 2019). When first learning to use software to interpret 3D seismic I was told to interpret faults every 5th increment in the seismic data I was using. However, when I asked why I should do it every 5th increment and not every increment or every 20th increment, I could not get a good and solid answer, not from fellow students or the teacher.

In 2019 Tao and Alves documented an optimum picking strategy based on the total length of the fault, introducing a new parameter "Sampling Interval/Fault Length Ratio" (δ). This parameter ensures that the longer the fault, the longer the sampling distance. Michie et al., (2021) found that in their study this interval was not sufficient to capture all details found within their study of the Vette Fault Zone and suggested an optimum picking strategy of 100 m.

Michie et al, (2021) suggested that further research should focus on faults of different scales. As the Vette Fault Zone is a more than 50 km long basement involved fault with throw values in some areas larger than 1000 m, this study focuses on six thin skinned faults in the footwall of the Vette Fault Zone, ranging from 900 to 13 000 m in length and with throw values less than 100 m. This study is performed in the same geologic setting as the Vette Fault Zone and the same seismic survey has been utilized, keeping variables besides picking strategies to a minimum, for better comparison.

Cunningham et al., (2020) recommend that in the main body of the fault should be picked at least every 100 or 200 m, and when approaching fault tips or complex fault intersection to decrease picking interval to maximum 50 m.

1.3 Research Objectives

The main objective of this master project is to improve the knowledge of the best practice for fault interpretation and show how different picking strategies will influence the fault growth interpretation and fault reactivation interpretation when assessing potential CO_2 storage sites.

By utilizing the GN1101 3D seismic data survey this study will make a geological model of the potential CO_2 storage site Smeaheia in the northern North Sea. Interpreting several faults within the footwall of the Vette fault using several picking techniques, generate fault cutoff lines using several picking techniques, examine fault Throw-Distance plots depending on picking technique and examine how fault stability and fault seal vary with picking techniques. The results of this project will be discussed in the light of previous studies investigating picking strategies for faults.

Results from this project have potential to not only have implications for assessing fault seal for CO2 storage, but also hydrocarbon production, ground water flow and other geological fields where subsurface fluid flow is important.

1.4 Study outline

Following the introduction of the study is a chapter describing the potential CO_2 storage site Smeaheia in detail, emphasizing on the structural framework. The third chapter introduces theoretical concepts such as fault geometry, fault segmentation theories and geomechanical analysis assessing fault reactivation. Chapter four present the data used, while chapter five describes the methodology used. Then the result of the study is presented in chapter six before results are discussed in chapter 7. At the end of the thesis a conclusion is given through the summarizing of the main finding of the study.

2.0 Geological setting

As mentioned in the introduction, the study area is the Smeaheia potential CO2 storage site within the Horda platform in the northern North Sea. The primary storage unit targeted for CO2 injection is the Sognefjord Formation located in the Upper Jurassic Viking Group, being a good reservoir quality sandstone, with the sealing Draupne Formation working as a cap rock. The focus of this chapter is the structural and lithological evolution of the North Sea in general, focusing specifically on the Horda platform, with emphasis on structures and lithological units close to the storage formation (the Viking Group) in time and space.

2.1 Structural framework

Located offshore the western and northern coast of Norway, the Norwegian Continental Shelf consists of three main provinces. The Barents Sea part of the Norwegian continental shelf is located between mainland Norway and Svalbard, the Norwegian sea stretches from the Barents Sea in the north to the North Sea in the south. From the southern border of the Norwegian sea (62ºN), the North Sea stretches between Norway and Denmark in the east to Great Britain in the west and continental Europe in the south. In the North Sea one of the dominant geological structures is the Trilete rift system. This rift consists of three main rift arms, the Viking Graben, Moray Firth Basin and the Central Graben meeting in the trilete junction (Davies et al., 2001). (Figure 2.1)

The area located approximately between 58ºN and 62ºN is defined as the northern North Sea. The northern North Sea can be described as a N-S trending basin located above continental crust (intracratonic). It is dominated by normal faults trending N-S, NW-SE, and NE-SW. The vertical component (throw) of these faults can be as big as 1,5km. Figure 2.2 shows the main structural features in the northern North Sea; the Viking Graben flanked to the east by the Horda platform and to the west by the East Shetland Basin. To the north of the Horda Platform is the Sogn Graben and west of Sogn Graben is Tampen Spur. (Figure 2.1)

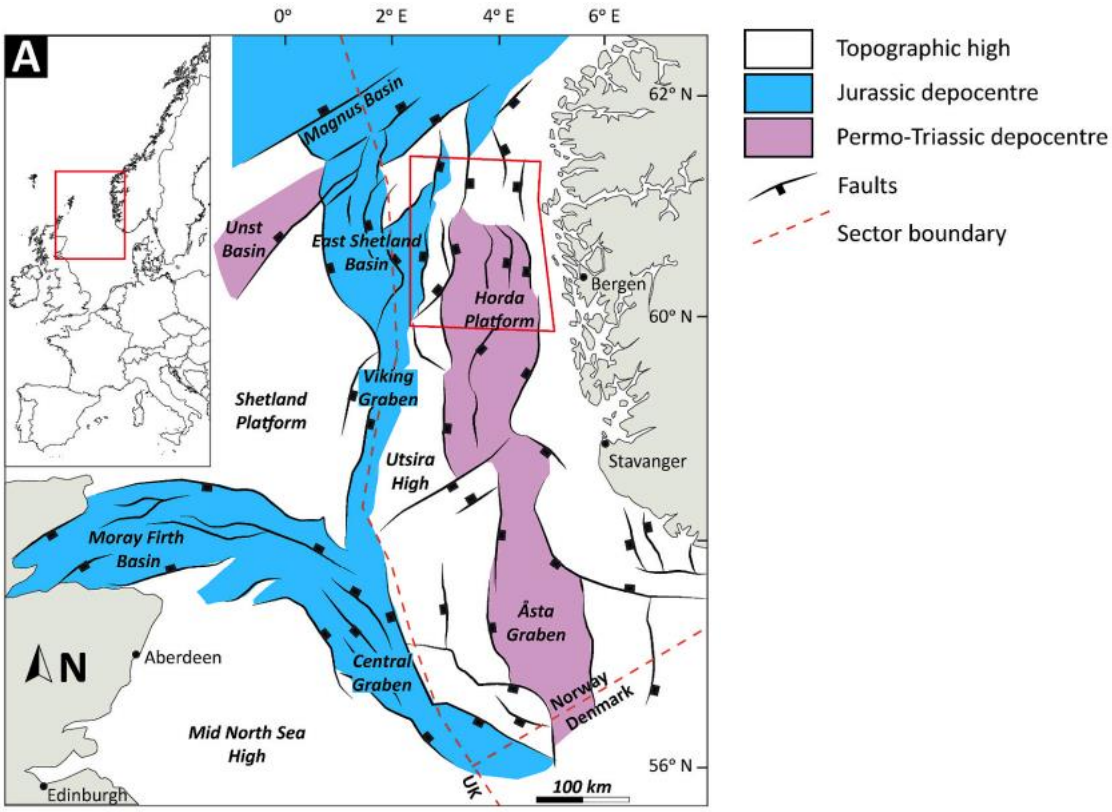

Figure 2.1 Presents a map view of the Northern North Sea. Red square highlights area of interest near Smeaheia Fault block, within the northern Horda Platform. Figure modified from Mulrooney (2020)

The Northern North Sea basin is characterized by large, rotated fault blocks (figure 2.2) The fault blocks mainly dip westwards in the eastern part of the North Sea and eastwards in the western part. Rotated fault blocks make half graben structures. Associated depocenters of each fault block are asymmetrically filled, with thicker sedimentary successions in the hanging wall, indicating syn rift deposition. The Viking graben represents the area with the thinnest crystalline basement and the thickest overlying sedimentary secession (Christiansson et al., 2000). Underlying the crystalline basement at the Horda platform is a lower crustal body characterized by high velocity and high bulk density (Christiansson et al., 2000).

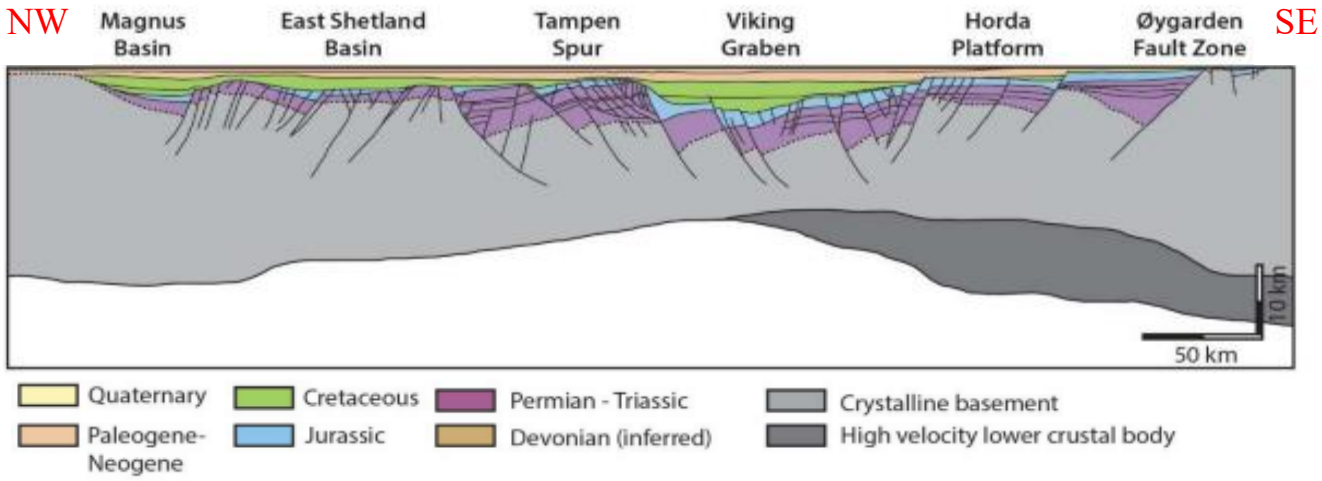

Figure 2.2 Presents a cross section of the Northern North Sea. Figure modified from Holden (2021) complied from Faleide et al. (2010) and Cristiansson et al. (2000).

The Horda Platform which has been used as the study area for this project is a N-S trending structural high, located on the eastern flank of the Viking Graben. The eastern extents of the Horda Platform is bound by the Øygarden Fault Complex (ØFC), which marks an abrupt change in thickness of the underlying basement rock. The southern section of the Horda Platform is bound by the Utsira High to the west and the Åsta Graben to the south. To the north, the Horda Platform is bound by the Sogn Graben and the Måløy Slope.

In section view the Horda Platform is comprised of four westward dipping fault blocks, divided by five major fault zones. From west to east the Troll, Svartalv. Tusse and Vette fault zones, and the Øygarden Fault Complex are large thick-skinned faults (displacing crystalline basement). These fault zones are up to 60 km long, N-S striking and have throw values larger than 1,5 km in some areas (Whipp et al., 2014). In this thesis these faults are termed first-order due to the involvement of basement rocks (after Gabrielsen (1984)).

A second population of smaller faults are also present at the Horda platform. These faults are not basement involved and are named second-order Mulrooney, 2020). This population of second-order faults are predominantly N-S and NW-SE trending, intersect Upper Triassic to Cretaceous succession and have throw values of less than 100 m (Whipp et al., 2014). They are also shorter in length and generally closer spaced than the five first-order faults. This population of faults tend to have their lower most tips in the Triassic Hegre Group and the upper most tips within the Cromer Knoll Group, indicating that this population of faults are

interpreted to have originated after, and become inactive before the first-order faults described in the section above (Whipp et al., 2014).

In the sedimentary overburden a third population of faults are present, they have low throw values and are described as polygonal faults (Wrona et al., 2017). They are chaotically oriented, but with a somewhat NW-SE organization, indicating that a minor degree of reactivation of older fault played a role even if a number of mechanisms are suggested in the creation of these faults (Mulrooney et al., 2020).

The easternmost fault block in the Horda Platform is the focal point of this project. The Smeaheia Fault block is bounded in the west by the Vette Fault Zone and in the East by the Øygarden Fault Complex (first-order faults). It is located within North Sea Block 32/4 and 32/1. Mulrooney et al., 2020 defined the northern extent of Smeaheia to be a sharp eastward jog in the Vette Fault Zone where the Uer Terrace and Bjornvin Arch bound each other, and the southern extent to be the point where the Vette Fault Zone tips out. By this definition Smeaheia extends more than 70 km from north to south. A selection of six second-order faults within the footwall of the Vette Fault Zone have been the focus of this study.

2.2 Geological evolution of the Horda Platform

This section describes the evolution of the northern North Sea in general and the Horda platform in particular. Description of the main events that led to the structural features and sedimental deposition (upper Jurassic Viking Group) relevant for entrapment and migration of CO2 at the Smeaheia storage site are given in more detail for the purpose of this study.

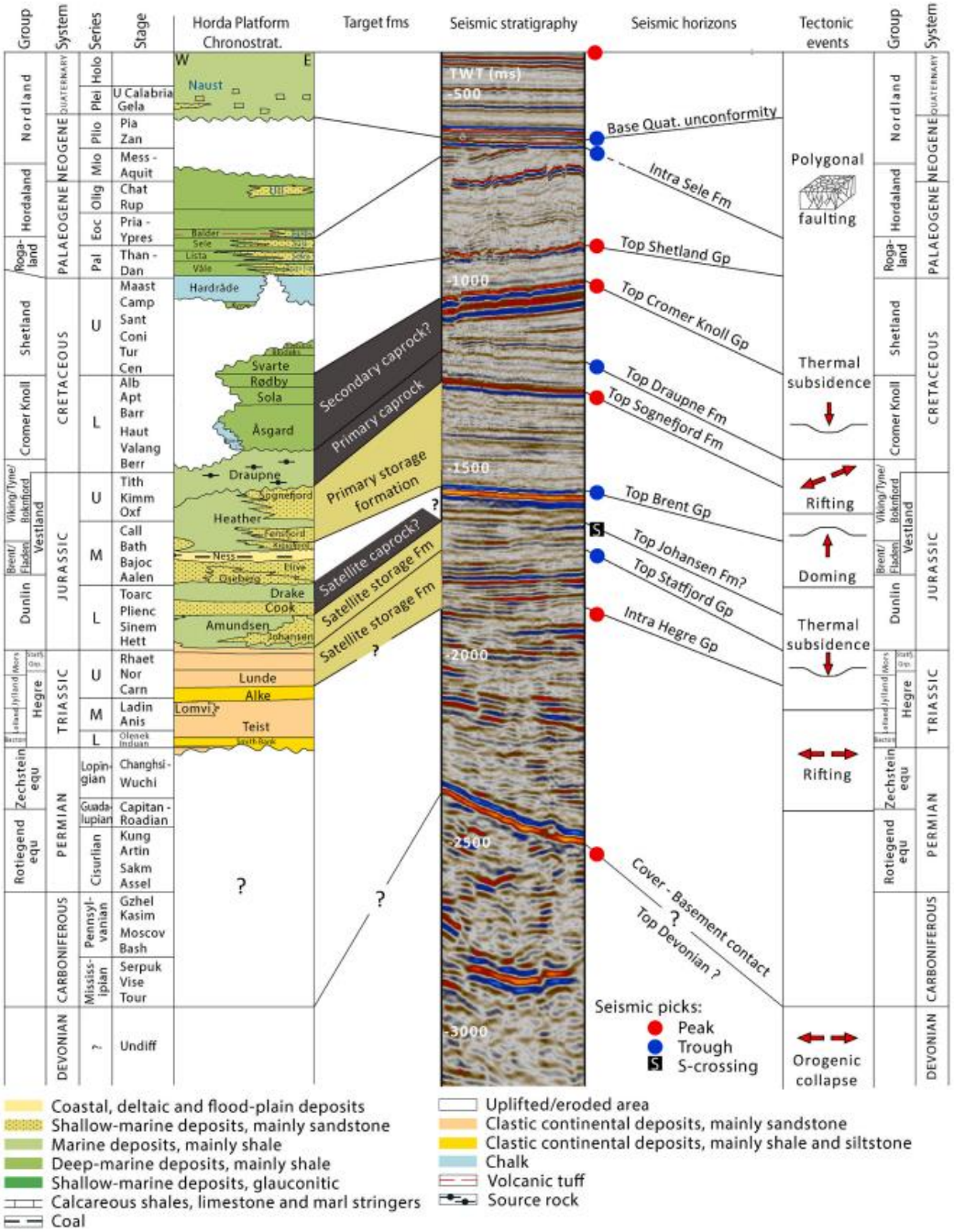

Figure 2.3 Gives an overview over Stratigraphy, target formations of the Smeaheia CCS prospect, the correlation to seismic stratigraphy in the GN1101 seismic survey and major tectonic events. Figure from Mulrooney et al., (2020)

2.2.1 Pre-Permian

The crystalline basement underlying the Northern North Sea initially formed during the Proterozoic Sveconorwegian orogeny, before being reworked during the Caledonian orogeny (Ordovician to Devonian) (e.g. (Phillips et al., 2019; Ziegler, 1975a)).

Due to contractional tectonics during the Caledonian orogeny, shear zones oriented NW – SE and EN -WSW were created (Andersen & Jamtveit, 1990). During the Scandian phase of the Caledonian orogeny, the Iapetus Ocean closed, and the western margin of Baltica was subducted under Laurentia (e.g. (Gee & Fossen, 2008). Allochthonous nappes from the Iapetus Ocean, Baltica and Laurentia were transported on weak décollement composed of weak Cambrian-Ordovician shales and phyllites and placed on Blatica (Gee & Fossen, 2008; Phillips et al., 2019). The high temperature and pressure needed to create the highly heterogeneous and metamorphic basement rocks that are exposed onshore Norway indicates creation at great depths. The area characterized by high velocity found under the basement of the Horda Platform is interpreted to be partially eclogitized rocks (Christiansson et al., 2000).

During the Early Devonian, gravitational collapse led to a phase of extension facilitated by reactivation of low angle Caledonian thrust zones (such as the Møre – Trøndelag Fault Complex and the Nordfjord – Song Detachment Zone) (Norton, 1987). Onshore Norway multiple Devonian continental basins were formed in the hanging wall of these shear zones. In the deeper parts of the eastern Horda platform, Devonian basins are visible in seismic sections as packages of intra basement reflectivity (Færseth, 1996; Lervik et al., 1989). Figure 2.4 presents an interpretation where asymmetric Devonian sediments are marked with a light brown color in the hanging wall of Vette Fault Zone and Øygarden Fault Complex (Whipp et al., 2014). These basins consist of low-grade clastic metamorphic rocks.

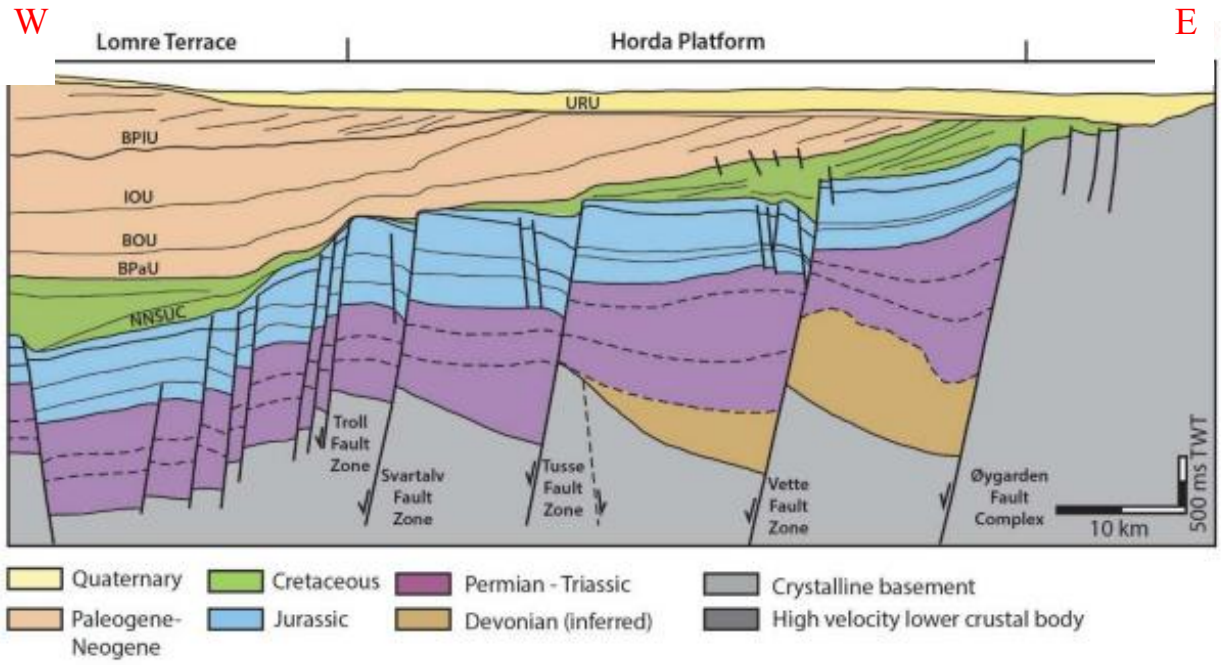

Figure 2.4 Presents a cross section of the Horda Platform. Figure from Holden (2021), modified from Whipp et al. (2014). Abbreviations: NNSUC = Northern North Sea Unconformity Complex, BPaU = Base Paleogene Unconformity, BOU = Base-Oligocene Unconformity, IOU 0 Intra-Oligocene Unconformity, BPlU = Base Pleistocene Unconformity, URU =Upper Regional Unconformity.

2.2.2 Permian to Early Triassic (Rift Phase 1)

The first major rift phase to influence the Northern North Sea rift initiated in the late Permian to early Triassic (Coward, 1995; Phillips et al., 2019), from here on called Rift Phase 1. Documented N-S striking Permian- Triassic dykes found onshore Norway suggests the regional extension direction during this rift phase is E-W (Fossen & Dunlap, 1999), forming a dominantly N-S striking rift (Bell et al., 2014). Rift Phase 1 is most likely related to the break-up of the Pangean supercontinent, and is suggested to last for 25–37 Myr, around 261 - 225 Ma (Bell et al., 2014; Ziegler, 1982).

A tick wedge shaped sedimentary package dated to be deposited approximately Asselian (ca. 290 Ma) to Rhaetian (ca. 207 Ma) is present at the Horda platform (Whipp et al., 2014). Locally this unit consists of more than 3 km syn rift sediments. The Permian- Triassic unit thickens toward the hanging wall of the first-order faults (e.g. Øygarden Fault Complex, Vette Fault Zone, Tusse Fault Zone and Svartalv Fault Zone), and fills tilted half graben structures (Færseth, 1996). Figure 2.4 show the interpreted Permian – Triassic unit as purple. During the

Triassic the North Sea experienced continental conditions resulting in deposition of the non-marine Hegre Group, comprising of the mud rich Smith Banken and Alke formations, and the sand-rich Teist, Lomvi, and Lunde Formations (Steel, 1993; Whipp et al., 2014).

Basins of Permian to Triassic age have also been reported on the East Shetland Basin and Unst Basin (e.g. (Færseth, 1996; Tomasso et al., 2008)). Underneath the Viking Graben Permian- Triassic basins have not been identified, if they ever existed they are buried to depth of >8 km due to extreme subsidence (Bell et al., 2014; Klemperer, 1988). Due to this uncertainty of Permian- Triassic basin beneath the Viking Graben the stretching factor (β – factor) is controversial. Færseth (2016) and Ter Voorde et al. (2000) suggests higher β – factor at the Horda Platform then at the Viking Graben, while Odinsen et al. (2000) suggest a more constant β – factor. The slip rate of Rift Phase 1 is calculated to 0,1-1,5 mm/year (Bell et al., 2014).

2.2.3 Middle Triassic to Early Jurassic

In the Middle to Early Jurassic, Rift Phase 1 was followed by an inter-rift period of 70 Myr dominated by tectonic quiescence and post-rift thermal subsidence (e.g., (Deng et al., 2017; Færseth, 1996; Roberts et al., 1993; Steel, 1993)). Even if it is generally assumed that this was a period of tectonic quiescence in the Northern North Sea, some authors report faults that were active during the later stage of the inter rift period (Deng et al., 2017). In the Oseberg area of the North Sea Deng et al. (2017) states that the tectonic activity during the inter-rift period is comparable to the activity of the established rift phases.

The depositional environment gradually transitioned towards a shallow marine environment towards the end of the Triassic and beginning of Jurassic (Røe & Steel, 1985). During the Rhaetian to Sinemurian the Statfjord Group, which exhibits a “coarsening upward” that represents a transition from continental to shallow marine environment, was deposited (Vollset & Doré, 1984). In northern North Sea the marine Dunlin Group was deposited from Early to Middle Jurassic (Hettangian to Bajocian). The Dunlin Group is subdivided into the Amundsen, Johansen, Burton, Cook and Drake formations (Deegan & Scull, 1977). The saline aquifer sandstones of the Johansen and Cook formation are proposed as primary storage units for CO2 at the Aurora CCS prospect (located approximately 25 km SW of the

Smeaheia prospect), while the clay rich Drake formation is proposed as a sealing unit (Holden, 2021).

The Brent Group overlaying the Dunlin Group was deposited during Middle Jurassic (Bajocian to Bathonian), and consists of sandstones, silt stones and shales with subordinate coal beds and conglomerates, interpreted to have been deposited in a large delta (Deegan & Scull, 1977; Vollset & Doré, 1984). The Statfjord, Dunlin and Brent Group experienced only minor syn-depositional faulting during this period of tectonic quiescence and thermal subsidence (e.g. (Bell et al., 2014; Whipp et al., 2014)). Thermal doming in the Central North Sea during Early to Middle Jurassic resulted in erosion strata across large parts of the North Sea (Davies et al., 1999; Phillips et al., 2019).

2.2.4 Middle Jurassic to Early Cretaceous (Rift Phase 2)

The collapse of this dome in the Central North Sea is interpreted by some authors to have been the start of the second major rift phase, Rift Phase 2 (Coward et al., 2003; Færseth, 1996; Phillips et al., 2019; Ziegler, 1990). Deflation of the central North Sea dome together with far field stress related to North Atlantic rifting (Davies et al., 2001; Whipp et al., 2014) resulted in a trilete rift system in the North Sea, comprising of the Central Graben, Moray Firth Basin and the Viking Graben (Davies et al., 2001).

Rift Phase 2 was active in the northern North Sea from Middle Jurassic to Early Cretaceous. Based on the analysis of sediment patterns adjacent to faults on the Horda Platform and the East Shetland Basin, the initiation of Rift Phase 2 is dated to be Bajocian (ca. 167-170 Ma) (e.g. (Davies et al., 2000; Færseth & Ravnås, 1998)). The initiation and cessation of this rift phase is interpreted to have been diachronous across the northern North Sea, the duration of activity on individual faults are estimated to range between 10 to 40 Myr (Bell et al., 2014; Cowie et al., 2005). Rifting during this rift phase was slower and less intense than under Rift Phase 1 with slip rates of 0.01 mm/yr (Bell et al., 2014).

Rifting during Rift Phase 2 in the northern North Sea is characterized by large scale reactivation of faults formed under Rift Phase 1, as well as the formation of a new smaller fault population striking N-S and NW-SE (e.g. (Bell et al., 2014; Deng et al., 2017; Færseth, 1996; Whipp et al., 2014)). This smaller fault population that abuts or cross cuts the larger N-

S striking Permian – Triassic faults, are from two to ten kilometers long(Færseth, 1996; Færseth & Ravnås, 1998; Mulrooney et al., 2020). These faults are thin skinned (not basement involved), with throw of less than 100 m and are closer spaced (0,5-5 km) than the thick skinned Permian – Triassic fault population (Mulrooney et al., 2020). The work of this study focuses on a selection of this new population of Jurassic – Cretaceous thin-skinned faults, located in the footwall of the Vette Fault Zone.

The rift orientation during Rift Phase 2 is highly debated, with some authors suggesting that the orientation of extension remined E -W, and that the observed change in strike orientation is due to stress perturbations surrounding pre-existing structures (e.g. (Badley et al., 1988; Bartholomew et al., 1993; Bell et al., 2014)), other authors suggest an anti-clockwise rotation of rift orientation from E – W to NE -SW (Deng et al., 2017).

Based on the observation of little syn-rift wedging in the Jurassic successions, but clear wedging in the Cretaceous successions in the easternmost Permian- Triassic faults (Øygarden Fault Complex, Vette- and Tusse Fault Zones), while this is not the case for faults located closer to the rift axis under the Viking Graben, some authors interpret the reactivation of Permian – Triassic faults to have migrated eastward over a period of 30 Myr (Bell et al., 2014; Mulrooney et al., 2020; Phillips et al., 2019). Øygarden Fault Complex marks the eastern extent of major activity (Bell et al., 2014).

Due to the increased rates of subsidence driven by faulting in Rift Phase 2 fully marine conditions developed, and the marine Viking Group was deposited (Bell et al., 2014; Dreyer et al., 2005). In the Norwegian North Sea five formations of the Viking Group are defined, the Heather and Draupne Formations are widely distributed, while the sandy developments of the Krossfjord, Fensfjord and Sognefjord Formations are more restricted (Vollset & Doré, 1984). On the Horda Platform silty claystone of the Heather Formation interfingers with Krossfjord, Fensfjord and Sognefjord formations, in well 32/4-1 on the Smeaheia fault block the Heather formation is recognized as relatively thin layers under, over and between all these sandy formations (NPD fact-pages).

The Krossfjord Formation (Bathonian) consists of medium to coarse grained, well sorted sandstone. The Fensfjord Formation consists of fine to medium grained well sorted sandstone. The Sognefjord Formation (Callovian) consists of medium to coarse grained, well sorted, and unconsolidated sandstone. These sandy formations are only recognized in the Troll Field area,

where the Sognefjord Formation is considered as the major reservoir interval (Vollset & Doré, 1984). The uppermost formation of the Viking Group is the deep marine Draupne Formation (Oxfordian to Ryazanian), consisting of grey-brown to black organic rich mudstone (Vollset & Doré, 1984).

According to the NPD fact-pages the formations of the Viking Group found in well 32/4-1, placed in close proximity of the study area and within the α-prospect of the Smeaheia CCS scenario is as follows (bottom to top): 5 m thick Heather Fm, 47 m thick Krossfjord Fm, 3 m thick Heather Fm, 229 m thick Fensfjord Fm, 60 m thick Heather Fm, 68 m thick Sognefjord Fm, 22 m thick Heather Fm and 107 m thick Draupne Fm.

2.2.5 Cretaceous and Cenozoic

Marking the change from syn-rift to post-rift deposition, the Base Cretaceous Unconformity (also called “Late Cimmerian Unconformity” (Ziegler, 1975b) or the “northern North Sea Unconformity”(Gabrielsen et al., 2001; Kyrkjebø et al., 2004)) formed. This widespread unconformity represent the transition from active stretching during Rift Phase 2 to the post rift period where sediment loading and thermal subsidence controlled subsidence in the North Sea (e.g. (Badley et al., 1988; Kyrkjebø et al., 2004)). This led to open-marine deposits, where sediments were deposited in shallow to deep marine environments (Isaksen & Tonstad, 1989). The Cromer Knoll Group deposited from Ryazanian to Albian/ Early Cenomanian in the North Sea, consists of mainly of calcareous claystones, siltstones and marlstone with subordinate layers of limestone and sandstone (Isaksen & Tonstad, 1989). The Shetland Group deposited from Cenomanian to Danian, consist of chalky limestone, marls and calcareous shales (Isaksen & Tonstad, 1989). Minor Creaceous reactivation of some large faults caused vertical movements (Gabrielsen, 1989; Mulrooney et al., 2020).

During Early Cenozoic in the northern North Sea is characterized by the deep marine deposition of the Rogaland and Hordaland Group (Isaksen & Tonstad, 1989; Mulrooney et al., 2020). Erosion and non-deposition of the Hordaland Group on the Horda Platform is linked to contractional inversion. during early to middle Miocene (Nottvedt et al., 1995; Rundberg et al., 1995). Polygonal faults nucleated in the Eocene to Early Oligocene have affected a less than 1000 m succession of the Cenozoic interval in the northern North Sea (Clausen et al.,

1999; Mulrooney et al., 2020; Wrona et al., 2017). On the Horda Platform the polygonal faults are generally confined to the Upper Cretaceous to Middle Miocene stratigraphy (Mulrooney et al., 2020; Wrona et al., 2017), occasionally they displace early Quaternary deposits (Eidvin et al., 2014; Eidvin & Rundberg, 2007). No faults within the Horda Platform displace the Upper Regional Unconformity, that marks the transition to horizontal Quaternary sediments (Ottesen et al., 2018; Sejrup et al., 1996). At the seafloor above Smeaheia Fault Block pockmarks are visible, they have been attributed to the destabilized hydrates during the last deglaciation period, but no correlation to underlying geologic features has been made (Forsberg et al., 2007).

3.0 Theory

Theory related to this study is presented in this chapter. Beginning with fault geometry (e.g., strike, dip, throw, heave, and fault segmentation) before analytical methods to assess fault reactivation potential is presented.

3.1.1 Fault Geometry

Assessing how CO_2 will migrate within the storage unit is essential in the de-risking of any CO_2 storage prospects. Injecting CO_2 subsurface, the CO_2 will likely act as a buoyant fluid migrating up dip within the storage unit. Intersecting faults can act eighter as a conduit to fluid flow or as a baffle/seal (Andersen & Sundal, 2021).

Oriented parallel to fluid flow faults can channel migrating fluid (e.g., CO_2) increasing the max plume front advancement, or if oriented at an oblique angle the fault can slow down or redirect the flow (Andersen & Sundal, 2021). For faults to act as a barrier or seal to CO_2 migration, the dip direction is important. Figure 3.1 presents two alternatives on how faults can eighter be sealing or not, depending on dip direction. I alternative A the CO_2 plume is in the footwall of a normal fault, and we can se how the juxtaposition of a sealing unit next to the storage unit traps CO_2. When a certain column height is reached CO_2 will further migrate through a spill point. In alternative B the CO_2 plume is located within the hanging wall of the fault. This time the storage unit is juxtaposed itself and there is no juxtaposition seal trapping CO_2 on the left side of the fault.

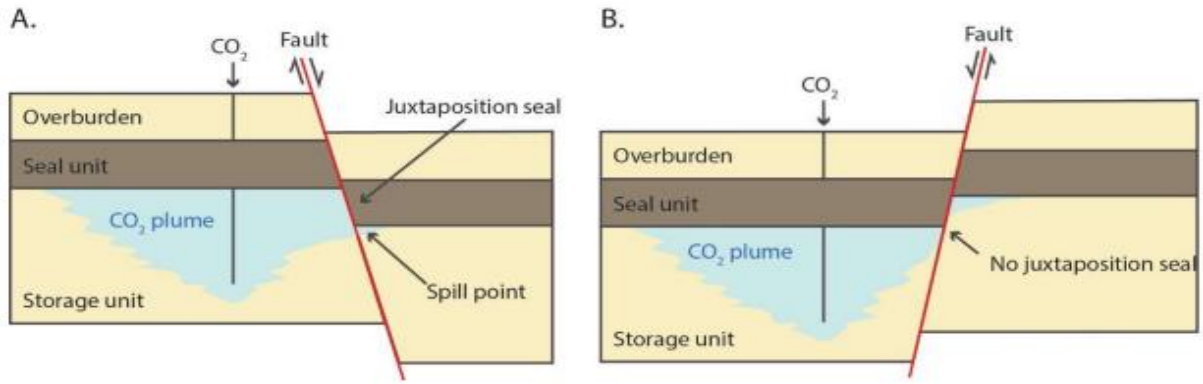

Figure 3.1 presents how dip direction influences juxtaposition seals and therefore the across fault CO2 migration. A) The CO2 plume is located within the footwall of the fault, in this example are CO2 trapped by a juxtaposed against a sealing unit. A CO2 column will develop until the CO2 reaches a

spill point. B) The CO2 plume is located within the hanging wall of the fault and CO2 can flow across the fault assuming no membrane seal. Figure after (Holden, 2021) and (Miocic et al. 2019).

When interpreting faults in seismic, faults are for simplicity treated as lines or surfaces even if they truly are bodies of rock, consisting of both a core zone (including the fault plane) and a wider damage zone and process zone (e.g., Cowie & Shipton 1998). This method of treating the faults as lines or planes serves the purpose of describing important parameters (strike, dip, displacement etc.), but it still important to remember that the damage zone and process zone are often highly fractured and have implications on fluid flow (e.g., (Peacock & Sanderson, 1994; Shipton et al., 2005)).

Lieth (1923) defined the displacement of a fault ass the relative separation of originally adjacent points. The separation of originally adjacent points can be described by the "real displacement" or more often when interpreting seismic by the "dip separation" due to difficulties resolving kinematic indicators (e.g., (Walsh & Watterson,1988; Peacock & Sanderson,1991; Whip et al., 2014). The real displacement is a description of how the points have moved spatially over time, considering that most fault surfaces are not flat surfaces. Dip separation, however, is describing a straight line from one point unit to the corresponding previously adjacent point on the other side of the fault. Dip separation is composed of a vertical component called throw and a horizontal component called heave.

3.1.2 Fault segmentation and growth models

Single normal fault that does not penetrate the surface are often described as elliptical, with maximum throw values found in the middle of the fault with gradually decreasing values towards the fault tips (e.g., (Peacock & Sanderson, 1991; Walsh & Watterson, 1988)). By assessing variations in throw, it is possible to estimate fault growth, timing of growth and interaction styles (Peacock & Sanderson, 1991).

Displacement vs length profiles or throw vs distance profiles (T-D plots) are often used to assess the lateral variations in throw (e.g., Bell et al., 2014; Whipp et al., 2014). It can be used to interpret fault segmentation and linkage history. Corresponding to largest throw values in the center of isolated faults, T-D plots for isolated faults will be near symmetrical, with

maximum values in the middle of the fault, decreasing towards the fault tips. If the throw maximum is skewed toward one of the fault tips this typically means an interaction with another fault, creating a relay zone (e.g., Walsh & Watterson,1988). Relay zones are important assessing migration of CO_2 as relay zones can create conduits for fluid flow (e.g., (Peacock & Sanderson, 1994; Rotevatn et al., 2009; Trudgill & Cartwright, 1994)). If two faults propagate to form one fault the relay zone will be breached, and the T-D plot will show two throw maximum, with a small minimum between. Figure 3.2 presents how faults grow laterally and eventually connects to other faults. In stage 1 the two faults are isolated and T-D plots show a symmetrical distribution of throw with largest values in the middle of the fault. In stage 2 the two faults have grown and started to interact, int the T-D plot throw maximums are not yet affected, but the two fault segments are soft linked creating a relay zone in between. Notice that the fracturing is increasing in the area where the two fault interact. In stage 3 the T-D plot show an increase in throw maxima as the two faults are interacting. Deformation in the relay zone is increasing. In stage 4 the two fault segments are now hard linked forming one fault. The relay zone is breached, and the relict fault segments are difficult to distinguish in the T-D plot.

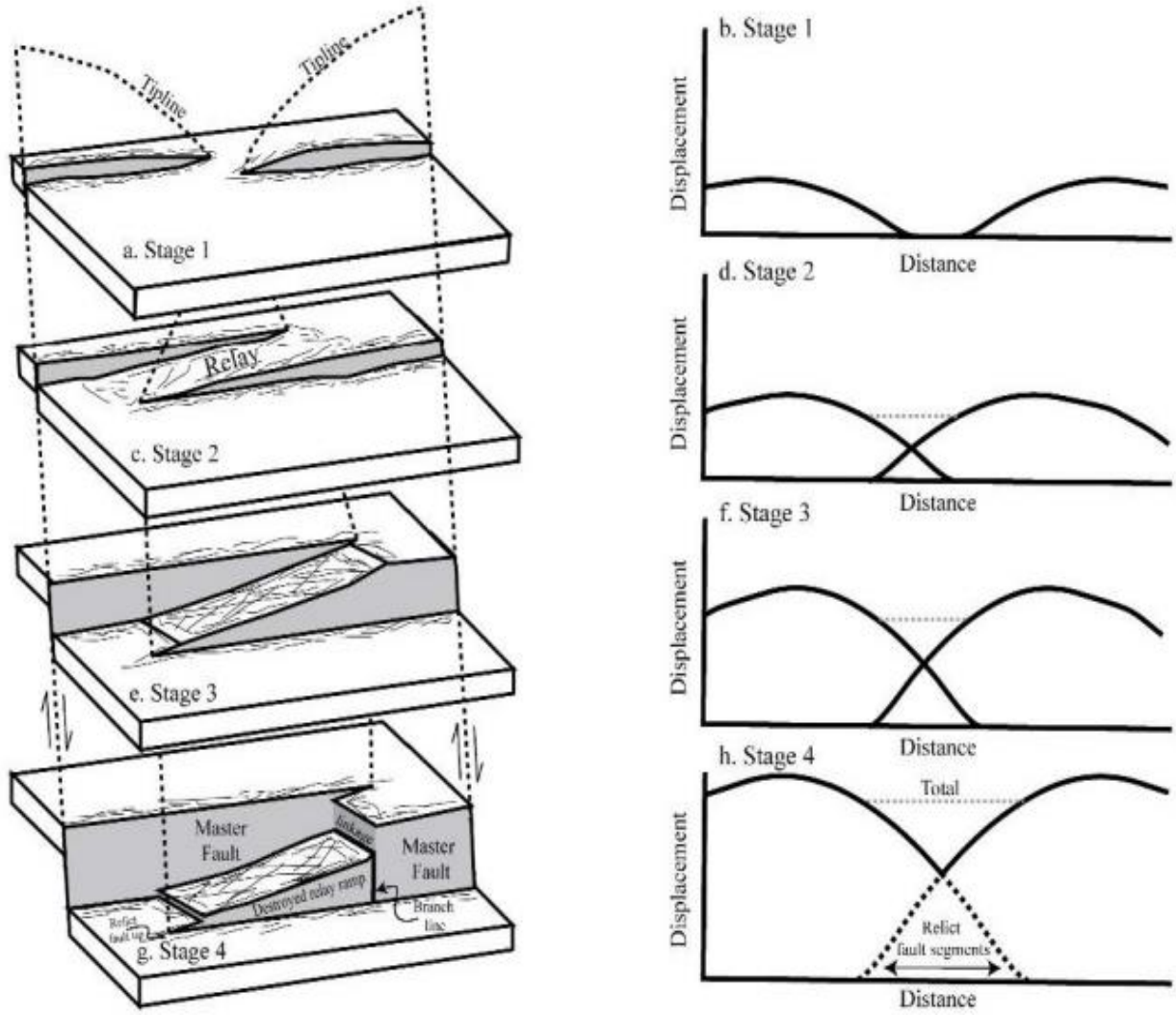

Figure 3.2 Present four stages of lateral fault linkage and the effect on calculated T-D plots. a+b) represents stage one, isolated fault segments. c+d) represents stage 2, faults have grown laterally and formed a relay zone T-D plots are overlapping but we can not yet see any impact on throw maxima. e+f) presents stage 3, relay zone is highly fractured and throw maxima is located close to the interacting fault. g+h) represents stage 4, the relay zone have become breached and the two fault segments are now hard linked. T-D plot show a sheard throw maxima with a small minima representing the link between them. Figure from Cunningham et al.(2021) inspired by Fachri et al.(2012), Long and Imber(2012), Peacock and Sanderson (1994), and Rotevatn et al.(2007).

Currently, two principal fault growth models are suggested, explaining growth over time (Rotevatn et al., 2019). The propagating fault model explains fault growth as a synchronous relationship between fault length and maximum throw (e.g., (Cartwright et al., 1995; Cowie & Scholz, 1992; Rotevatn et al., 2019; Walsh & Watterson, 1988)). As the fault grow in length the maximum throw will also grow. The constant length fault growth model on the other hand assumes that the fault in early stages of its life will grow rapidly in length. Then, when the length is near maximum the displacement (throw) will start to accumulate (e.g.,(Childs et al., 1995; Cowie, 1998; Rotevatn et al., 2019)). Other growth model has also been proposed, a combination of the two end members where fault growth is divided in two stages, the first being best described by the propagating fault model and the next stage being described by the constant length model (Rotevatn et al., 2019).

To distinguish between fault growth models the interaction with growth strata is important and looking at T-D plots alone can lead to ambiguous conclusions (Jackson et al., 2017). As this study focuses on the picking strategy, growth strata are not discussed, and growth models are not proposed. However, the identification of displacement minima, indicating breached relay zones are important in CO2 storage sites as they may impact fluid flow through enhanced fracturing, deformation bands or zones where juxtaposition changes (e.g., (Peacock & Sanderson, 1994; Shipton et al., 2005)).

Along strike variations have been interpreted to represent areas where faults segments are linked (Schlische, 1995).

3.2.0 Fault Reactivation

3.2.1 Principal Stresses

One of the most used classification of faults are based on the work of Ernest Anderson from 1905. He described three classes of faulting based on the relationship of principal stresses ($\sigma_1 > \sigma_2 > \sigma_3$).

1) **Normal faults**: In a normal faulting regime the biggest principal stress (σ_1) is vertical, while σ_2 and σ_3 (H_{max} and h_{min}) are horizontal and perpendicular to σ_1. This results in faults where the hanging wall is downthrown relative to the footwall.

2) **Reverse faults**: In a reverse faulting regime the σ_1 is horizontal while σ_3 is vertical. This results in faults where the hanging wall is upthrown related to the footwall.

3) **Slip-Strike faults:** In a strike slip regime σ_2 is vertical while σ_1 and σ_2 are horizontal. In such a regime the dominant movement is lateral.

The study area in this thesis is regarded as a normal faulting regime where the maximum principal stress (σ_1) is vertical and a product of the weight of the overburden. The intermediate principal stress ($\sigma 2$) and the minimal principal stress (σ_3) are horizontal. In this case σ_1, σ_2, and σ_3 can be called σ_v, σ_H and σ_h respectively. The differential stress (σ_d) is the magnitude between maximum and minimum principal stress (σ_1-σ_3). Normal stress (σ_n) is the stress impacting a surface at a 90 degrees angle, while the shear stress (τ) is the stress impacting the plane from a parallel angle.

Besides stress acting on a surface, several fault rock properties are important when considering fault reactivation. The pressure of fluids in pore spaces in rocks is called Pore pressure (P). Principal stress minus pore pressure is the effective principal stress acting on a surface giving equation 1.

Equation 1: $\sigma_1' = (\sigma_1 - P) > \sigma_2' = (\sigma_2 - P) > \sigma_3' = (\sigma_3 - P)$

When a rock is critically stressed the relationship between the normal stress and the critical shear stress is described by the constant tanφ, where φ is called the angle of internal friction. If the normal stress increases, the shear stress required to generate a shear fracture also increases (equation 2).

$$\textit{Equation 2: } \tau = \sigma_n \tan\varphi$$

The coefficient of friction μ (μ=tanφ) is often considered to be 0,6 -0,85 for un faulted crustal rock (Byerlee, 1978). For fault gauges and phyllosilicates μranges from 0,2-0,4 while sandstone generally have μ=0,6 (Ferrill et al., 2017).

Cohesion (C) is the inherent shear strength of a rock. Previously it var normal to assume that already faulted surfaces are cohesionless (Zoback, 2010), this assumption do however not consider cementation and cataclasis processes happening after faulting, that might cause rocks to regain cohesive strength (e.g., Weiss et al., 2016)

3.2.2 Fault Reactivation Potential

Regional increase in compressional strength, local increase in pore pressure or present-day stress field aligning with the orientation of fault surfaces might cause a fault to reactivate (Wiprut &Zoback,200). Reactivation presents a threat to potential CO2 storage sites as it can lead to e.g., up section fluid flow. To reactivate a fault the shear stress (τ) applied to the fault surface must exceed the cohesion (C), the coefficient of internal friction (μ) and the resolved effective normal stress (σ_n) (Coulomb, 1973). Formula 3 presents the Mohr-Coulomb failure criteria, while figure 3.3 presents the failure criteria as a Mohr circle.

$$\textit{Equation 3: } \tau = C + \mu\sigma_n$$

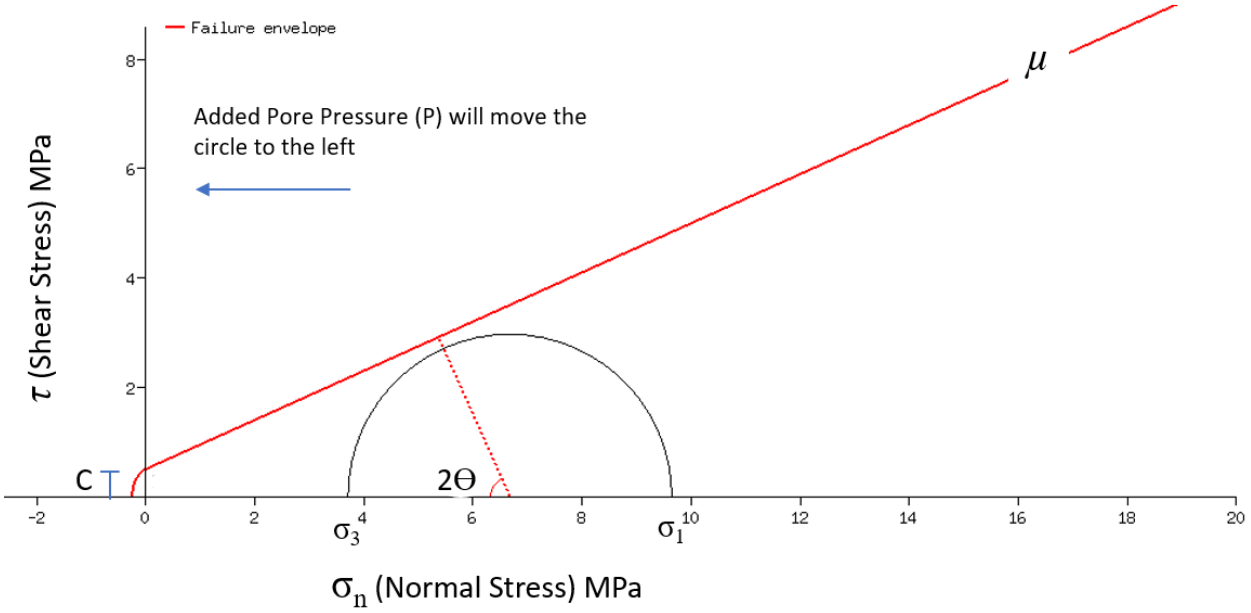

Figure 3.3 presents a Mohr diagram. Red line represents the Failure envelope. C = Cohesion, τ = Shear Stress, σ_n = Normal Stress, μ = coefficient of internal friction

3.2.2.1 Slip Tendency

Morris et al., (1996) defined slip tendency as "the tendency of a surface to undergo slip in a given stress field". Slip tendency is given by the formula $T_s = \tau/\sigma_n$. This shows that T_s (slip tendency) is given by the ratio between shear stress and normal stress acting on a fault plane. It is a ratio between 0 and 1, and slip is likely to happened when Ts are higher than the coefficient of friction (Ts >μ), or said in other word when resolved shear stress exceeds the frictional resistant (Morris et al., 1996).

3.2.2.2 Dilation Tendency

Ferrill et al., 1999 defined dilation tendency as: $Td = (\sigma_1 - \sigma_n)/(\sigma_1 - \sigma_3)$. It describes how the magnitude and direction of the resolved normal stress as a function of the tectonic pressures can cause failure by dilation. It is a ratio between 0 and 1 where a higher value translates to a higher possibility of reactivation. Ferrill et al., (2020) presents that values above 0,8 passes the criteria for failure by dilation.

As slip tendency and dilation tendency are only relying in the impact of the local stress field, it is independent of the geomechanical properties of the rock (Ferrill et al., 2020). However, if a rock will experience failure also depends on the angle of internal friction and the cohesive and tensile strength.

3.2.2.3 Fracture Stability

Fracture stability (Fs) or FAST can be used to calculate how much the pore pressure (critical perturbation pressure) must increase for the fault to reactivate or put in other words it measures the horizontal distance it takes to hit the failure envelope in the Mohr-Coulomb diagram. The lower the CCP or fracture stability is the higher the risk of reactivation. Fracture stability considers both tensile and shear failure and can be expressed by the equations:

$$Tensile\ failure = \sigma_3 + C/2$$

$$Shear/tensile = \sigma_n + (C^2 - \tau^2)/2C$$

$$Shear\ failure = \sigma_n + (C - \tau)/P$$

When CO_2 are injected into a storage unit the pore pressure will increase and fracture stability is therefore an effective analysis to assess the effect of CO_2 injection.

4.0 Data

The data utilized in this study is a 3D seismic survey (GN1101) and well data. An in-house velocity model was used to convert the seismic survey from two-way-time to depth (Michie et al., 2021). The data have been used to create a 3D geomodel of the study area and perform fault modeling and fault analysis.

4.1 3D Seismic Data

Seismic reflection data provides an image of the subsurface by measuring the time (ms) it takes for a seismic wave to penetrate down to a reflector and then back to the surface to be registered at a receiver, known as two-way-time (TWT).

Different stratigraphic layers have different rock densities (ρ), which vary as a function of depth and petrophysical properties. If the density changes at the interface between different stratigraphic layers the wave velocity (υ) will change, and part of the seismic wave will be reflected. The strength of this reflection depends on the bulk rock density (ρ) and the velocity of the seismic wave (υ). The product of rock density (ρ) and wave velocity (υ) gives the acoustic impedance (IA)(Reynolds, 2011). A large change in the acoustic impedance results in a strong reflection. (Mondol, 2010).

Seismic reflection surveys can be conducted along single lines (2D seismic) or systematically over a survey area (3D seismic). 3D seismic surveys provide data cubes where cross sections in any orientation can be generated.

The GN1101 3D seismic survey used in this study was conducted in 2011 by Gassnova SF and covers an area of 442,25km2. This survey is located inside the Norwegian quadrants 32/1,32/2, 32/4 and 32/5, it partly covers two proposed CO2 storage sites in the Smeaheia fault block. The Alpha-prospect, located in the western part of the survey, and the Beta-prospect in the eastern part of the survey.

GN1101 has inline and crossline spacing of 12,5 and 25 m respectively. The survey penetrates a thick sedimentary succession (~4000-6000 m thick) down to the crystalline basement. Inlines are orthogonal to faults interpreted in this study. Seismic processing focused on

resolving the Jurassic interval, and within this interval the vertical resolution is approximately 15 m. The quality of imaging in the Jurassic interval is excellent (e.g. Mulrooney et al., 2020 and Michie et al.,2021).

4.2 Well Data

15 wells in the area were used in this study: 31/2-1, 31/2-2R, 31/2-4R, 31/2-5, 31/2-8, 31/3-1, 31/3- 3, 31/5-2, 31/6-1, 31/6-2R, 31/6-3, 31/6-6, 32/2-1, 32/4-1 T2 and 32/4-3 S. These wells were used for horizon correlation, to make a velocity model and to make a stress model.

4.3 Velocity model

To get a more realistic presentation of structural features the 3D survey has been converted from time domain (measured in ms TWT) to the depth domain (m). This was done using an in-house velocity model made by the CCS team at the University of Oslo (Michie et al., 2021). This model was created using time-depth curves from wells in the Smeaheia and Troll area. The15 wells aforementioned wells contain velocity data and were used to create the velocity model: (Michie et al., 2021). For further details on depth conversion the reader is referred to Michie et al., (2021).

As T7 only calculates values for slip tendency dilation tendency and fracture stability for projects in the depth domain, the in-house velocity model was essential for these calculations.

4.4 Geomodel

The Northern Horda platform and Smeaheia have been extensively studied. The GN1101 survey has been the basis of multiple studies (e.g. Mulrooney et al.,2020, Michie et al.,2021). Five horizon surfaces made by Michie et al. (2021) have been used as input when creating the geomodel this study is based on. This has been done to prevent unnecessary repetition when good data already exists and are available in the study area. The Top- Shetland Group, Top-Cromer Knoll Group, Top-Draupne Formation, Top-Sognefjord Formation and Top-Brent Group are the key horizons used in this study. When creating the seismic horizons the same wells as used for the velocity model was used to aid the interpretation (Michie et al., 2021).

4.5 Stress model

A key input when calculating the fault reactivation potential is the stress scenario used to perform the calculations. In this study in situ stress data have been derived from an unpublished Equinor data package. Wells 31/6-3, 31/6-6, 32/4-1 and 32/2-1 are inside or close to the study area and have been used. Vertical stress (σv) was determined from the overburden gradient while the minimum horizontal stress (σHmin) was determined from extended leak-off test. Pore pressure (Pp) was measured to be hydrostatic (Michie et al., 2021). Previous studies of the northern North Sea have found that the study area are within a normal faulting regime with almost isotropic horizontal stress at levels shallower than 5km (Andrews et al., 2016; Hillis & Nelson, 2005; Skurtveit et al., 2018). The maximum horizontal stress (σHmax) is assumed to be the same at σHmin. The frictional coefficient has been set as 0.45 and the cohesion as 0.5MPa (Michie et al., 2021).

Figure 4.1 gives an overview of the stress model. Note that the same in situ stress profile have been used for each fault and picking strategy. Any differences in reactivation potential will because of this be due to picking strategies.

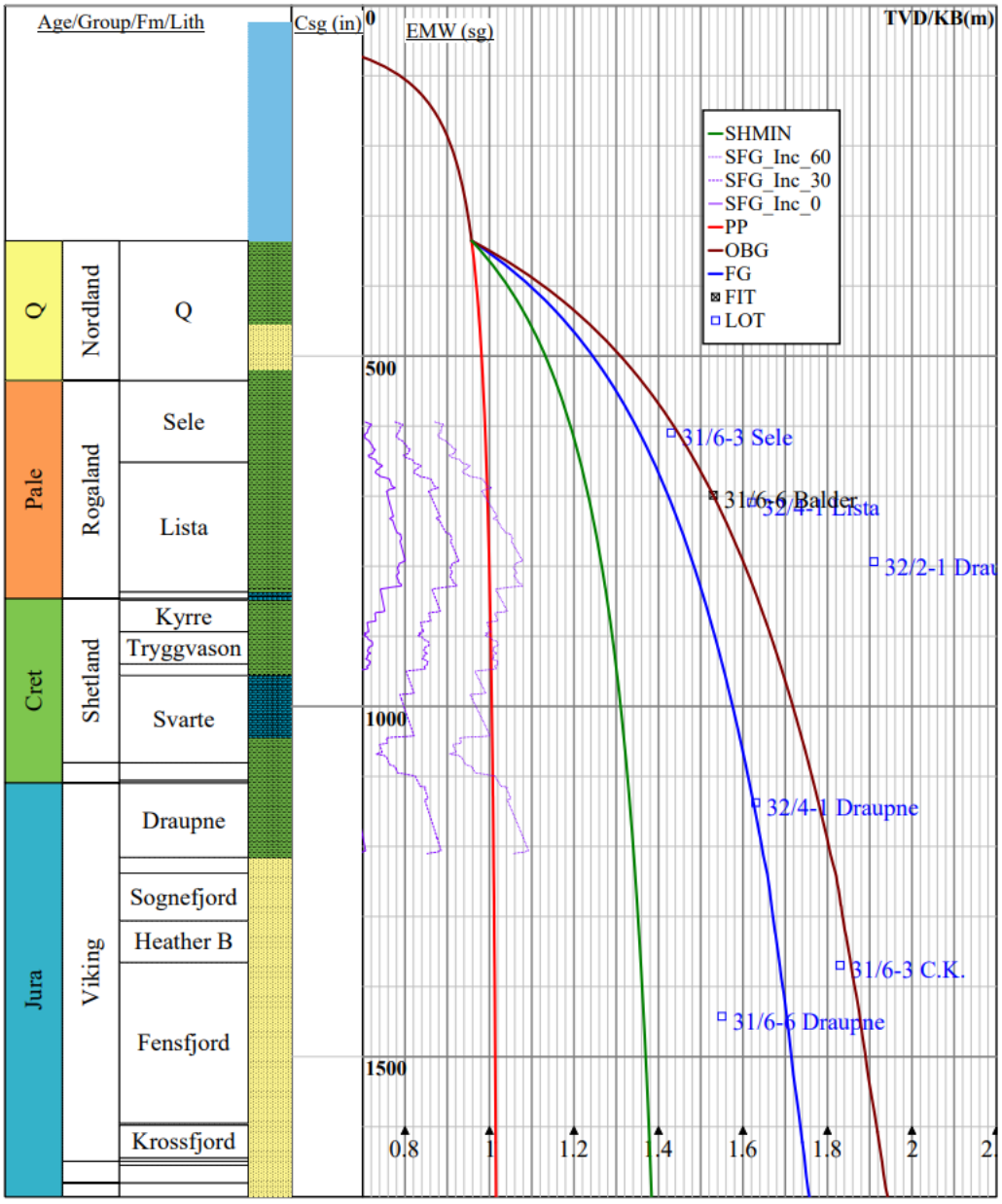

Figure 4.1: The figure presents an overview of the stress scenario used when calculating the reactivation potential in this study. SHMIN= minimum horizontal stress, PP=pore pressure, OBG= overburden gradient, FG= fracture gradient. LOT=leak off test. Figure by (Gassnova, 2021)

5.0 Methodology

Methods are chosen to achieve the objectives of the study: i) improve the knowledge of the best practice for fault interpretation, ii) show how different picking strategies influence the fault growth interpretation, across fault sealing capabilities and fault reactivation potential iii) testing results from previous studies on a new case study of faults with different characteristics than those previously studied.

The workflow of this project can be described in three main stages. The preparation stage consisted of literature studies and software training. The second stage consisted of examination of input data and seismic interpretation. In the third stage fault modeling and analysis were performed before a comparison of the results.

All interpretation, modeling and analysis were performed using Badleys Geoscience's software T7, provided on an academic license. As stated in the Data sub-chapter the depth-converted GN1101 3D seismic survey was used as a foundation for this study.

5.1 Fault interpretation

Testing different fault interpretation strategies was the main objective with this study. A good structural geomodel providing reliable analysis is dependent on the strategy chosen by the interpreter. Choice of interpretation strategy is influenced by data quality and time available. The overall goal when creating a geomodel in industry should be to use a strategy that captures all necessary details, but also limit time invested.

In a 3D seismic survey, the maximum horizontal resolution is defined by the inline and crossline spacing (Brown, 2011). As inlines in GN1011 are almost orthogonal to the fault strike direction of faults interpreted in this study, the inline spacing (25 m) is a good approximation for maximum horizontal resolution when interpreting these faults. A cube of 3D seismic can also produce an arbitrary seismic section in any direction. Arbitrary seismic sections are however a product of the information given by inlines and crosslines and will not provide a more detailed interpretation of faults orthogonal to the inline direction. Arbitrary sections can however be helpful visualization or when interpreting fault oblique to inline and crosslines. In this study arbitrary sections were used for visualization, while faults were picked only at inline sections.

5.2 Triangulation methods

Faults are identified in cross section by an offset of seismic reflections, representing an offset lithological boundary. In the software T7, nodes are picked marking the extent and shape of the fault in 2D cross sections. The software connects points with straight lines creating 2D fault sticks. After multiple seismic sections are interpreted the software creates a fault surface connecting points and lines to one plane. Figure 5.1 illustrate the workflow of creating fault surfaces in T7. Three options for triangulation methods are available in T7 when creating fault surfaces: (i) constrained triangulation, (ii) unconstrained triangulation and (iii) gridded. Constrained triangulation combines both the points picked by the interpreter and the lines generated between points. Unconstrained triangulation combines all points created but not the lines. If gridded modelling is chosen T7 models a surface consisting of regularly sampled points spaced according to a chosen cell dimension. T7 reference manual states that the cell dimension should be set to approximately the distance between seismic lines (T7 reference manual), therefore dependent on picking strategy. As stated by Michie et al. (2021) unconstrained triangulation is considered to be the "middle ground" as it allows for some smoothing of the fault surface but still honors all points picked by the interpreter. For this reason, unconstrained triangulation is used throughout this study. No further smoothing of fault surfaces was used.

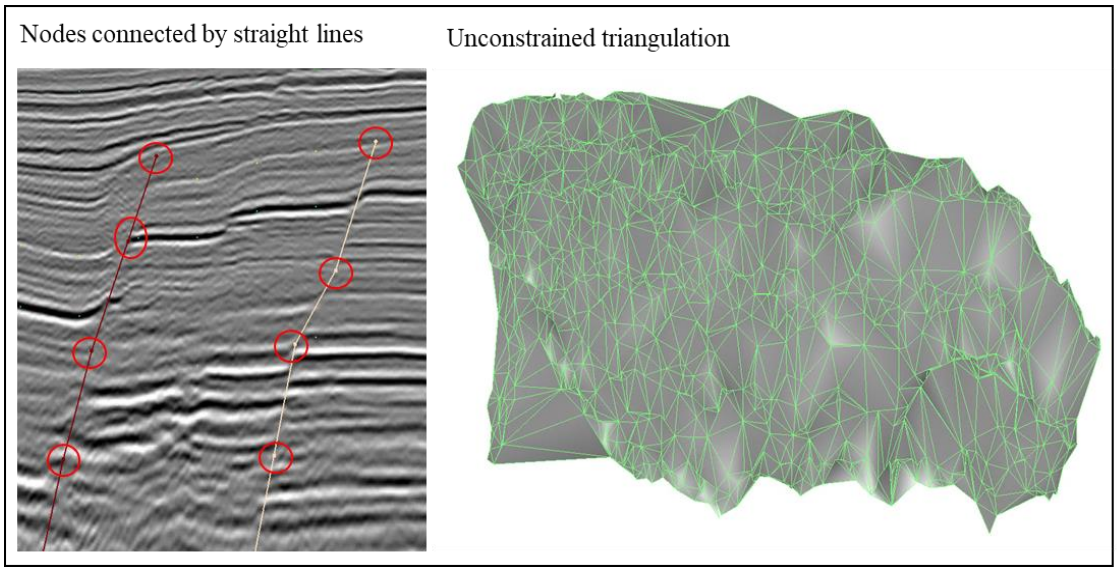

Figure 5.1 illustrate the workflow of making fault surfaces. Red circles marks nodes made by the interpreter. The software then connects the nodes by straight lines. When the full length of the fault is interpreted the software connects nodes by triangulation to make a surface, in this case by unconstrained triangulation.

5.3 Picking strategy

Six second order faults have been interpreted using different line spacing to assess the optimum picking strategy (figure 5.2). Faults have been picked every 1, 2, 4, 8, 16, and 32 inline. This corresponds to 25, 50, 100, 200, 400 and 800 m spacing, respectively. Creating a total of 36 fault surfaces (6 versions of each fault).

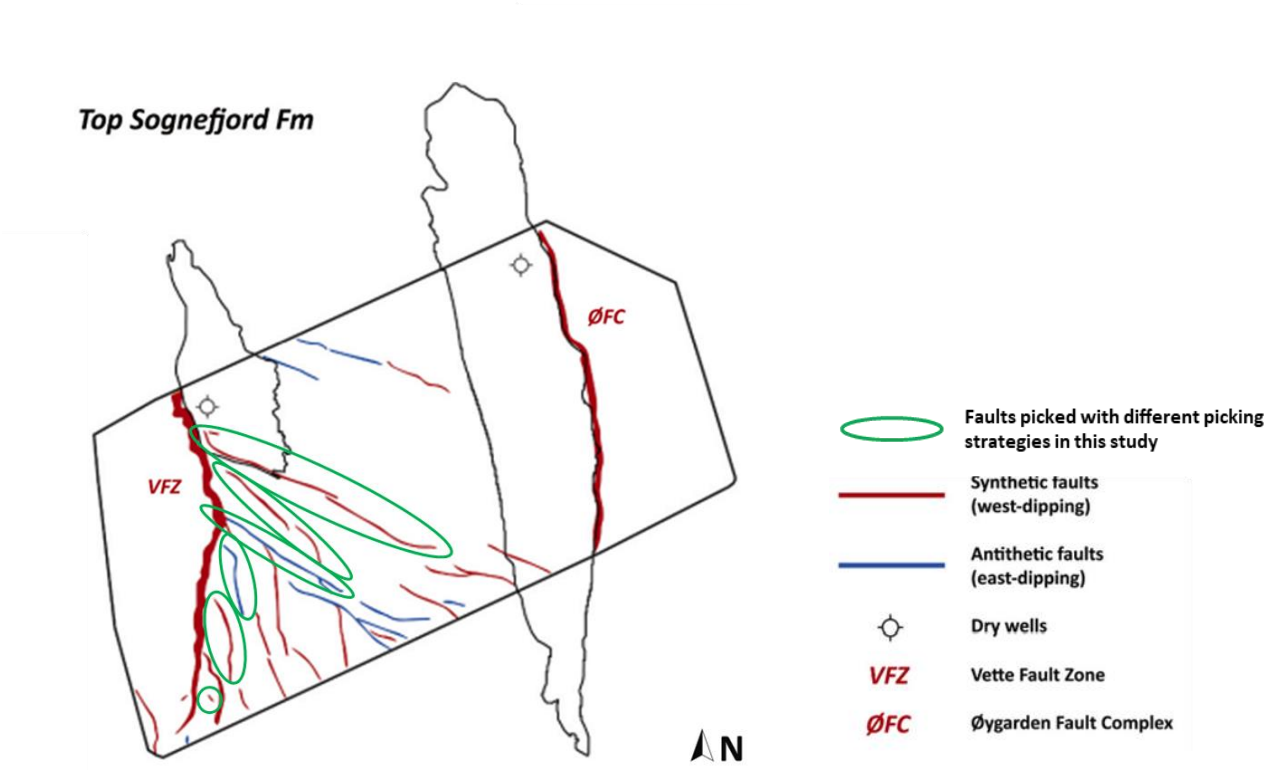

Figure 5.2: The six second order faults interpreted with different picking strategies are highlighted by green circles. Alpha and Beta prospects are shown in grey. Modified from (Mulrooney et al., 2020).

Michie et al. (2021) used the same method to find the optimum line spacing when interpreting the Vette Fault Zone (VFZ). The VFZ is a ~50 km long first order (basement involved) fault zone with a maximum throw of 1000 m. The six faults that are the focus of this study are smaller second order splay faults of the VFZ with a maximum throw of less than 100 m. Interpreted faults range from 0.8 km to 12 km in length. The full fault length of all faults is within the area covered by the seismic survey. To ensure continuity faults are treated as individual faults, even though they might be hard linked to the VFZ.

The faults interpreted in this study were chosen because they represent a different scale than those previously studies using the same method. As the faults in this study have a wide range of lengths (0.8 – 12 km), it is also possible to compare picking strategy chosen on this smaller scale. All faults are within the same seismic survey as the interpreted part of VFZ by Michie et al. (2021), therefore no additional "noise" created by seismic survey quality should affect the comparison between results.

Fault segments were picked at every inline increment (25 m spacing) for the entire length of each fault. To make sure the picking was consistent, every other fault segment was deleted to make the 2-increment spacing (50 m), three out of four segments were deleted to make the 4-increment spacing and so on. This keeps the picking consistent as the same segments are used for every picking strategy, ignoring possible human error picking and difficulties in QC-ing due to large distances between increments. Adding crossline interpretation when faults are parallel to the crosslines represent significant uncertainty. It is very easy to get a mismatch between inline and crossline interpretation creating a false zig-zag pattern to the fault surface. Keeping to inlines only, also makes comparison between each picking strategy easier.

5.4 Horizon interpretation/ Use of existing geomodel

The Smeaheia fault block is an area of the North Sea that has been the subject of multiple previous studies. Because of this good quality models of the area already exists. To avoid unnecessary work already existing horizon interpretation made by (Michie et al., 2021) was used in the work of this study. This also ensures that there is no difference in horizons within this study or between the easily comparable study of (Michie et al., 2021). Keeping fault interpretation as the only variable.

A total of five horizons have been used in this study: the top Brent Group, top Sognefjord Formation, top Draupne Formation, top Cromer Knoll Group, and top Shetland Group. Horizons was chosen as the Sognefjord Formation is the primary storage unit of the Smeaheia scenario and the Draupne formation is the primary cap rock while Brent Group and Cromer

Knoll Group might work as secondary storage and cap rock respectively. Faults interpreted in this study terminate up-section around the top Shetland Group (Mulrooney et al., 2020).

5.5 Cut-off lines

After the fault surfaces are created, surface intersections between faults and horizons are created. Intersections are represented by cut-off lines at the fault surface. The method of creating cut-off lines is commonly used to assess characteristics such as juxtapositions, membrane seals and fault growth models (e.g., Mulrooney et al., 2020, Michie et al. 2021). An offset horizon is characterized by a cut-off line representing the footwall intersection and a cut-off line representing the hanging wall intersection.

These lines are generated by the software using “fault trim distance (m)” and “patch with (m)”. The fault trim distance is the horizontal distance (on the horizon) on either side of a fault surface that is excluded when creating a fault – horizon intersections. The patch width defines a patch zone beyond the fault trim distance that are used to create fault – horizon intersections. By default, the software defines fault trim distance to 1,5 x (√ (total survey area / 50 000)) in this project 150 m, and the patch zone is defined as 4/3 of the fault trim distance (200 m). This was the values used when crating intersection lines in this study. However, these values are not important as all cut-off lines were re-picked using the different picking strategies described above.

Corresponding to the picking strategy chosen for fault interpretation, each cut-off line was re-picked guided by seismic sections every 25, 50, 100, 200, 400 and 800 m (figure 5.3). Greater distances significantly reduce time invested in the project (re-picking cutoff lines for one fault of 12 km at a 25 m spacing took the author an excess of 40 hours of work), but also leads to smoothing and possibly losing important data.

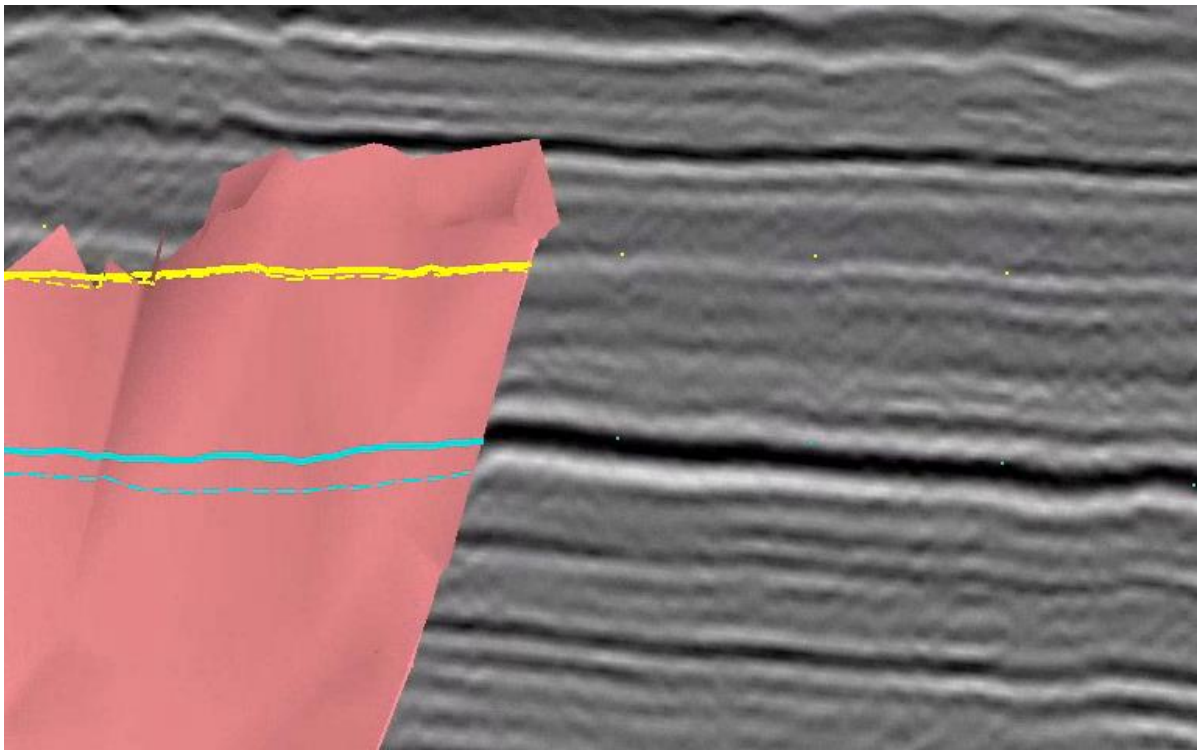

Figure 5.3: Figure of cut-off line picking being guided by seismic sections. This was done every 25, 50, 100, 200, 400, and 800 meter, corresponding to the chosen picking strategy.

Cut-off lines can be challenging to create, even at a fine spacing to guide picking. They are also dependent on high quality fault interpretation. Picking cut-off lines on faults with a low throw can be specifically challenging as a few mm on the computer screen translates to multiple meters in reality. A substantial amount of time has, therefore, been spent into re-picking cut-off lines. At areas where fault throw was close to the seismic resolution, specifically near the fault tips, automatically generated cut-off lines was often erroneous drawing the hanging wall above the footwall, indicating reverse movement. After careful manual editing, this was no longer the case even at large spacing between sections (400 and 800 m).

Some faults interpreted have a significant drag in the hanging wall or footwall. Some faults also have areas along strike where the reflectors show subtle folding, rather than showing a sharp offset. This forms complications as cutoff lines could be interpreted to honor the drag or not. By honoring the drag the representation of juxtaposition could be better represented, playing an important role in across-fault sealing analysis. Figure 5.4 present an example of areas dominated by drag vs. areas dominated by sharp offset. However, for the proposed CO2 storage scenarios in Smeaheia, the sealing capabilities of these second order faults are not of great importance. Because of the low throw, most stratigraphic units are self-juxtaposed and will at most work as a baffle for migrating fluids. To best capture the throw of each fault and accurately interpret fault growth, drag was removed when picking fault cutoff lines.

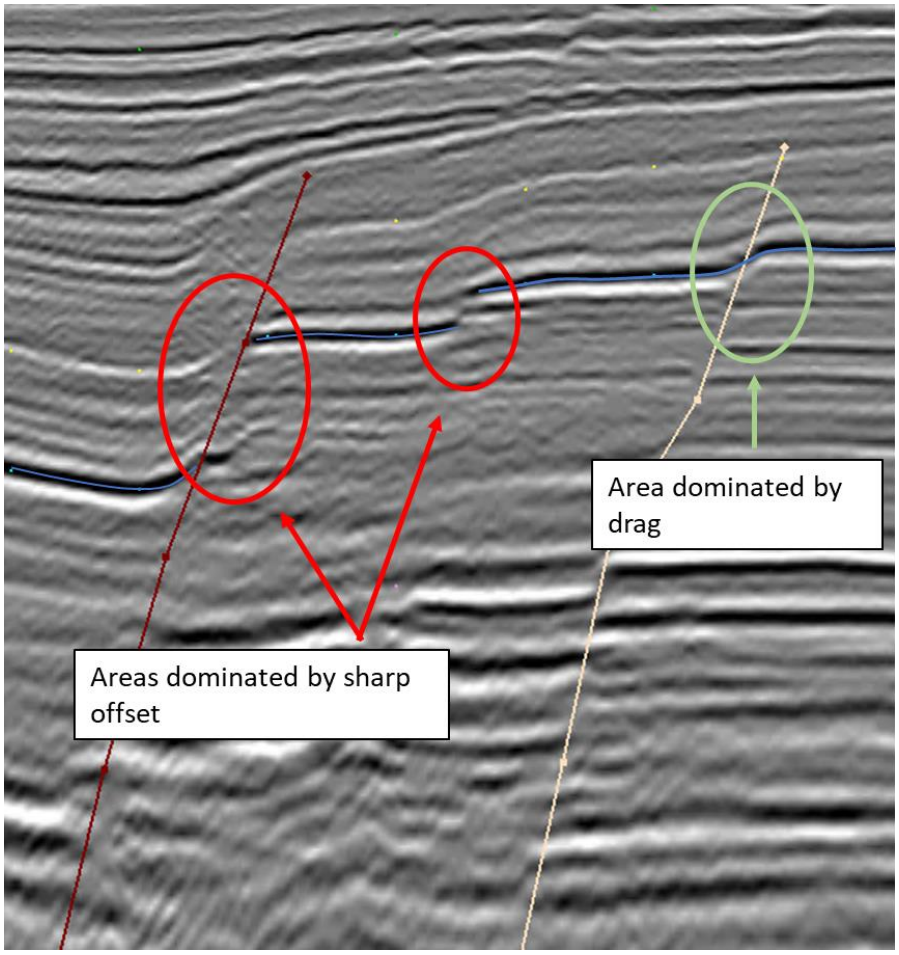

Figure 5.4: Examples of areas that are dominated by drag vs. areas that are dominated by a sharp offset. The blue line is the top Sognefjord formation. The red circle to the left highlights the Vette Fault Zone, notice that in the hanging wall there I some drag, but there is also a sharp offset between hanging wall and footwall. The red circle in the middle highlights an area with very little or no drag. The green circle to the right highlights an area with no sharp offset, only drag.

5.6 Fault modeling and analysis

When using different software for seismic interpretation and fault modeling, issues may arise during export and import process. Because of this, careful quality control must be performed to verify that the newly generated faults are structurally valid. In this study seismic interpretation, fault modeling and analysis were all performed using T7, thus issues concerning import/ export were eliminated.

Fault analyses are regularly performed to assess the presence of across fault seals, evolution of faults and the reactivation potential of faults. This study presents fault throw, throw vs. distance diagrams, fault dip, dilation tendency, slip tendency and fracture stability on a selection of faults interpreted using differing picking strategies (see sub section 3.2).

To map attributes on fault surfaces the “synchronize attribute” display function in T7 was used. To optimize resolution without the need to extend processing time a resolution of 8 m lateral and 4 m vertical was chosen.

To identify fault segmentation and create fault growth models, throw was mapped on fault surfaces by using the synchronize attribute function and throw - distance profiles was generated using the fault statistics function in T7 (measuring the vertical distance between footwall and hanging wall cut-off lines). For the throw distance profiles the throw of the top Sognefjord formation was plotted against the distance. This was because the Sognefjord formation is the main target of CO2 injection at the Smeaheia scenario.

To help identify fault segmentation, strike and dip was calculated and mapped onto the fault by the software. Strike and dip are also essential when calculating the reactivation potential of faults combining the faults spatial properties with a set stress scenario. Then “slip tendency” and “dilation tendency” were calculated and mapped onto the fault. These parameters result in ratio values between 0 and 1 equating to a higher tendency for leakage. To provide a measure of the increase in pore pressure required to force a fault into extensional or shear failure “fracture stability” was calculated. For this measure lower values equate to a higher tendency of reactivation (T7 reference manual).

6.0 Results

The aim of this study has been to improve our knowledge of the best practice for fault interpretation and show how different picking strategies will influence fault growth interpretation and fault reactivation analysis. This chapter describes how fault surfaces, fault cutoff lines and fault attributes vary with picking strategy.

6.1 Fault characteristics

All six faults picked are normal faults within the footwall of the Vette Fault Zone. They are thin-skinned faults (not basement involved). Fault numbers 1,2, 5, and 6 are synthetic to the Vette Fault Zone while faults 3 and 4 are antithetic and dip to the east (figure 5.2). The faults vary from 800 to 13 000 m in length, though the length of the corresponding fault surfaces varies with the picking strategy. When picking with a wide spacing, information close to fault tips is lost and the surface generated is shorter than when picking at every inline. Table 4.1 summarizes fault characteristics for each fault and shows how different picking strategies influenced the length of the Sognefjord Formation cutoff lines for each fault.

Table 6.1: Summary of fault characteristics for the 6 faults interpreted with 6 different picking strategies.

	Fault 1	Fault 2	Fault 3	Fault 4	Fault 5	Fault 6
Strike direction	NW-SE	N-S	N-S	NW-SE	NW-SE	NW-SE
Dip direction related to VFZ	Synthetic	Synthetic	Antithetic	Antithetic	Synthetic	Synthetic
Length when picked at 25 m increment	930 m	4446 m	3830 m	5232 m	6483 m	12 934 m
50 m increment	911 m	4428 m	3751 m	5081 m	6338 m	12 587 m
100 m increment	765 m	4280 m	3689 m	4932 m	6024 m	12 021 m
200 m increment	868 m	4277 m	3638 m	4754 m	6268 m	12 378 m
400 m increment	809 m	4255 m	3472 m	4711 m	6122 m	12 367 m
800 m increment	754 m	4090 m	2960 m	4648 m	5689 m	12 341 m

6.2 Fault segmentation analysis

To interpret how faults have grown at the seismic scale two main attributes are used within this study: throw profiles and strike variations. Abrupt changes in fault strike may indicate where fault segments initially isolated were subsequently linked (e.g. Mansfield & Trudgill, 1996). However, not all variations of fault strike indicate fault linkage, and not all fault linkage results in fault strike changes. Because of this, integrated analysis of throw profiles and fault strike variation is used to better understand the fault growth history. It is also important to note that fault segmentation below the seismic resolution can not be detected by this analysis. In this study faults with throw values of less than 100 m have been analyzed, and changes in throw variations might come close to the vertical seismic resolution of 16 m.

6.2.1 Throw-distance profiles

Changes in throw along strike are used to identify the location of fault segmentation (e.g., (Michie et al., 2021; Mulrooney et al., 2020; Tao & Alves, 2019)); areas of throw minima might indicate areas where fault segments are linked. In this section, throw-distance profiles (T-D plots) for the top Sognefjord Formation are shown alongside throw attributes plotted on fault surfaces for visualization. T-D plots and throw attributes are then compared to variations in strike.

6.2.1.1 Fault 1:

Figure 6.1 presents throw measurements of the top Sognefjord formation for all picking strategies for Fault 1. Towards the northwest, where the displacement tips out, the throw-distance profiles show throw values from 5 m to 20 m; in the southeast, fault throw values are between 60 and 75 m. Along strike, throw values gradually increase to reach the maximum in the southeastern part of the fault. Notice that along the entire fault there is a variation of approximately 15 m between all picking strategies, which is on the same scale as the vertical resolution of the seismic survey. Picked at 25 m increments there are subtle variations along strike that are not seen with coarser picking strategies. This may indicate a breached relay.

The fact that Fault 1 shows an increase in throw values to the southeast may indicate that Fault 1 is a splay fault of a larger fault. More precisely a splay fault to a N-S trending second order fault that extends to the south of the study area.

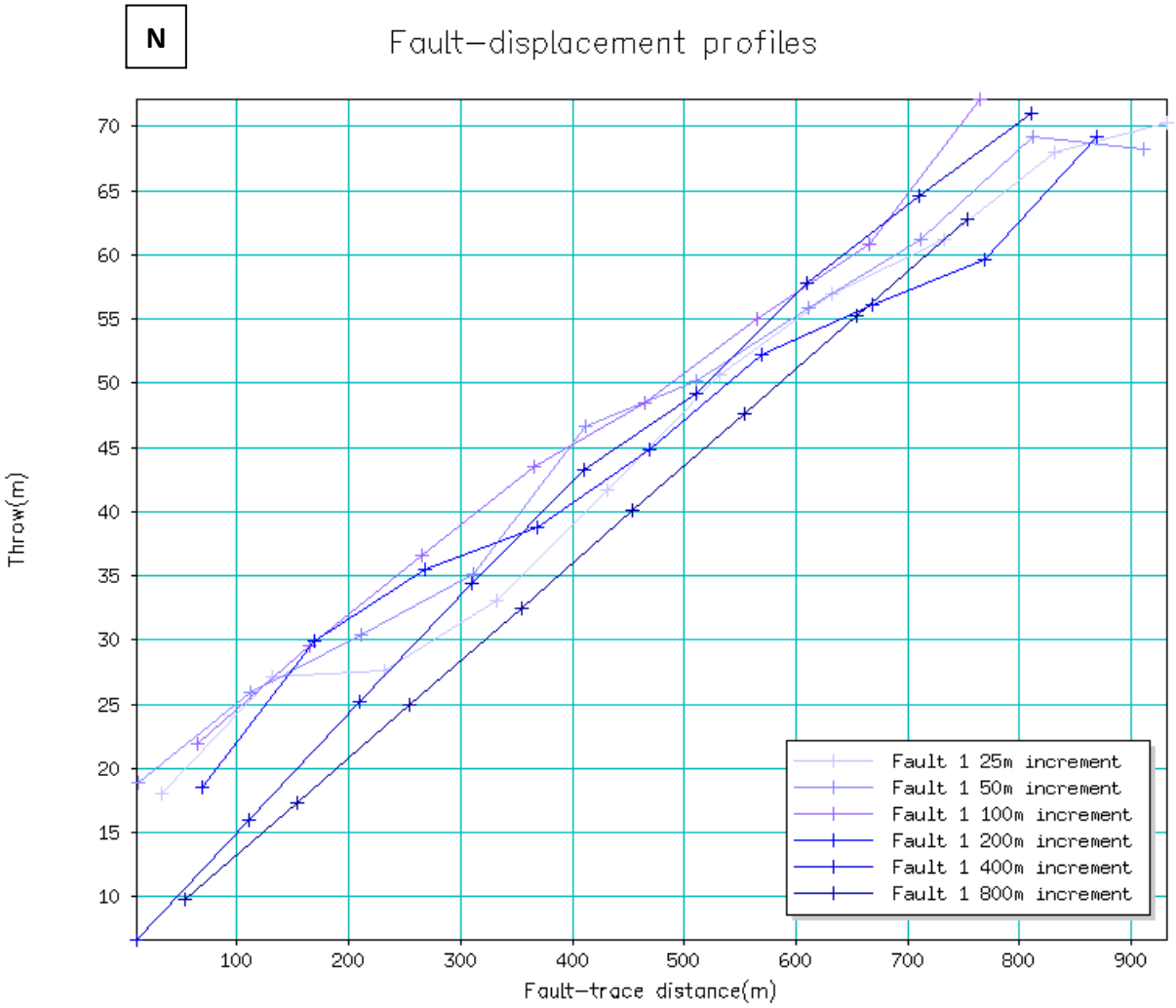

Figure 6.2: Throw- Displacement profile (T-D plots) Fault 1. Lighter colors represent a more densely spaced picking strategy, while darker colors represent wider spacing in the picking strategy.

Figure 6.2 presents throw values plotted on the fault surface of Fault 1 when picked at 25 m spacing. Throw values are largest (70 m) at the depth of the top Sognefjord Formation (approximately 1500 m) in the southeastern part. Up-dip, down-dip, and to the northwest, throw values gradually decrease. All picking strategies showed the same trends for throw plotted on fault surface for Fault 1 and only the most densely spaced strategy is shown. Appendix A presents all attributes for all picking strategies on all faults.

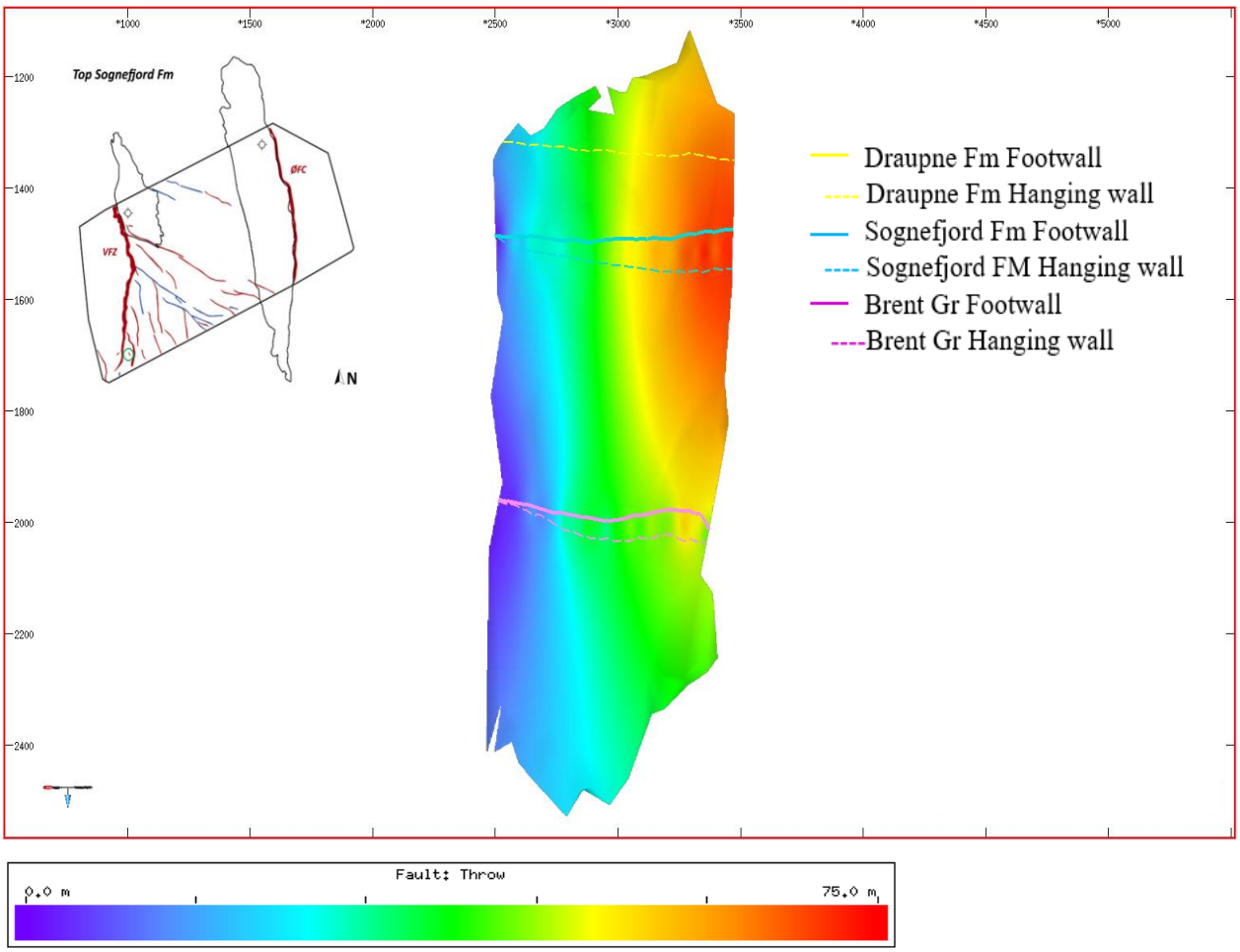

Figure 6.3: Throw values plotted on the fault surface of Fault 1 picked at 25 m inline spacing. Figure from software T7 taken in strike view. Inset show the spatial position of Fault 1, marked in green circle

Strike

Fault 1 is a fairly straight fault without significant variations in strike. When strike direction was plotted onto the fault surfaces and the color range was set to vary between 270 degrees and 360 degrees some variations were visible (figure 4.3). Picked at an increment of 25 m, it is visible that the northwestern half of the fault has a strike orientation of around 315 degrees while the southeastern half is oriented at around 340-350 degrees. Some “bulls-eye” patches of different strike orientations are also visible with this picking strategy. Picking at 100 m inline spacing the differences in strike on the northwestern half and the southeastern half are

still visible, but the “bulls-eye” patches are no longer visible. When picking at every 800 m inline spacing no differences in strike are visible.

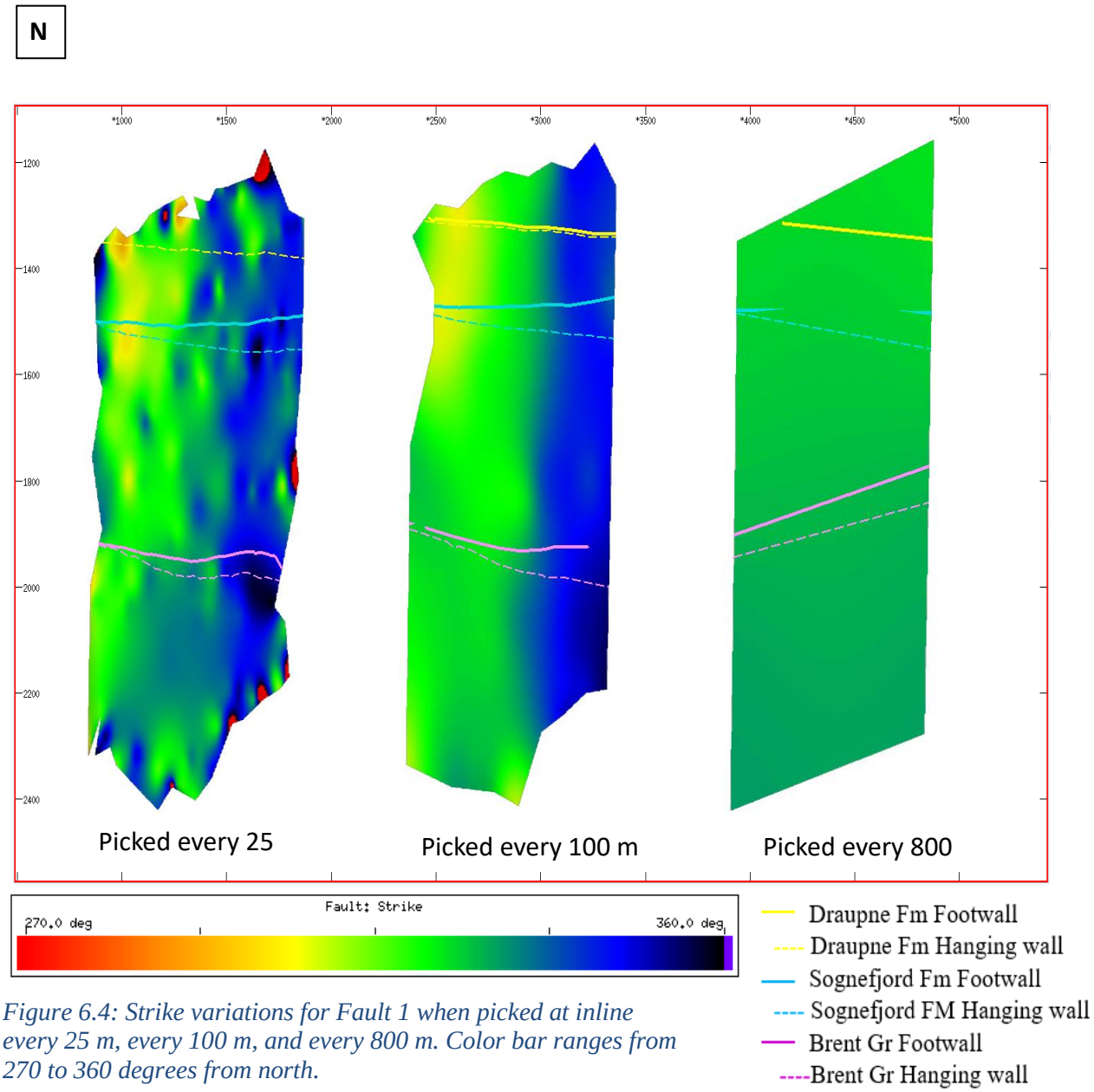

Figure 6.4: Strike variations for Fault 1 when picked at inline every 25 m, every 100 m, and every 800 m. Color bar ranges from 270 to 360 degrees from north.

6.2.1.2 **Fault 2**

Figure 6.4 presents T-D plots for the top Sognefjord Formation on Fault 2 picked at every increment (25m). There are two notable throw maxima of throw up to 32 m separated by a minima of 17 m. Throw maxima is located at 2100 m and 3300 m along strike with the minima at 2850 m. Toward the southern tip of the fault the throw value decreases.

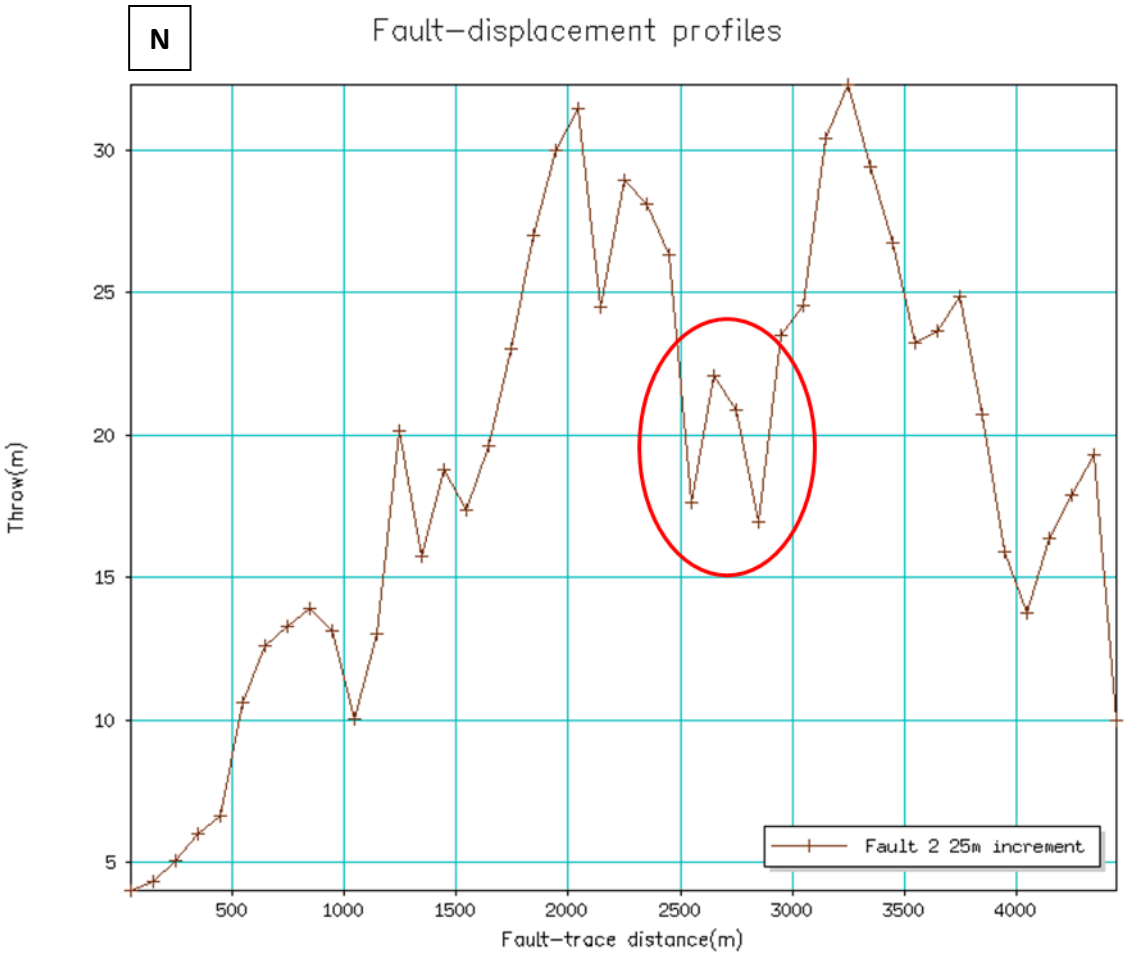

Figure 6.4: Throw- Distance profile (T-D plots) Fault 2, picked at 25 m spacing. Red circle highlights area of throw minima.

When looking at T-D plots for all picking strategies (figure 6.5) the overall trend is the same for picking strategies up to 200m increments. The lightest color represents picking with 25 m increments, lines drawn in the T-D plot gets gradually darker when increments increase. In the northern part of the fault throw values are low (0- 10 m depending on strategy), then gradually increases to 30 to 35 m at 2100 m south along strike, there throw values decreases to approximately 20 m (one picking strategy showing 10 m) around 2600 m along strike, before increasing to a new maximum of 30 - 35 m at 3300 m along strike. It then decreases towards the southern tip of the fault.

However, there are some differences between the results given by each picking strategy. Picking at 100 m increments resulted in the same general trend, but the first throw maxima is

smaller and harder to identify than picked at 25, 50, and 200 m increments. When picking at 800 m increment the throw profile does not show the second throw maxima or decrease towards the southern tip of the fault surface. Instead, it quickly increases in the northern part of the fault and then stays between 25 to 30 m to the end of the fault. The T-D plot for the fault picked at 200 m spacing gives the most pronounced throw minimum.

The same trend is noticeable when looking at throw values plotted on fault surfaces. Figure 6.6 presents this for picking at 25 m spacing and 800 m spacing. Picking at shorter increments identifies fault segmentation while 800 m increments does not. This presentation also shows that throw maxima is at top Brent Group and not within the Sognefjord Formation.

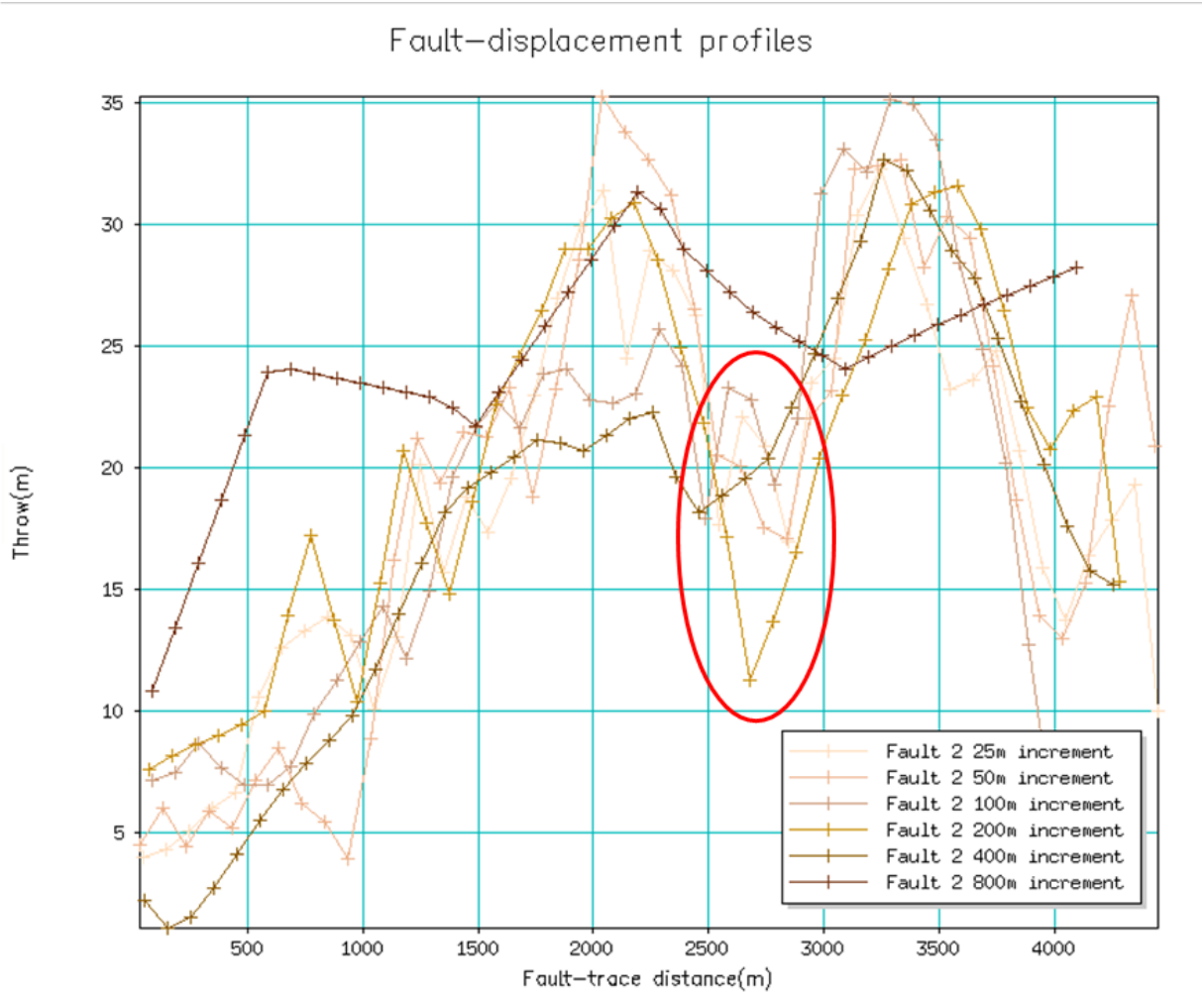

Figure 6.5: Throw- Displacement profile (T-D plots) Fault 2. Lighter colors represent a densely spaced picking strategy, while darker colors represent wider spacing in the picking strategy.

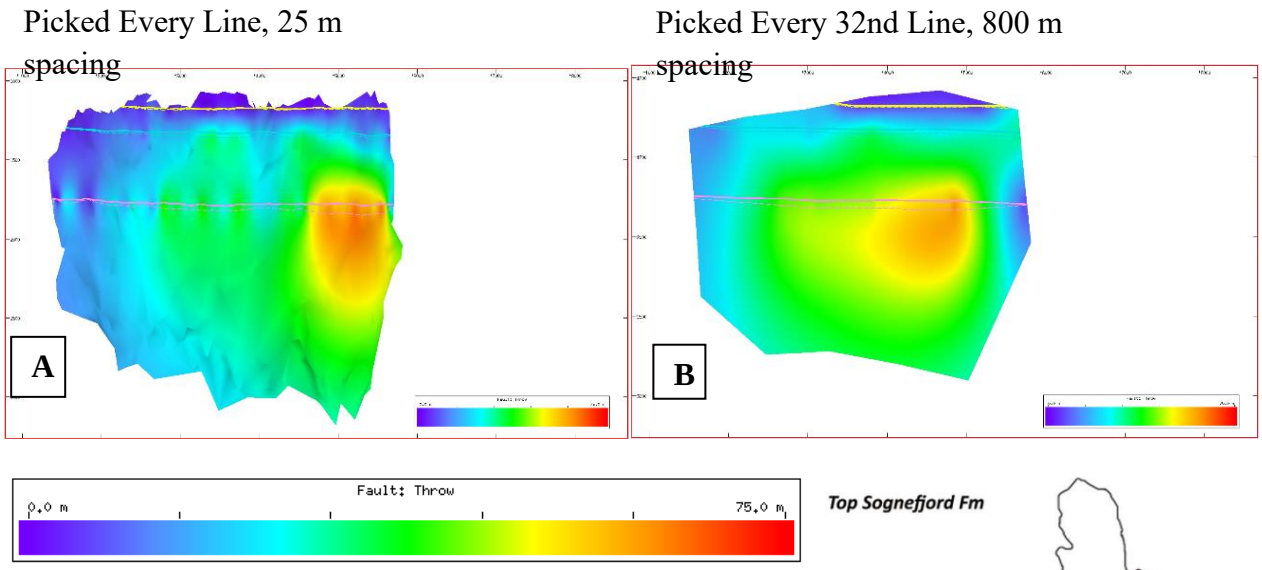

Figure 6. 6: A) Throw plotted on the fault surface of Fault 2 when picked at 25 m spacing. Notice that there is two separate throw maximums, corresponding to the two throw maximums in the Throw- Displacement profile (fig. 6.4 and 6.5). B) Throw plotted on the fault surface of Fault 2 when picked at 800 m spacing. Here only one throw maximum is visible. Color bar ranges from 0-75m. To the right, spatial reference, Fault 2 marked with green circle

Strike

Figure 6.7 presents the variation in strike for all picking strategies on Fault 2. To highlight small differences, the color bar is set to range from red at 180 degrees from north to blue/black at 360 degrees. There is a noticeable difference in strike at 2500 m along strike where the color changes from blue to red. This corresponds to the area of throw minimum, leading to a possible identification of fault segmentation. This variation of strike is visible for all picking strategies. However, when the fault was picked at 25 – 400 m spacing another variation in strike is visible at 3000 m along strike, but when picked at 800 m spacing this second variation is not visible.

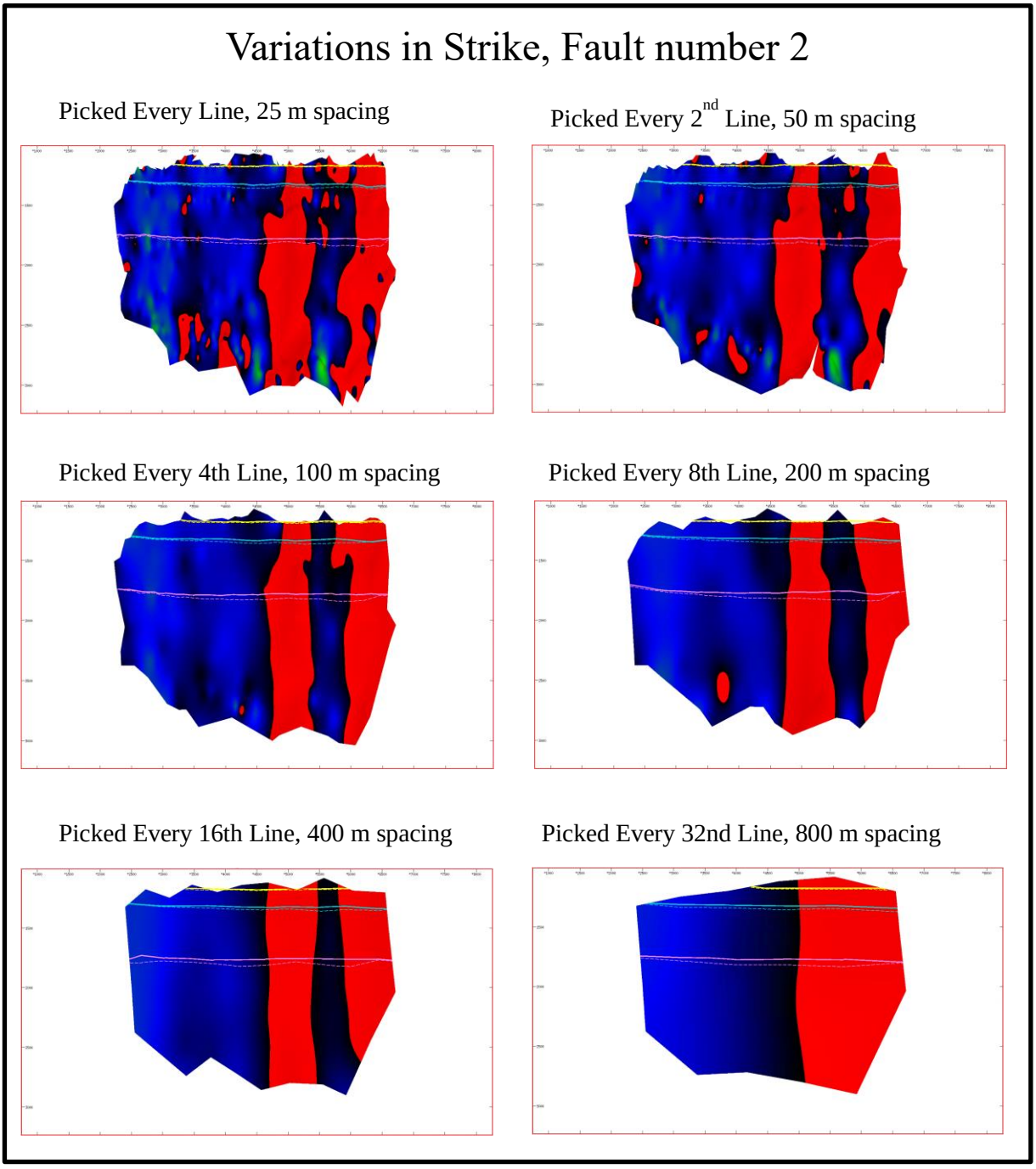

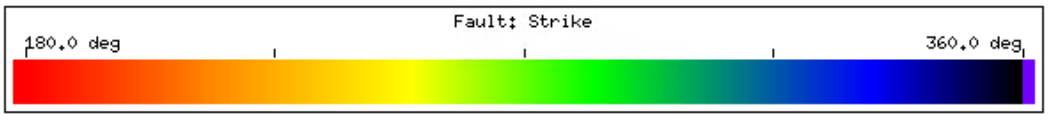

Figure 6.7 Strike plotted on fault surfaces for all picking strategies on Fault 2

6.2.1.3 Fault 3

Figure 6.8 presents T-D plots for the top Sognefjord formation on fault 3 with every picking strategy presented. Note that Fault 3 is antithetic in respect to the VTZ and that the left part of the T-D plot (fig 6.8) is to the south. In the southern part of the fault, throw values increase to approximately 15 m, at 2000 m north along strike throw values start to increase. At 3100 m along strike throw values reaches a maxima before it decreases towards the northern tip of the fault. At this point of maximum throw, picking strategies from 25 to 400 m have throw values ranging from 35 to 55 m. There is no apparent trend that larger increment spacing gives higher or lower throw values. Throughout the entire fault, all throw values have a variation up and down with an amplitude of approximately 10 – 15 m.

When looking at the T-D plot for Fault 3 picked at 800 m spacing the irregularity in throw values is higher, throw values start to increase further south and reaches a higher maxima (65 m) than the rest of the picking strategies. No fault segmentation can be identified on Fault 3, and only Throw- Distance profiles are shown, for throw and strike plotted onto the fault please see appendix A.

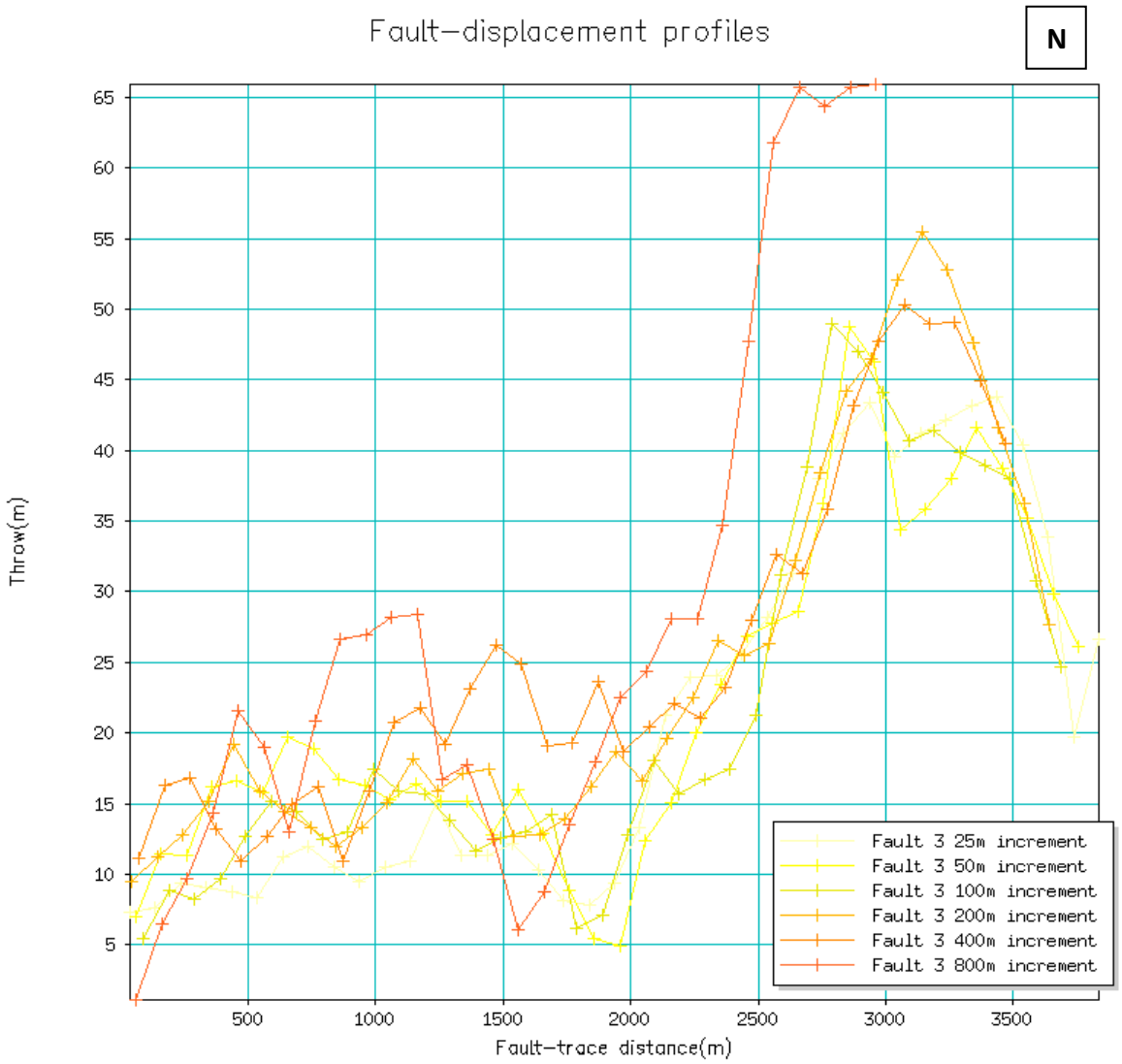

Figure 6.8: Throw- Displacement profile (T-D plots) Fault 3. Lighter colors represent a densely spaced picking strategy, while darker colors represent wider spacing in the picking strategy. To the right is the position of Fault 3 highlighted with a green circle

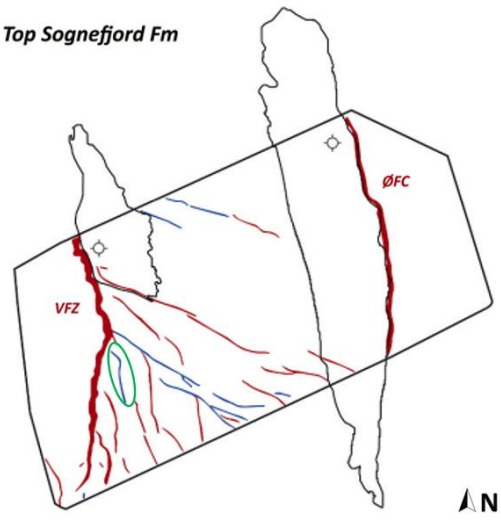

6.2.1.4 Fault 4

Figure 6.9 presents T-D plots for the top Sognefjord formation on Fault 4 with all six pic strategies shown. In the southern end of the fault throw values increases to approximately 30 m for all picking strategies, it is then relatively constant for most of the fault before it tapers out at the end of the fault. All picking strategies have an irregular pattern with an amplitude of roughly 10-15 m. At each end of the fault, differences between picking strategies are larger than in the middle with picking at 25 and 50 m increments show lower throw values related to other strategies in the southern end of the fault and larger values in the northern end (difference of up to 40 m).

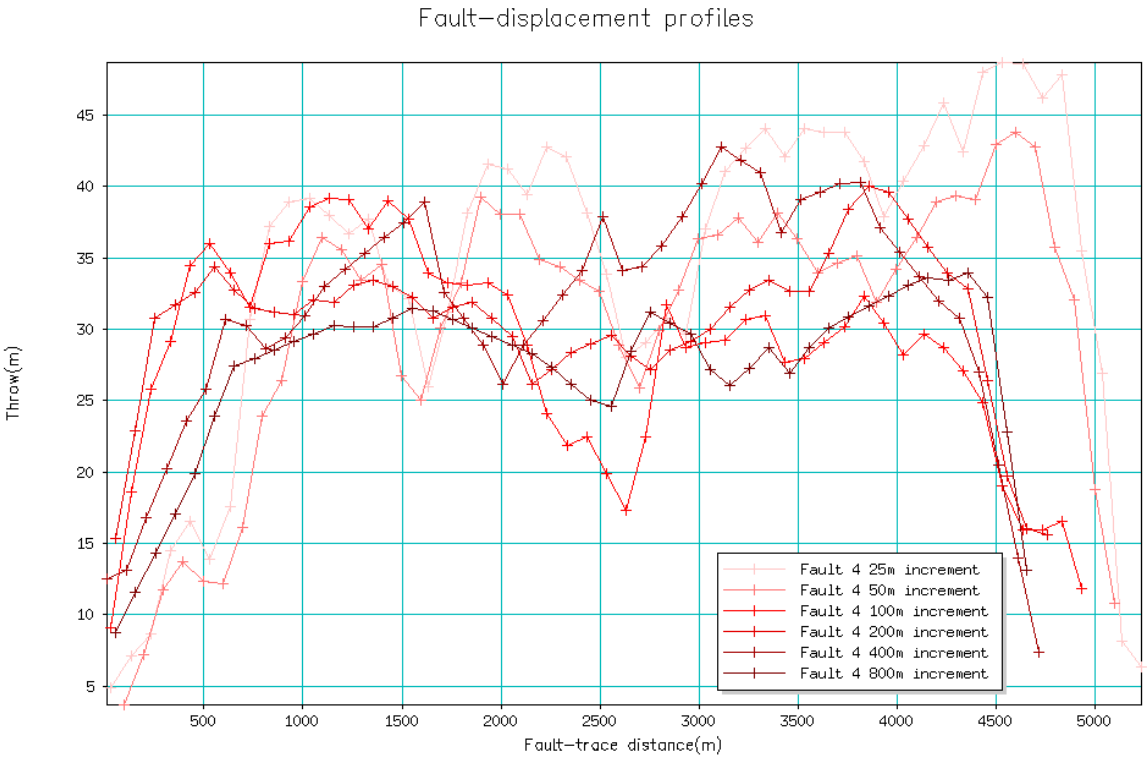

Figure 6.9: Throw- Displacement profile (T-D plots) Fault 4. Lighter colors represent a densely spaced picking strategy, while darker colors represent wider spacing in the picking strategy. To the right is the position of Fault 4 highlighted with a green circle.

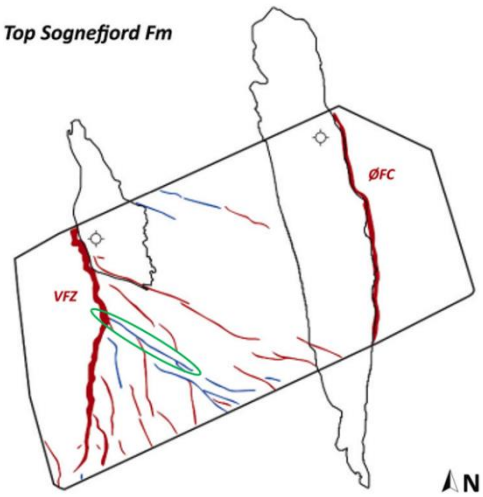

6.2.1.5 Fault 5

Figure 6.10 presents T-D plots for the top Sognefjord Formation on Fault 5 with all six picking strategies shown. In the northern end of the fault most picking strategies show throw values that steadily increase to 55-60 m at 2200 m along strike. At 3500 m along strike throw starts to decrease and reaches zero at the end of the fault. Notice that when picked at 100m inline spacing the T-D plot looks very different from the rest. This picking strategy produced a T-D plot with low throw values for the first 2000 m relative to other strategies. The throw maxima is also "skewed to the right". This T-D plot does not fit at all with the others and are being interpreted to be due to human error and is not given significant attention in analysis.

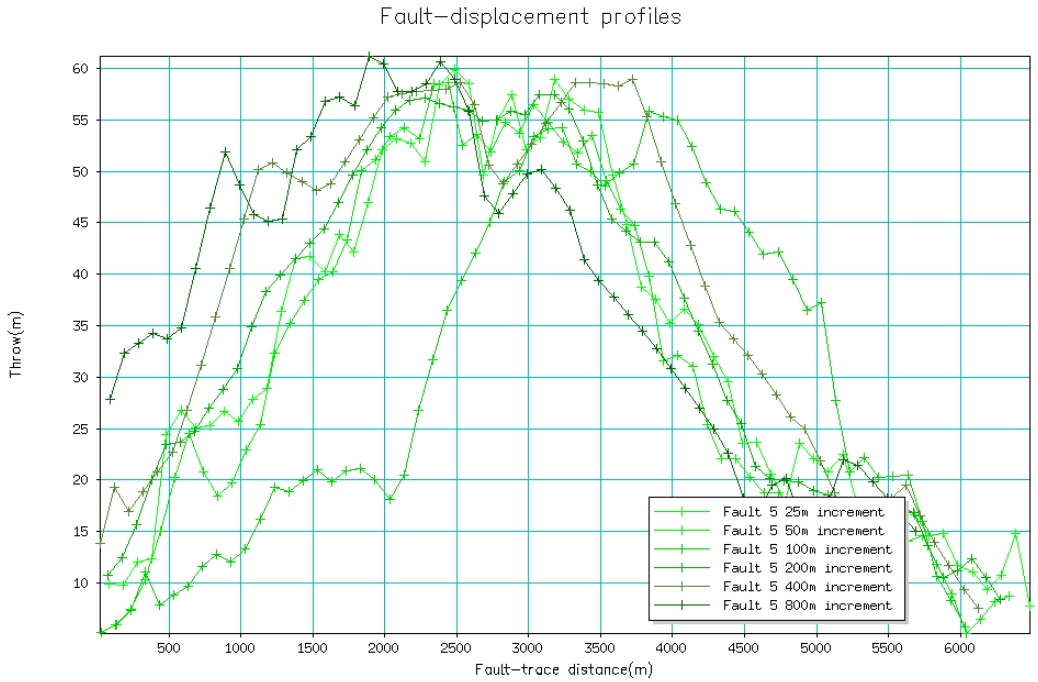

Figure 6.10: Throw- Displacement profile (T-D plots) Fault 5. Lighter colors represent a densely spaced picking strategy, while darker colors represent wider spacing in the picking strategy.

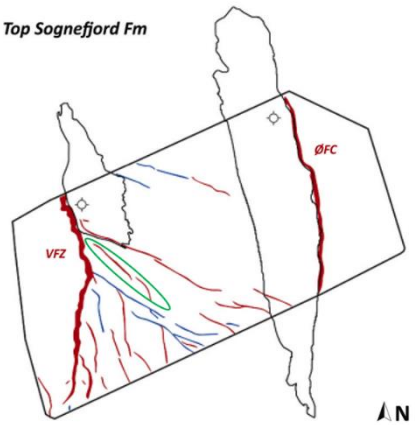

6.2.1.6 Fault 6

Fault 6 is the longest fault in the study, it is 13 000 m in length and show some interesting properties. Figure 6.11 presents T-D plots at the top Sognefjord Formation for every picking strategy separately. When picked at every inline with 25 m spacing the T-D plot show throw values of 15-20 m in the northern part, after 1000 m throw values start to rise and have a first maxima of 45-50 m at 3000 m along strike. It then decreases to 40 m at 3000 m along strike before it reaches a new throw maxima of 55-60 m 6000 m along strike. At 7500m we can see a new throw minimum, at 8-9000 m a new maxima before it gradually gets lower towards the southern tip of the fault.

Picking at 50 and 100 m increments show the same general trend. The deviation (zig zag pattern) of the T-D plot varies from that picked at 25 m, but the same throw minimum and maxima are found on the same places. Note that the amplitude of the deviation is low (5-10 m). Further, towards the northern tip of the fault, both picking strategies show a big increase in throw values. The reason for this is likely that as information is lost towards the tip of the fault, fault cut-off lines might have been picked on the wrong reflector at the very end as large intervals make it hard to follow the same reflector.

T-D plots picked at 200, 400 and 800 m do not show the same trend. Picked at 200m it is skewed to the right and the throw minimum and maxima does not match that of denser picking strategies. The T-D plot for 400m has a big spike at 5000m along strike showing throw values of 70m. When picked at 800 m spacing, the deviation is around twice the size of deviation in other strategies (10-20m). The only trend possible to identify with such a large sampling interval is that throw values are generally larger in the middle of the fault. This might even lead to a conclusion of only one fault segment on false premises. A general trend is that the irregularity decreases with picking strategy until 400 m, but at 800 m it shoots back up. This is interpreted to be because the long increments between “guiding sections” when creating cutoff lines make makes it difficult to follow the correct seismic reflection consistently.

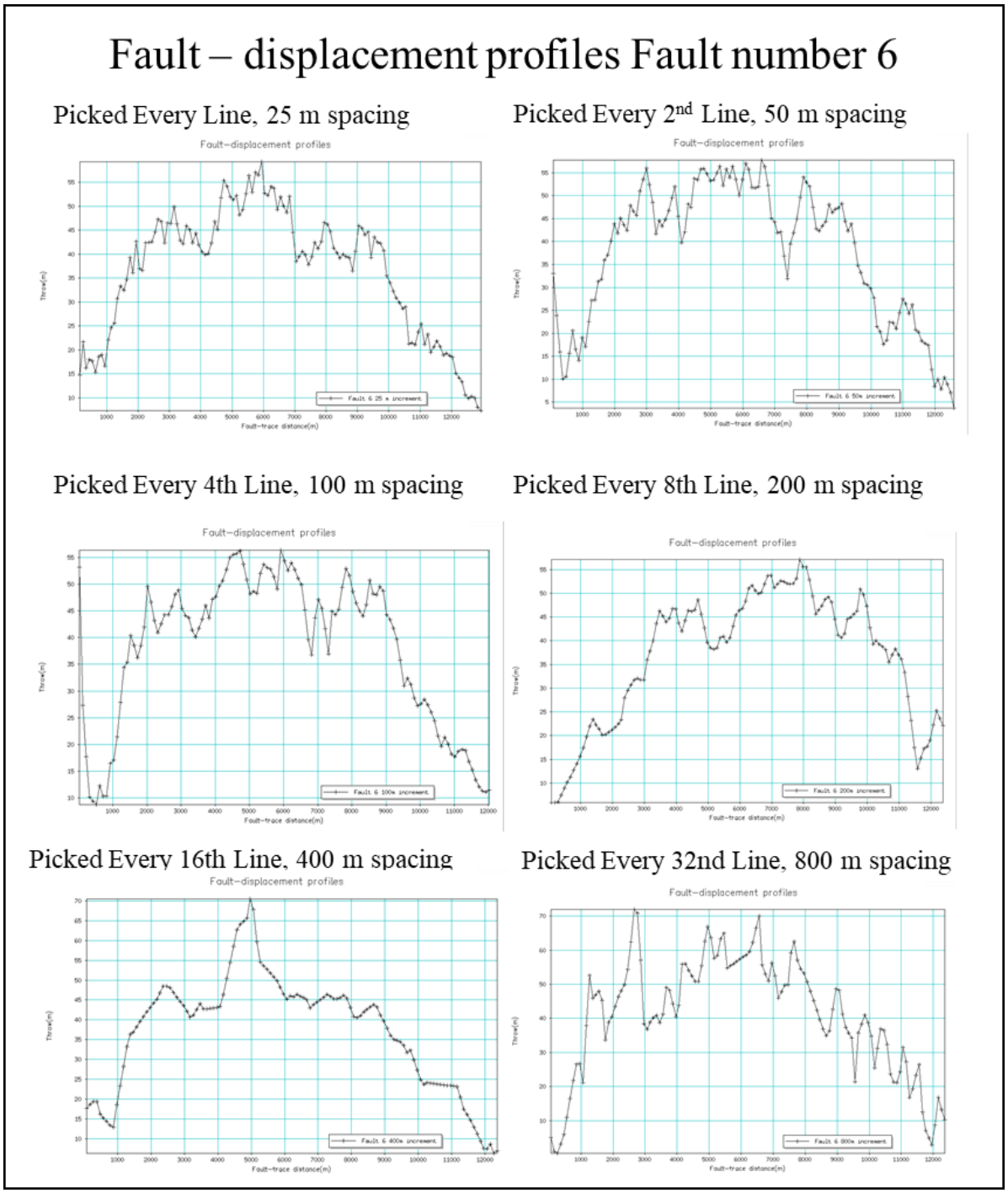

Figure 6.11 Presents T-D plots for all picking strategies on Fault 6

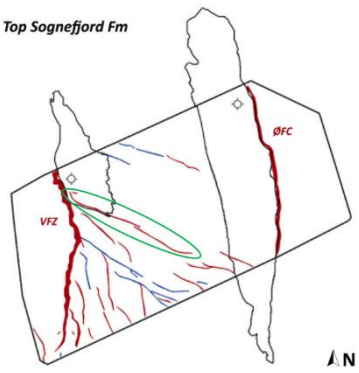

Figure 6.12 presents throw values plotted on the fault surface for all picking strategies. Picked at 25 m increments it is possible to identify the same throw minima as identified in the T-D plots. To see the northern most minimum a correlation with T-D plots makes it easier, while the southernmost throw minimum is more obvious also when looking at fault surfaces. Picked at 50 m and 100 intervals, the northern most throw minimum is no longer easily found (looking at top Sognefjord levels), but a small trend of lower values can be identified when looking for it. From figure xx it is clear that the maximum throw values are found deeper than the top Sognefjord Formation. Maximum throw values are observed close to the top Brent Group. At this depth it is easier to distinguish throw maxima and minima. For the three densest picking strategies throw values show the same trend at top Brent Gr. level as top Sognefjord Fm, but a bit more obvious.

Surfaces picked at 200- and 400-meter intervals show three maxima and two minimums when you look at top Brent Gr. levels. When picked at 800 meters interval, no trend is visible and throw plotted on the surface appears chaotic. This matches results from T-D plots where it is possible to identify segmentation at narrow increment spacing. When increments exceed 100m it is harder to identify (only possible at the depth of maximum throw), at 800m spacing no segmentation is possible to identify and results appears chaotic.

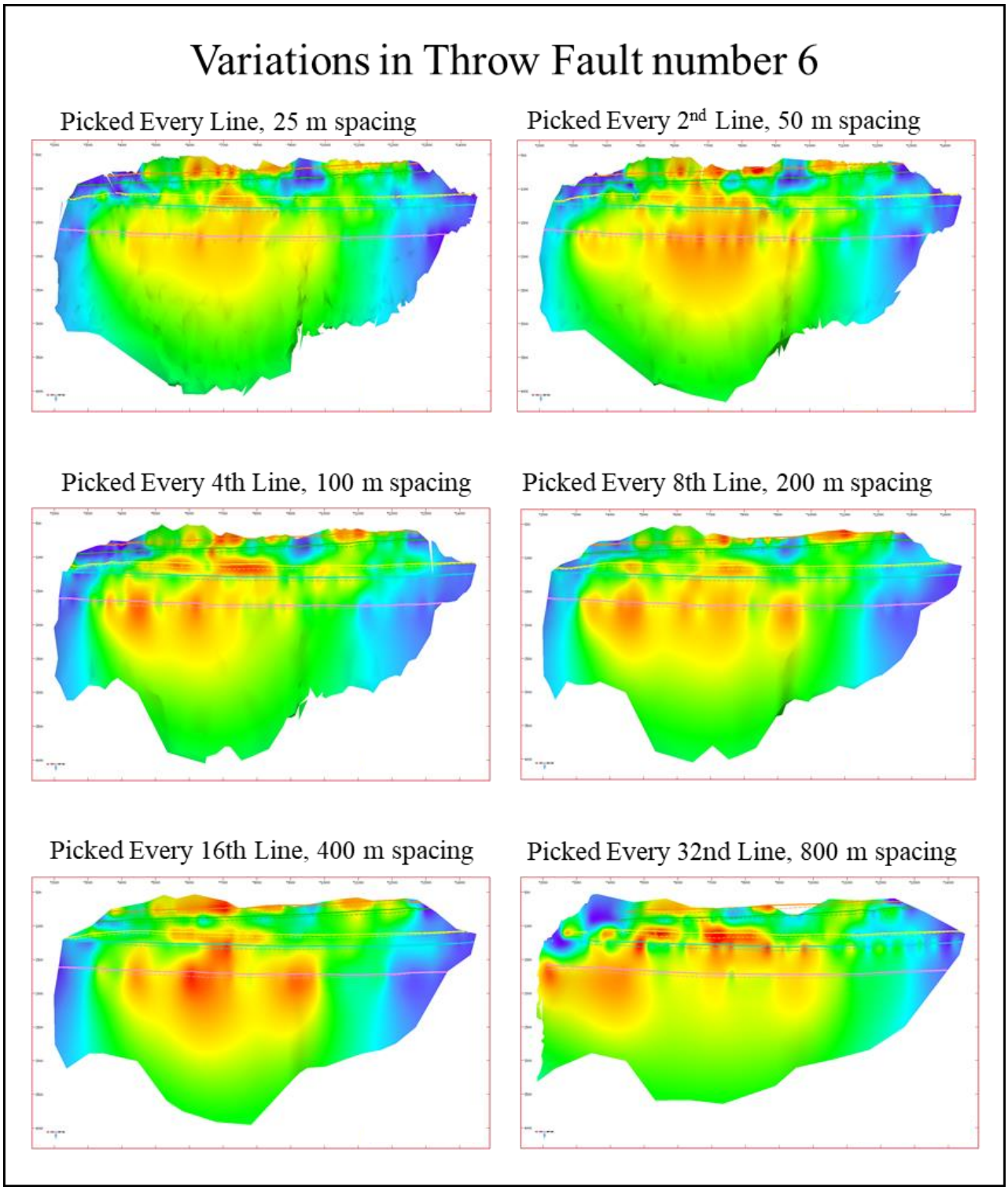

Shetland Gr Footwall
Shetland Gr Hanging wall
Cromer Knoll Gr Footwall
Cromer Knoll Gr Hanging wall
Draupne Fm Footwall
Draupne Fm Hanging wall
Sognefjord Fm Footwall
Sognefjord FM Hanging wall
Brent Gr Footwall
Brent Gr Hanging wall

Figure 6.12 Presents throw plotted on fault surfaces for all picking strategies for Fault 6

Strike

Figure 6.13 presents variations in strike for Fault 6. The colorbar is set to range from 180 to 360 degrees from north. Fault 6 generally shows values between 270 and 360 degrees. Picked at every inline, it is quite easy to see that strike varies a lot within short distances (color changes from green to blue). Overall the fault is oriented NW-SE. It is also possible to identify two areas of abrupt change in strike of the fault where it is oriented more N-S (where the color plotted on the fault is more blue than green).

Picked at 50 m interval, the same trend is visible, but the variability over short distances reduces. At 200m picking interval, the northernmost variation in strike is no longer possible to identify, while the southernmost variation is visible for all picking strategies.

As the variation in strike are at the same place as throw minima found in the T-D plots. This supports the results from T-D plots and throw plotted on the fault surface, Fault 6 is interpreted to consist of at least two fault segments connected at around 7500 m along strike where throw minima and variation is found. When picking at intervals of 25m, 50m and 100m, it is possible to identify throw and strike values that might indicate that the fault consists of three fault segments. Connected at throw minima and the subtle variation in strike at around 3000 m along strike. These subtle variations are lost when picking at larger intervals. Picking at 200 and 400 m intervals identified two fault segments, while picking at 800m interval lost all details necessary to make any meaningful interpretation of fault segmentation. Losing the possibility to contribute to the understanding of the fault growth history.

At shorter picking intervals a lot of fault plane rugosity is observable that does not correlate to fault segmentation observed in T-D plots. It is assumed that this can be either due to human error, making the fault surface “rougher” than in reality, or due to heterogeneous rock properties making the surface rough {Schöpfer, 2006 #68}. When picking at larger intervals this “smooths” the fault surface such that these corrugations over short distances are no longer visible. At 200m picking interval the surface appears smooth but the corrugation marking the fault segmentation identified in T-D plots is still visible. At 800m picking interval the whole fault seems to be straight with only a subtle change where southern segmentation was identified.

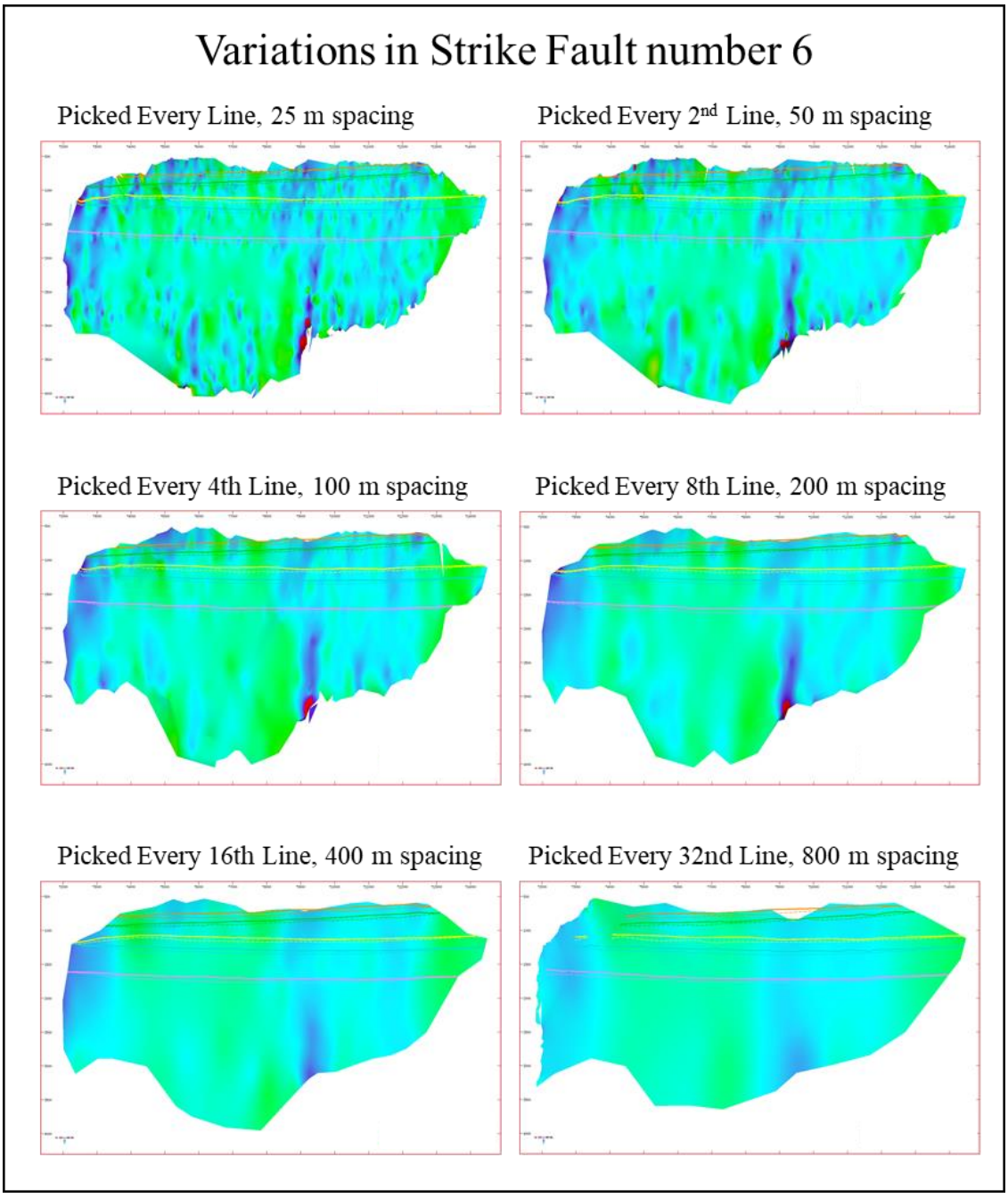

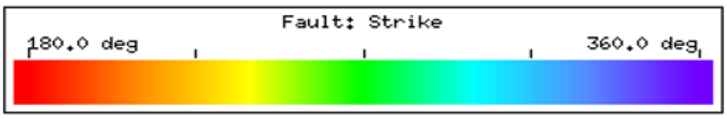

Shetland Gr Footwall
Shetland Gr Hanging wall
Cromer Knoll Gr Footwall
Cromer Knoll Gr Hanging wall
Draupne Fm Footwall
Draupne Fm Hanging wall
Sognefjord Fm Footwall
Sognefjord FM Hanging wall
Brent Gr Footwall
Brent Gr Hanging wall

Figure 6.13 Figure presents variations in strike draped on fault surfaces for all picking strategies on Fault 6.

6.3 Geomechanical modelling /fault reactivation

The fault stability is influenced by both external factors such as the in-situ stress conditions, and fault attributes such as strike and dip (see chapter 3, theory). In this study the focus has been to investigate how picking strategy influences the predicted fault stability. Keeping the stress model constant, the only variables are the fault attributes. In the Smeaheia study area the horizontal stress is isotropic, thus variation in strike does not impact the modeled stability. Changes in dip are therefore the main variable when assessing fault reactivation in this area. Note, the calculated fault stability is meant to highlight differences in picking strategy, not be used as final calculations for stability in the area.

6.3.1 Dilation tendency

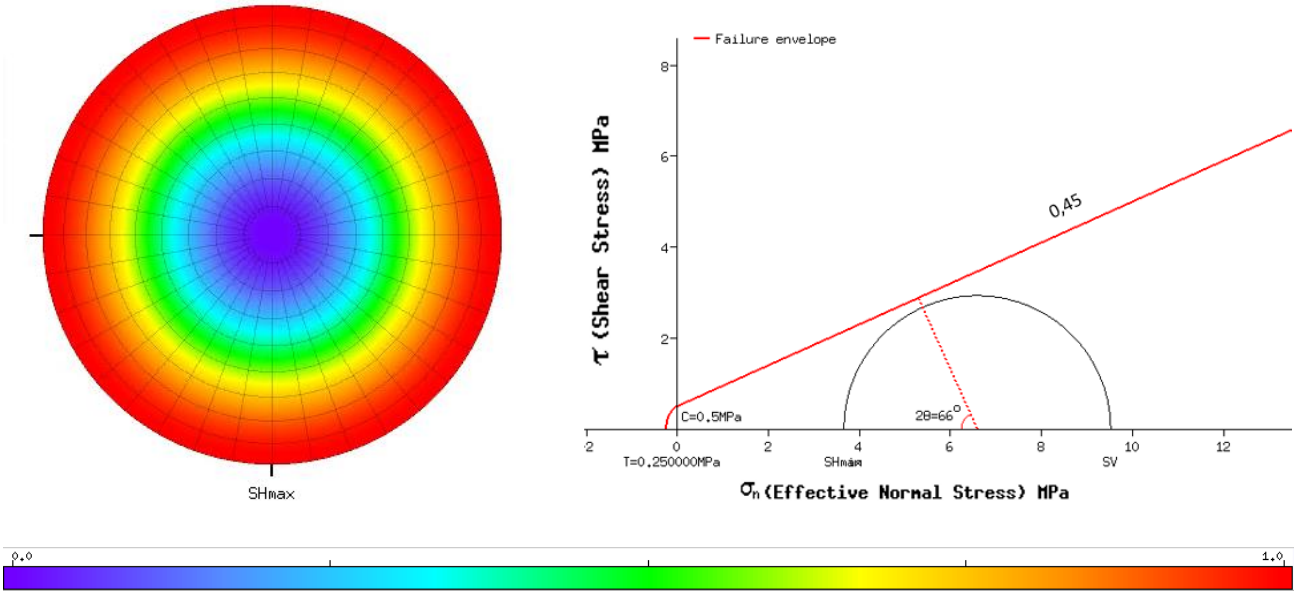

Figure 6.14 presents the dilation tendency for the stress scenario used in this study for the depth of the top Sognefjord Formation. It is presented on a lower hemisphere stereograph. On the right is the corresponding Mohr circle for dilation tendency at top Sognefjord Formation level.

Dilation tendency is calculated as a ratio between 0 and 1, where a higher number (closer to 1) represents a greater possibility of tensile failure. Figure 6.14 presents the dilation tendency for the stress scenario used in this study for the depth of the top Sognefjord Formation. It is presented on a lower hemisphere stereograph, and with the corresponding Mohr circle. The

stereograph clearly shows that as the horizontal stress is isotropic in this area, the magnitude of dip dictates the dilation tendency for a given depth. A horizontal fault has a dilation tendency of 0, while a vertical fault parallel to the maximum principal stress (σ_1) has a dilation tendency of 1. The dilation tendency increases as a fault gets steeper in this study.

6.3.2 **Slip tendency**

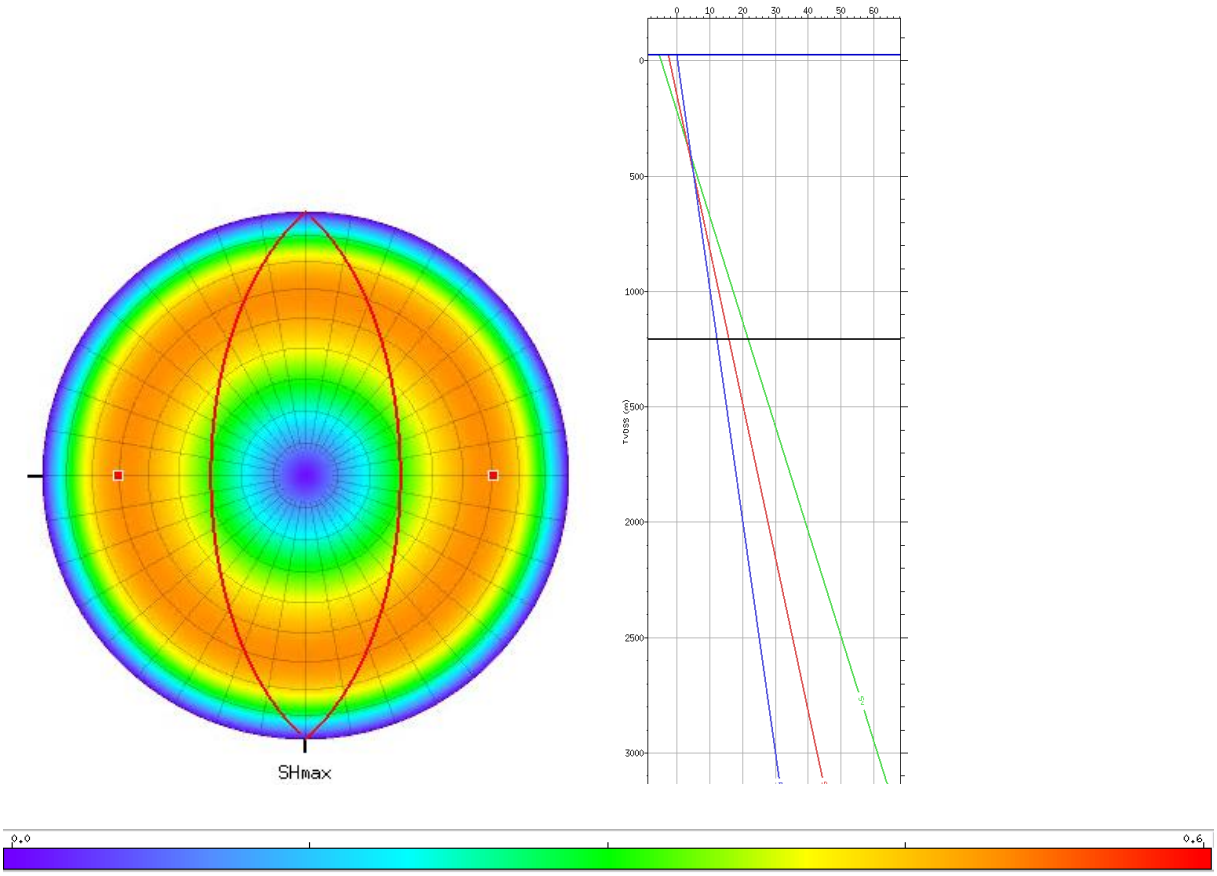

Figure 6.15 presents the Slip tendency for the stress scenario used in this study for the depth of the top Sognefjord Formation. It is presented on a lower hemisphere stereograph. On the right is the stress profile used for calculations, green line is σ_v, red line is σ_H and σ_h, blue line is pore pressure.

Slip tendency represents the likelihood of shear failure. Higher values indicate a higher chance of failure. Usually, the coefficient of static friction represents the value at which a fault will be critically stressed, in this study set as 0,6. For a normal faulting regime slip tendency will be highest at 60 degrees (see chapter 3). As the horizontal stress is isotropic variations in strike will not influence slip tendency in this study. Figure 6.15 presents the slip tendency at the top Sognefjord Formation, at 60 degrees the slip tendency is 0,5.

In the stress scenario used in this study the vertical stress σ_v increases with depth at a greater rate than the horizontal stress (σ_H and σ_h) (figure 6.15). Combining this with the formula for slip tendency ($Ts= \tau/\sigma_n$) means that as depth increases the slip tendency decreases. Figure 6.16 A presents a Mohr diagram for slip tendency at the depth of 850 m (top Shetland Group), while 6.16 B presents a Mohr diagram at 1240 m (top Sognefjord Formation). Note that the distance between the Mohr circle and the failure envelope has increased, which means that a greater increase in pore pressure is necessary to cause reactivation for the deeper part of the fault.

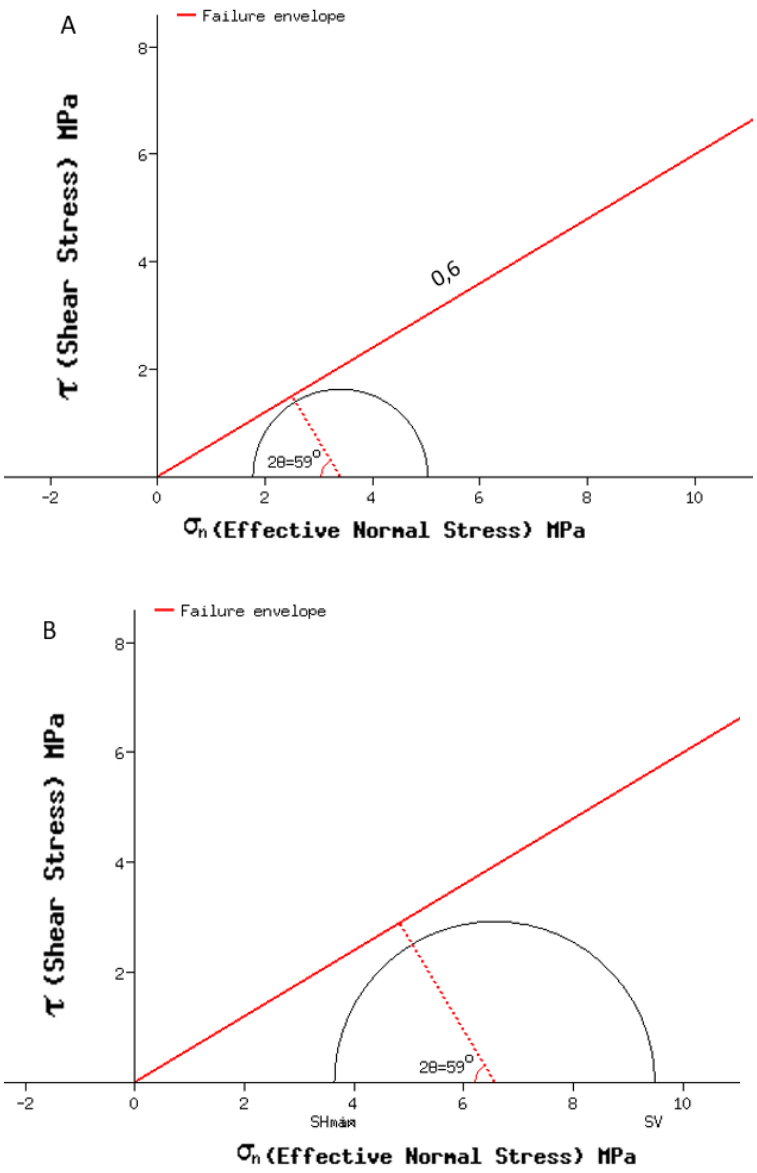

Figure 6.16 Figure 6.16 A presents a Mohr diagram for slip tendency at the depth of 850 m (top Shetland Group), while 6.16 B presents a Mohr diagram at 1240 m (top Sognefjord Formation)

6.3.3 Fracture stability

Figure 6.17 presents a projection of fracture stability on a lower hemisphere stereograph at top Sognefjord Formation depths. In this case dip at ~60 degrees give the highest chance of reactivation. Both a higher and lower dip angle will result in higher pore pressure needed to reactivate a fault. Figure xx presents fracture stability at top Shetland depth, comparing this top figure xxC we can see that as we get deeper very low- and very high dip values require a higher added pore pressure for reactivation, while dip values of 60 degrees requires a constant 0,5 MPa for reactivation. As the difference between the vertical stress σ_v and the horizontal stress (σ_H and σ_h) increases with depth near vertical and near horizontal faults gets more stable, while fracture stability on faults with a dip angle of around 60 degrees is not affected.

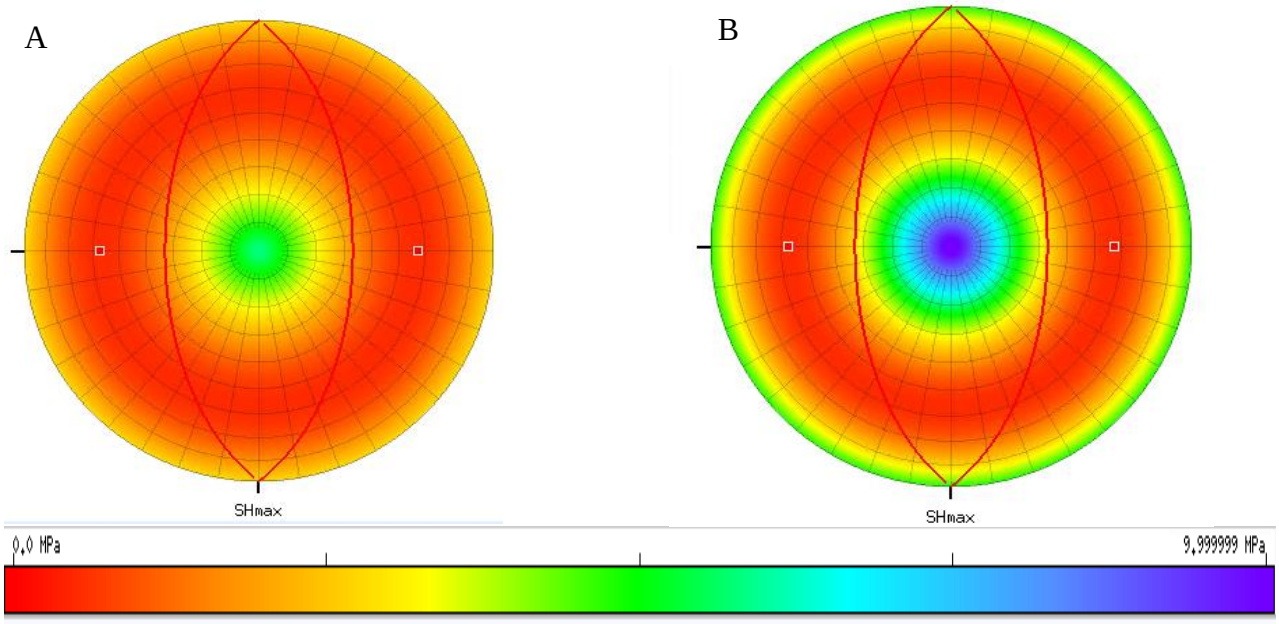

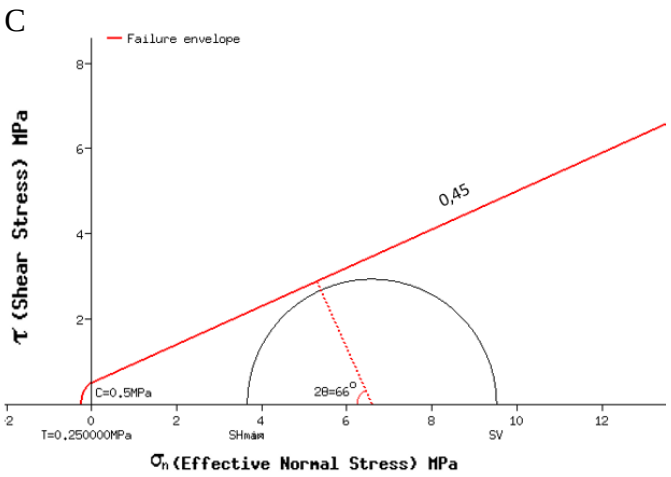

Figure 6.17 A) Present lower hemisphere stereograph of fracture stability at top Shetland depth (850 m). B) Presents lower hemisphere stereograph of fracture stability at top Sognefjord level. C) Presents Mohr circle for fracture stability at top Sognefjord level.

6.4 Dip

Figure 6.18, 6.19 and 6.20 presents the dilation tendency, slip tendency and fracture stability for all faults picked at every line (25m), every 4th line (100m) and every 32nd line (800m). All faults follow the same general trend of losing detail with increasing picking strategy and generally demonstrating fewer extreme high and low values. As an example, fault number 4 is described in detail, while all picking strategies for all faults are available in appendix A.

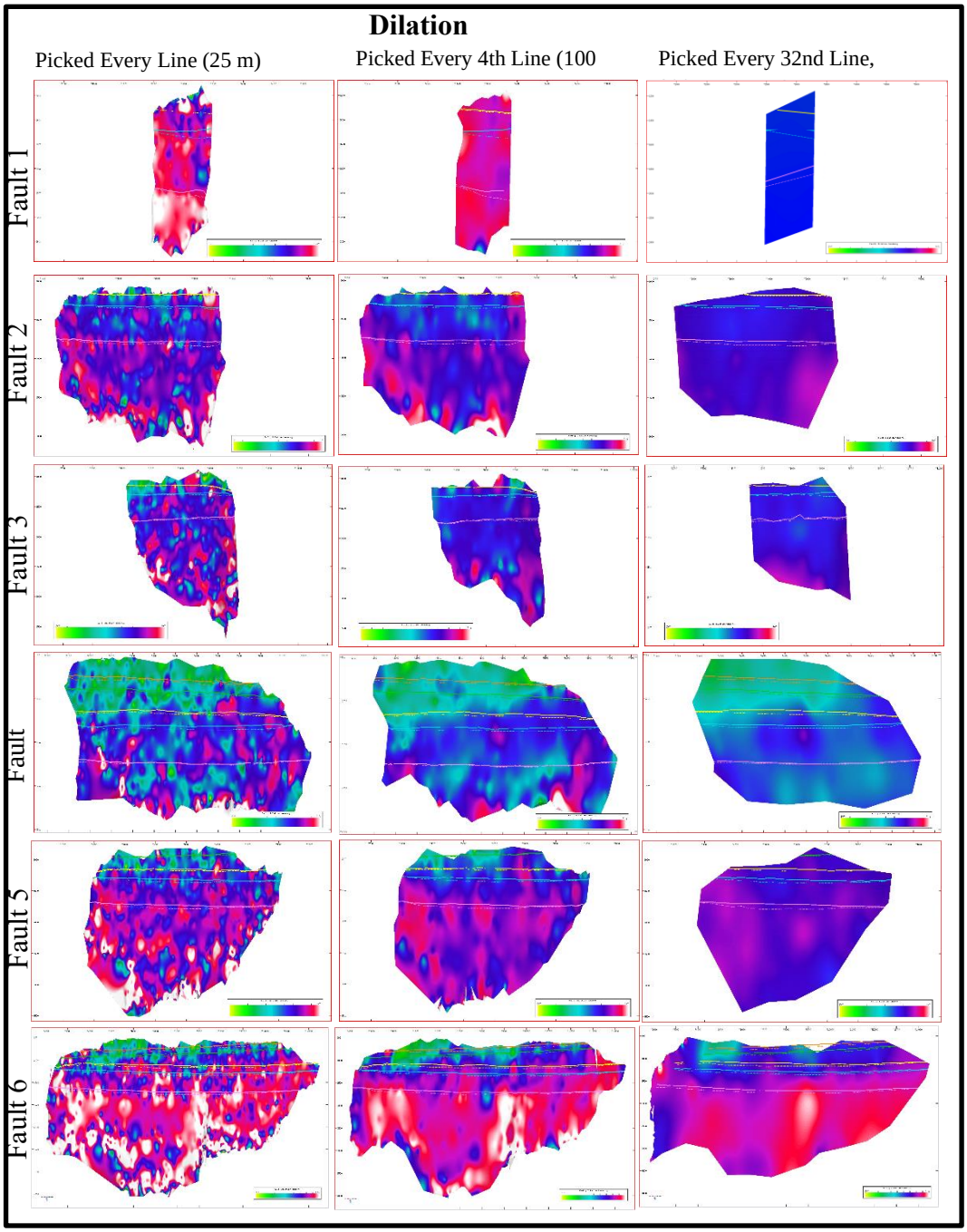

Figure 6.18 Presents dilation tendency for all faults

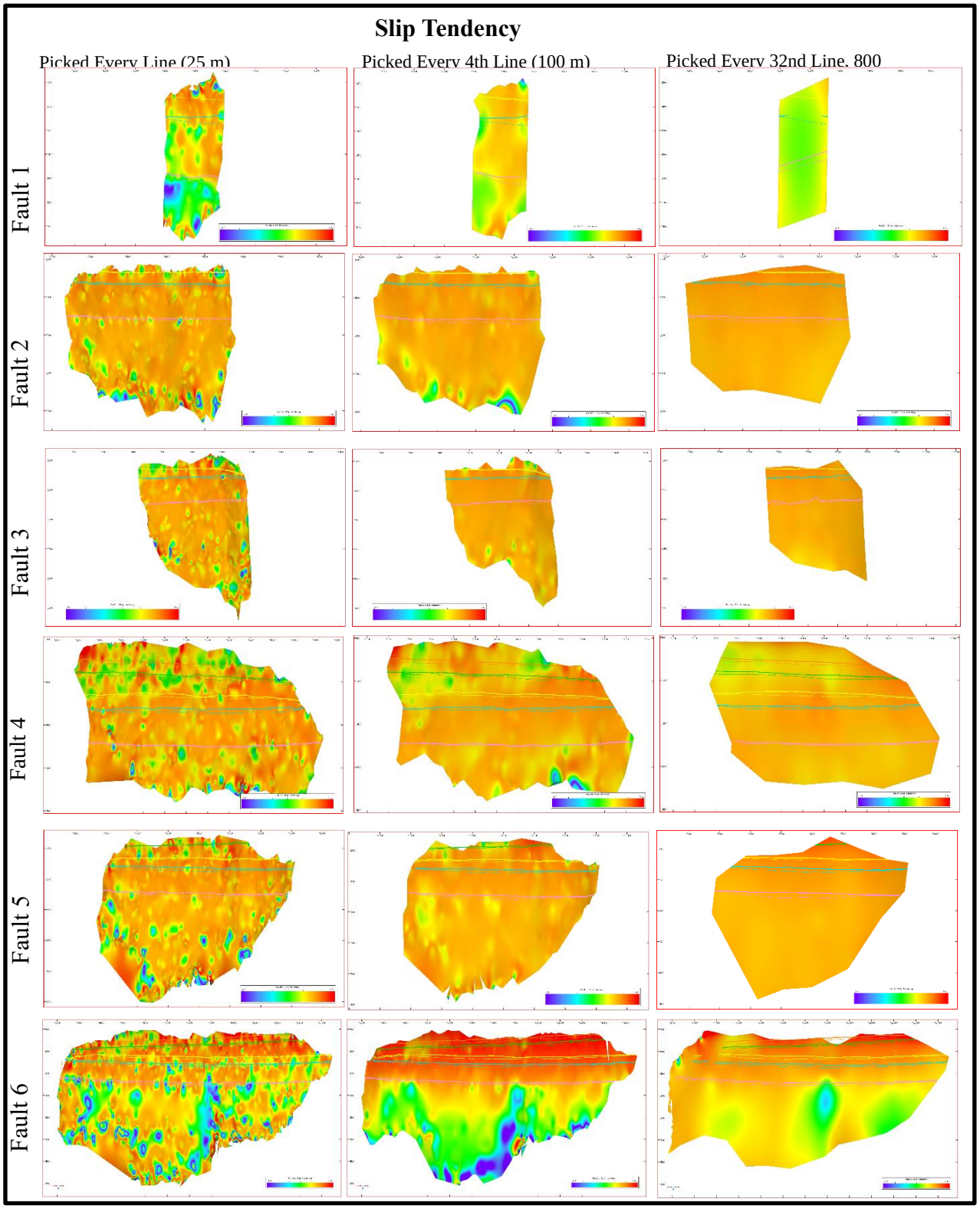

Figure 6.19 Presents slip tendency for all faults

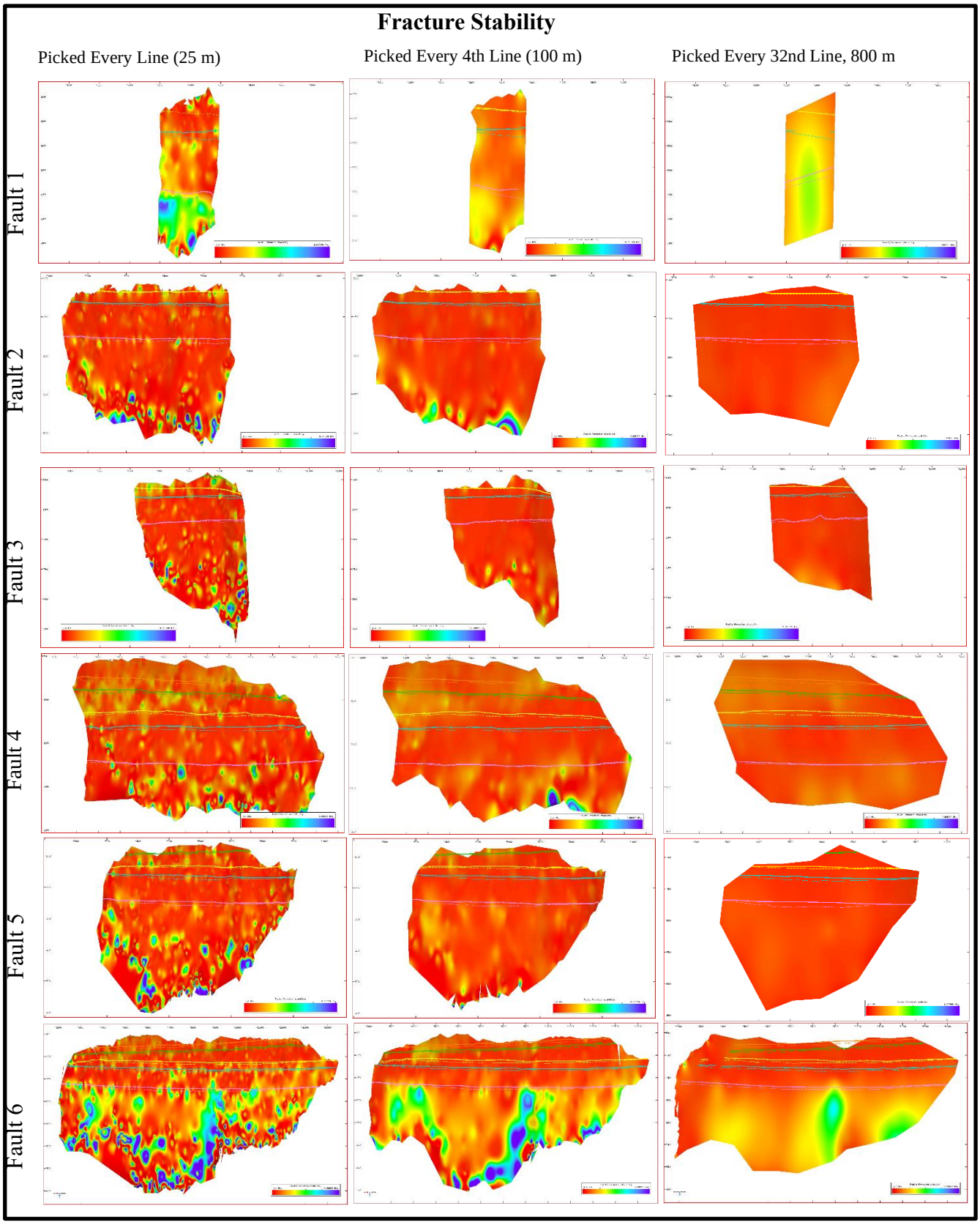

Figure 6.20 presents fracture stability for all faults

6.5 Fault 4

Figure 6.21 presents variation in dip on Fault 4 for all picking strategies. Picked at 25m intervals the top of the fault show dip values of 30 degrees with a few small areas with dip lower than 15 degrees. Deeper down, at around top Draupne Formation the fault becomes steeper with patches of areas that are steeper than 60 degrees. At these lower levels, there are still areas of less than 45 degrees. Looking at the fault picked at a 50 m spacing, it is still less steep in the top and steeper deeper than the Top-Draupne Formation. The few steep patches in the top third of the fault are almost gone. In the lower two thirds of the fault the southern part does not seem as steep as it does when picked at every line. In the northern part of the fault, steep areas are not as widespread that it is when picked at 25m intervals.

Picked at 100m interval the fault has very few steep areas and they are mostly restricted to the northern part of the fault. This trend is more obvious with increased increment spacing. At 800m interval the fault surface show almost no sign of ever being steeper than 45 degrees.

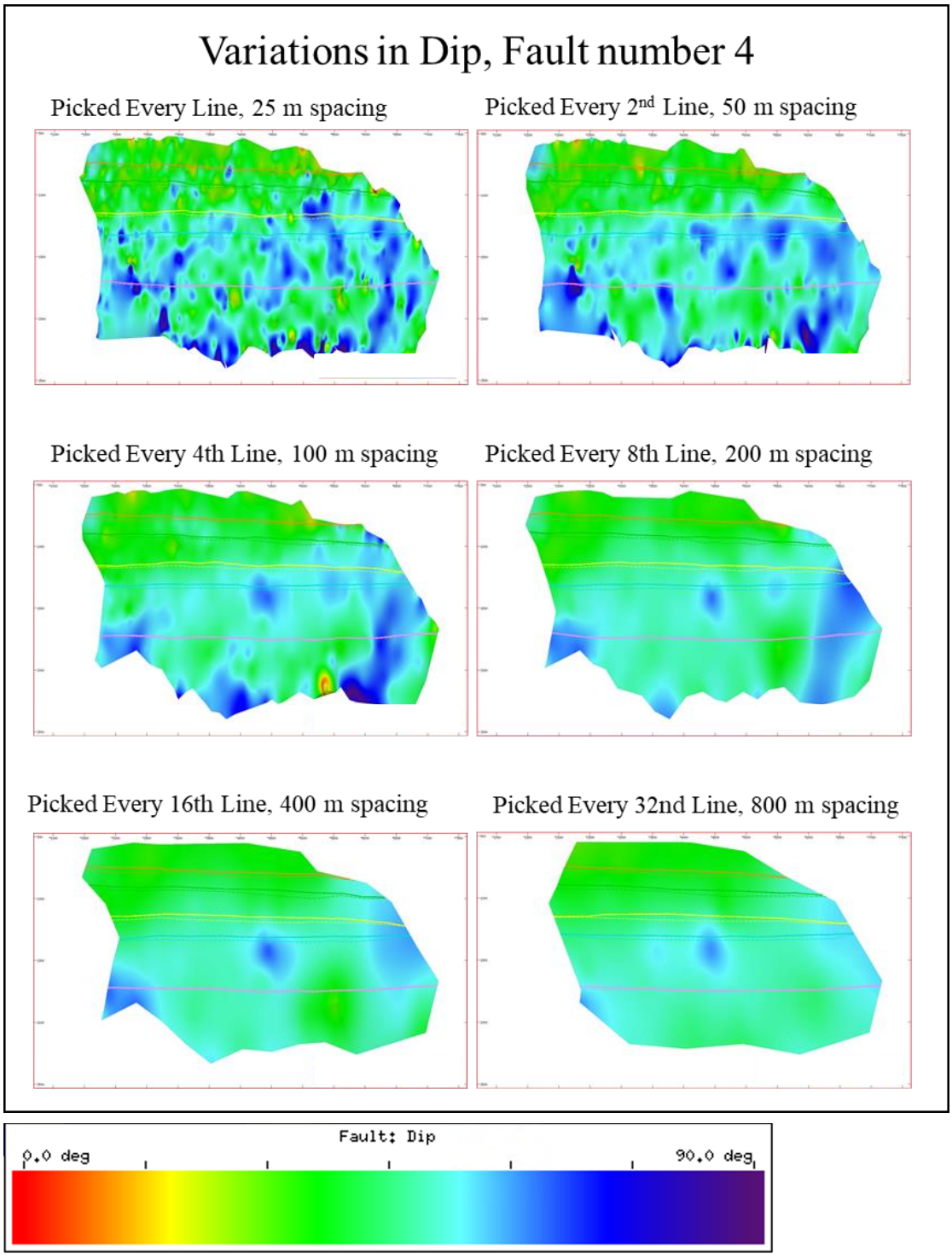

Figure 6.21 presents variation in dip for Fault 4

6.5.1 **Fault Stability**

As stated above, the variation in dip is the main variable in fault stability predictions in this study. When dip varies between picking strategies, so does the fault stability. Figure 6.22 show how fault stability varies between picking strategies for Fault 4. Picked at 25m intervals Fault 4 show a low dilation tendency (~0,3) in the flatter top part of the fault and higher values approaching 0,8 and 1,0 in the lower part. There is a clear pattern that shows that steep areas also have values of high dilation tendency. These high values represent high risks of reactivation. With increased sampling interval most of the high-risk areas disappear. At a sampling interval of 200m only a very small area in the middle, and an area to the northern part of the fault show values that exceeds the 0,8 criteria for failure. Picking at 800 m show a fault surface that does not have dilation tendency close to failure, while picking at closer intervals have many areas close to failure.

Slip tendency, which is dependent on the ratio between shear stress and normal stress acting on the surface is also highly dependent on dip in this study. It is usually represented as a value between 0 and 0,6 where 0,6 represent the coefficient of static friction. A higher value relates to a higher risk of shear failure (closer to the coefficient of static friction). Picked at 25m intervals the top part of the fault is altering between low values (0,3) and high values (close to 0,6). The rest of the fault show values between 0,3 and 0,45. Picking at 50 m increments the same trend is visible, but there are fewer and larger areas of altering high and low values. When picking strategies are further increased the high and low value spots gradually disappears and are replaced of middle values all over the fault. Picked at 800 m interval the whole fault has slip tendency values of 0,45.

When assessing fracture stability (FAST), which considers both shear failure and tensile failure, the predicted color plotted onto the fault represents the amount of added pore pressure required to put the fault into a critical stress state. In this study the pore pressure values should not be taken as absolute numbers for when the fault is going to reactivate, but rather highlight areas where the fault is more and less stable. In general, when every line is picked the fault is more stable at the top of the fault, while the bottom two thirds are generally close to failure, but with some local areas of greater stability. With increasing picking strategy, the stable areas decrease in size, and areas that are close to failure become more stable. This means that the “extreme” values (highs and lows) are averaged out. Thinking of fracture stability in this

study as a method of assessing areas of relative stability, means that the fault is interpreted as more stable with increasing picking strategy. In details, the areas that are most likely to reactivate first are no longer visible, as resolution is lost.

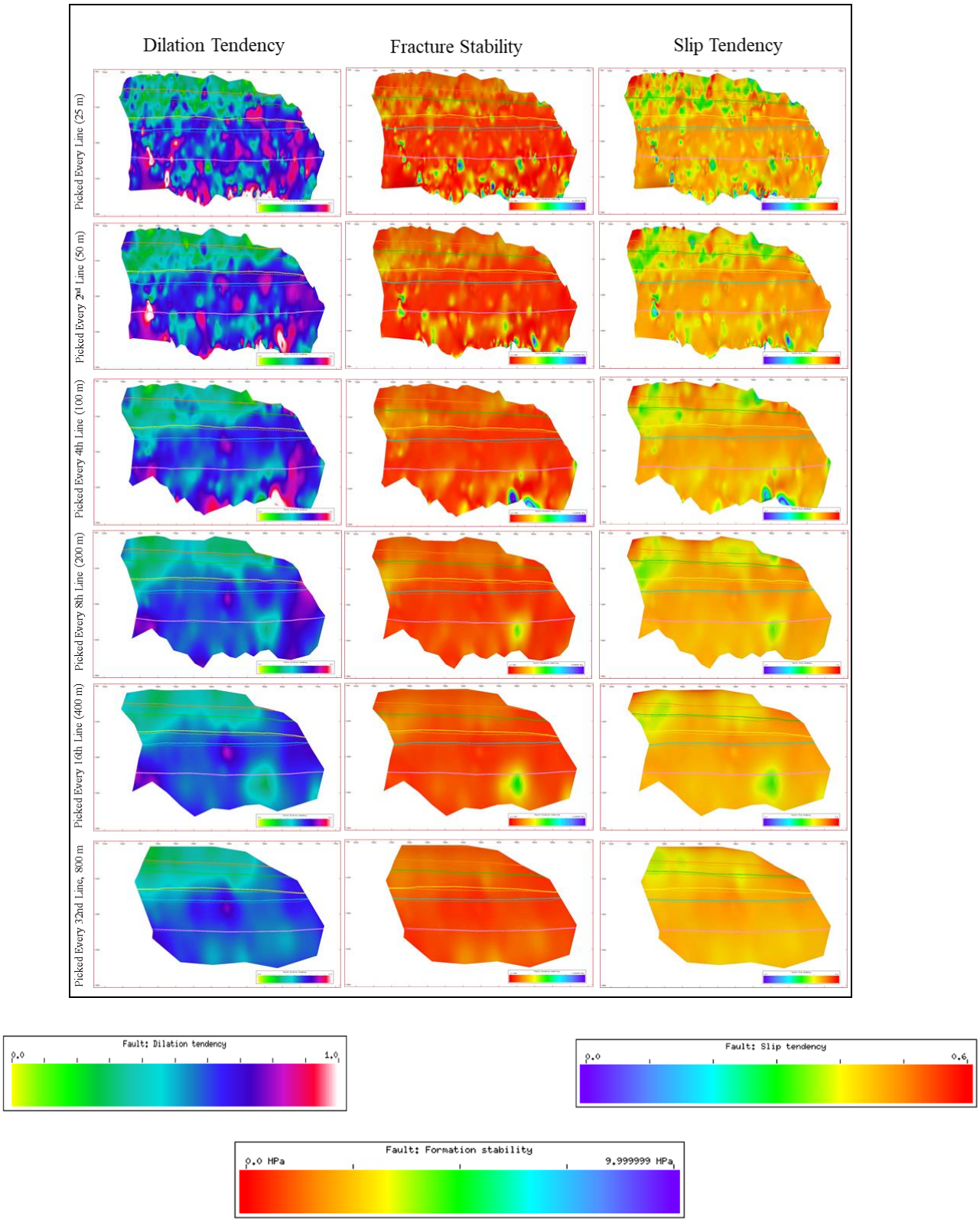

Figure 6.22 show how different picking strategies influence predicted fault reactivation potential.

7.0 Discussion

Several studies present the workflow and technics on how 2D and 3D seismic surveys are used to interpret faults in the subsurface (e.g., (Badley, 1985; Boult & Freeman, 2007; Yielding & Freeman, 2016; Michie et al., 2021)). Being used for fault growth analysis, across fault sealing analysis and fault reactivation potential, the creation of fault surfaces and fault cutoff lines are crucial when analyzing subsurface fluid flow, or the geomechanics of possible CO2 storage sites. However, the influence of sampling strategy on fault interpretation, and its impact on the resulting fault risk analyses, have received little attention until recently. In the last few years several published studies have proposed optimum picking strategies (Cunningham et al., 2020; Michie et al., 2021; Tao & Alves, 2019). While some results appear to be consistent in these studies (coarser picking strategies miss important details), the conclusions are not unanimous (no consensus on optimum picking strategy for different analysis). This case study investigates seismic scale faults ranging from 900 to 13 000m in length, and the results are discussed here in comparison with those of previous studies.

We show that picking strategy greatly influences the characteristics of faults (length, throw, strike, and dip), how this influences analysis of fault growth, the reactivation potential of these faults, and further how our results compare with previous studies. In a time of strict deadlines in industry, the optimum picking strategy would capture all important details within the fault, minimize human error and do this with as little time invested as possible.

7.1 Fault segmentation

In 2019 Tao and Alves presented an optimum picking strategy based on the total length of the fault. By looking at sub-seismic scale faults in Bristol, Great Britain, seismic faults in SE Brazil and a rift related fault (Ierapetra Fault Zone) in SE Crete, they propose a new parameter called “Sampling Interval/Fault Length Ratio” (δ). This parameter ensures that the longer the fault, the longer the sampling distance (sampling intervals on Ierapetra Fault Zone could be much larger than that of the cm scale faults of Bristol). They state that with no prior knowledge of fault segmentation, a δ-value of 0.05 should be applied. For faults longer than 3,5km in length the δ-value required is 0.03 (Tao & Alves, 2019). Table 7.1 summarizes what this means in terms of sampling interval for faults interpreted in this study.

Fault nr.	Fault 1	Fault 2	Fault 3	Fault 4	Fault 5	Fault 6
Length	930 m	4446 m	3830 m	5232 m	6483 m	12 934 m
δ-parameter	0.05	0.03	0.03	0.03	0.03	0.03
Suggested sampling interval	47 m	134 m	114 m	156 m	195 m	388 m

Table 7.1: The table presents suggested sampling intervals based on the δ-parameter presented by Tao and Alves (2019).

Michie et al. (2021) investigates the optimum picking strategy for the Vette Fault Zone, which is approximately 50 km long. This would have resulted in a sampling interval of up to 1500 m, using the strategy proposed by Tao and Alves (2019). However, even when looking at only the 14 km inside the study area (corresponding to picking interval of minimum 420 m) this led to overly smoothed surfaces and was not able to identify all fault segmentation found within the study. To capture all necessary information while also smoothing out any irregularities caused by human error or poor seismic resolution, Michie et al. (2021) propose an optimum picking interval of 100 m for the Vette Fault Zone.

The results of Cunningham et al. (2020) show that picking strategies with more than 200 m spacing were insufficient to capture critical details such as fault length and relay ramps. They also acknowledge that it was difficult to capture the entire length of the fault if using more than 50 m spacing. Based on their study of the Snøhvit field in the Barents Sea, they recommend that in the main body of the fault should be picked at least every 100 or 200 m, and when approaching fault tips or complex fault intersection to decrease picking interval to maximum 50 m.

Following the δ-value suggested by Tao and Alves (2019) a sampling interval of 134 m would have been sufficient to capture fault segmentation on Fault 2, as a sampling interval of 200 m was able to identify a throw minimum in this study. On Fault 4 the suggested sampling interval of 156 m sits right between the interval (100m) that was able to identify a small throw minimum and the first that was not (200 m). The suggested sampling interval could be just enough to capture this important detail. On Fault 6 on the other hand the suggested sampling

interval of 388m would have been too coarse to capture any important variations in throw vs. distance. On this fault the maximum sampling interval able to identify segmentation was 100 m.

These results are in agreement with those of Michie et al. (2021), who found that a suggested sampling interval of 420 m (based on the δ-value presented by Tao and Alves (2019)) was not sufficient to capture all details within their study of the Vette Fault Zone. The sampling interval of 100 m suggested by Michie et al. (2019) would however be exactly the interval necessary to identify all details and fault segmentation also in this study.

Looking at the suggested picking strategy by Cunningham et al. (2020) of 100 or 200 m, one should opt for the densest strategy as 200 m would not have identified all details within this study. An important observation made by Cunningham et al. (2020) was that coarser picking strategies loose important details near fault tips. Table 6.1 summarizes fault characteristics of all picking strategies, and highlights a key result of different picking strategies, fault length. With increasing picking strategy, we can also see that information is lost towards the tips of the faults. From 25 m intervals to 800 m intervals there is a reduction in total length of Fault 3 by 870 m. Excluding the tips of the faults might also exclude some of the most important detail, as it is crucial to understand how the faults interact with nearby faults. To capture the entire length of the fault we therefore recommend that when approaching the tip of the fault picking intervals are decreased to capture the maximum extend of the fault within the seismic resolution, also stated by Cunningham et al. (2020). This can be done by simply decreasing the sampling interval until the last segment of the fault is interpreted and does not necessarily have to be related to picking strategy used for the main body of the fault.

While Tao and Alves (2019) suggested a sampling interval based on fault length, results from our study show that for faults large enough to require a reduced δ- value from 0.05 to 0.03, the suggested intervals were too coarse to capture all important information. However, the T-D plot from Fault 1 suggests that smaller faults might lose details with picking at 100 m suggested by Michie et al. (2021). Picking at 25m intervals reveals small variations in throw values across the fault which might indicate a breached relay ramp (if they are in fact real geologic features and not a product of human error/seismic quality). These variations are not found with coarser picking strategies. It is also easy to imagine that faults on a sub seismic scale will not get meaningful interpretations when sampled at 100 m intervals.

I recommend that when interpreting faults smaller than ~3500m (the point at which the δ-parameter suggest 100 m sampling interval), the sampling interval based on fault length suggested by Tao and Alves (2019) should be followed when interpreting for fault segmentation/fault growth analysis. At a certain fault length this interval becomes so wide that important irregularities and details are lost. Based on this study and the studies of Cunningham et al. 2020 and Michie et al. (2021) it appears that this limit is at a sampling interval of 100 m. Faults ranging from 3,5km to more than 50 km should be interpreted with 100 m as a maximum sampling interval. As information towards fault tips are missing for every sampling strategy coarser than 25m, all faults should be interpreted with a strategy close to vertical seismic resolution at fault tips. Note that there is "always" a sub-seismic part of the fault missing in seismic data and faults are in fact even longer than that shown by the densest picking strategy available (Hemingway et al., 2013).

7.2 Fault reactivation

As horizontal stresses in the area are isotropic the fault attribute that effects the reactivation potential the most in this study is dip. Throughout the study results show that the densest picking strategies show bulls-eye pattern of dip variation, while coarser strategies smooths over these areas. This results in overall more stable faults with coarser picking strategies, as small areas of high risk are smoothed over. It also results in very stable areas being smoothed over, but this does not impact the overall stability of the fault that much as unstable areas are going to reactivate before areas showing medium stability.

The smoothing of fault surfaces can potentially lead to areas with high potential for reactivation being missed. However, the nature of the difficulty being consistent from one segment to the other is apparent picking the fault. Dip variation over short distances might be a result of human error and not a result of geologic features.

In the field, faults are often observed with highly irregular surfaces (e.g. (Childs et al., 1997; Peacock & Xing, 1994)) However, irregularities must be larger than the seismic resolution to cause any meaningful interpretation of geologic features. A fault surface honoring irregularities found within the seismic survey will most likely be smoother than the real fault.

Michie et al. (2021) attributed the bulls-eye pattern of dip found in their study to be caused by human error and triangulation method, producing severely uneven fault surfaces despite rigorous QC. Figure 7.1 show how fault surfaces (of the Vette Fault Zone) created by Michie et al. (2021) is affected by picking strategy. Because of this they proposed a line spacing of 100 m to smooth out irregularities made by human error, but still be able to capture fault details. They point out that this suggested line spacing is specific for their case study as it likely to be different for varying sized faults, different tectonic regimes, fault complexity and seismic resolution (Michie et al., 2021).

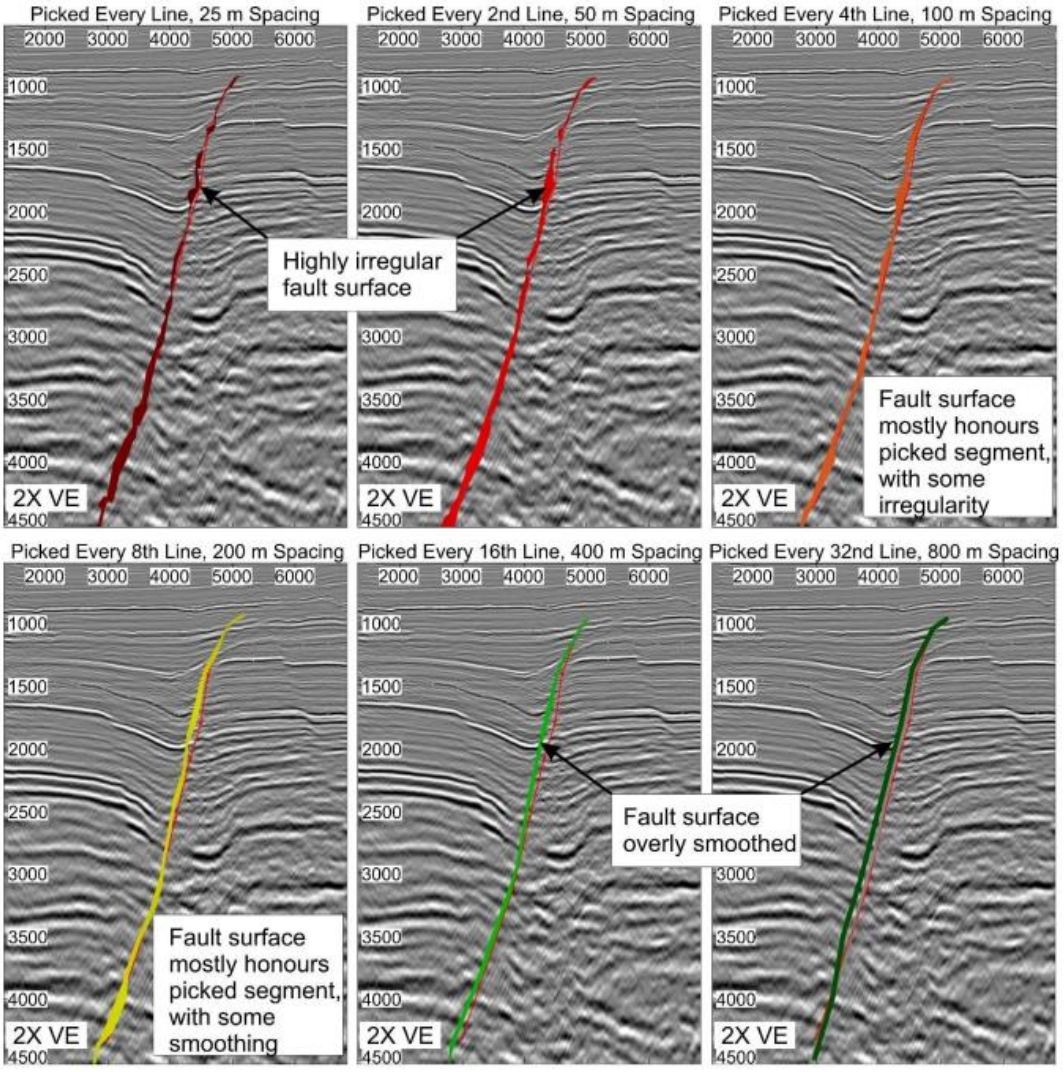

Figure 7.1 Presents how fault surfaces are affected by picking strategy. Note that when picked at 25 m and 50 m intervals the fault surfaces are highly irregular but when picking intervals surpasses 100m fault surfaces are smoothed, not honoring picked segments. The fault picked is the Vette Fault Zone, figure from Michie et al. (2021).

However, if irregularities are not a product of human error but of geologic features the strategy suggested by Michie et al. (2021) would underestimate the reactivation potential leading to false assumptions regarding prospect of CO2 storage. Tao and Alves (2019) also investigate how slip tendency is influenced by picking strategy. They assumed that fault surfaces picked at the shortest intervals (12,5m) represent the most accurate slip tendency. Tao and Alves find that the magnitude of slip tendency decreases with coarser picking strategies. When coarser strategies are used fault surface becomes so smooth that the slip tendency is underestimated (Tao & Alves, 2019). Tao and Alves (2019) suggest that for slip tendency picking strategy should reach maximum data resolution. Meaning that for seismic interpretation every line should be interpreted, and for field-based studies LIDAR technology is favorable. Cunningham (2020) does not investigate implication for fault reactivation.

In this study we find similar results as both Michie et al. (2021) and Tao and Alves (2019). Faults are most prone to reactivation when picked at every line, and with increasing picking strategy areas of high and low reactivation potential is smoothed out. Fault surfaces picked at every line show bulls-eye pattern with small areas representing extreme reactivation risk, however in the case of reactivation larger parts of the fault would likely reactivate and the presentation of only small parts of the fault being prone to reactivation would be wrong (Michie et al., 2021).

It is important to note that in another stress regime where the horizontal stresses are not isotropic, variations in strike would also affect the reactivation potential. Similar results are found on variations of strike as variations in dip within this study (although not effecting reactivation in this case). Picking at maximum resolution results in strike variations over short distances, while coarser picking strategies smoothens the surfaces resulting in average values over larger areas.

The recommendation of optimum picking strategy comes down to the level of human error and the resolution of the seismic survey. Optimum picking strategy captures all available detail within the resolution of the data, while also smooths out human error. Because of this, human error and the effect of seismic resolution is discussed further. For this case study we see that bulls-eye patches of extreme dilation tendency, slip tendency and fracture stability is removed at a sampling interval of 100 m. This is therefore the recommended picking strategy, but we also acknowledge that this strategy might lose some detail that can be present within the data resolution, if not overshadowed by human error.

7.3 Seismic resolution and human error

Alcalde et al. (2017) documents how seismic quality impact the interpretation uncertainty. They find that areas of low contrast and continuity corresponds to a greater range of interpreted fault geometries, leading to changes in fault geometrics such as throw or heave. Faleide et al. (2021) also documented that different interpreters chose to interpret faults differently, possibilities could be in the hanging wall side, in the middle or in the footwall side of the fault, resulting in different fault geometry. Prior knowledge based on geological concepts and biases such as availability bias, anchoring bias and confirmation bias greatly influences interpretation, (Bond et al., 2007; Shipton et al., 2020). Bond (2015) document that because of the limited resolution and spatial distribution of seismic surveys, field data and borehole data, significant uncertainties occur in the interpretation to create a geological model. Highlighting areas of uncertainty is important in the process of making geological sound models.

Besides the possibility of human error when assessing reactivation potential, described over, a major uncertainty in this study has been the seismic resolution being close to variations in throw values in T-D plots. All faults picked at 25 m intervals show variations in throw over short distances with an amplitude of 5-10 m. Variations in throw used to identify fault segmentation are from 10 – 25 m, and the vertical resolution in the GN1101 seismic study is approximately 15 m. Figure 7.2 shows the picking of the Sognefjord Formation hanging wall guided by a seismic section. Highlighted is an example of how only a few millimeters on computer screen translates to multiple meters in the T-D plot. If the cut-off line by mistake was picked at the lower of the two points this would result in a throw value 9 m larger than what the top point result in. The difficulty in being consistent between seismic sections result in uneven throw values not made by geologic features but by human error despite rigorous QC.

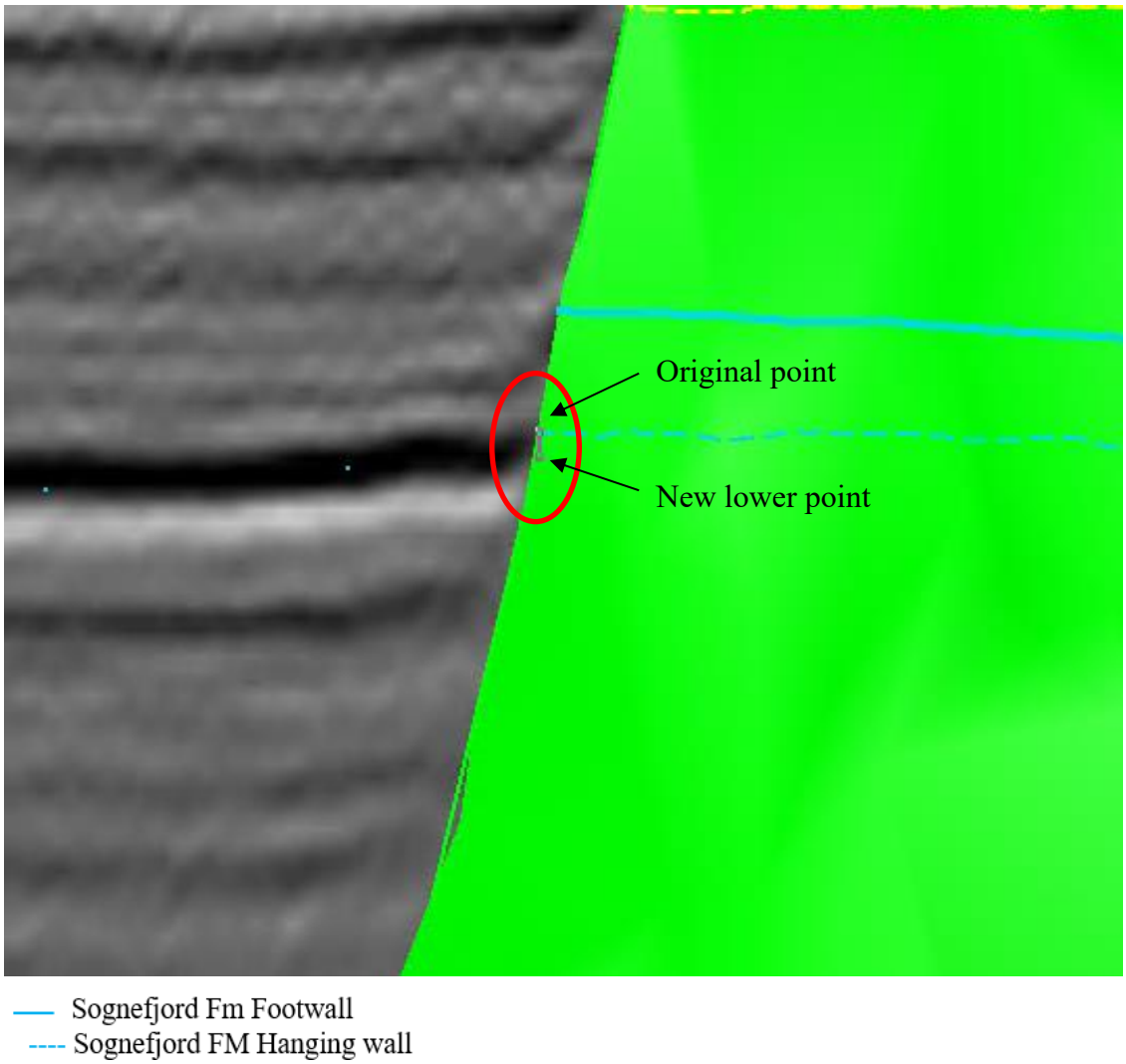

Figure 7.2 show the picking of the Sognefjord Formation hanging wall guided by a seismic section. Highlighted are two points, if picked at the lower of the two points it would result in a 9m variation in throw values.

When the picking strategy is increased this smoothens out both T-D plots and fault surfaces, and the optimum picking strategy will be a balance between capturing all geological details, but also smoothing out irregularities made by human error and seismic resolution.

Time spent picking each segment and the amount of QC being performed also alters the interpretations. More detail is added when extra time is available (Michie et al., 2021).

7.4 Implications of picking strategy on CO2 storage at Smeaheia

We have documented how picking strategy influences throw-distance profiles and variations in strike. This has major implications in fault geometry and will further have implication on fault segmentation analysis. Areas of soft-linked relay zones can act as conduits to fluid flow (e.g. (Peacock & Sanderson, 1994; Rotevatn et al., 2009; Trudgill & Cartwright, 1994)) and the intensity of fractures and deformation bands are higher in areas where faults interact (e.g.(Peacock & Sanderson, 1994; Shipton et al., 2005)). Understanding how CO_2 flow in the sub surface is crucial when assessing the possibilities of the Smeaheia area as a possible CO_2 storage site. Choosing a picking strategy with intervals larger than 100 m will lead to areas of fault segmentation being missed and the understanding of CO_2 migration within the Smeaheia CCS site lacks important details. At fault tips however one should decrease the picking interval so that the last visible trace of the fault is picked. We show that choosing a coarse strategy can lead to hundreds of the total fault length being lost, these lost parts of the faults are near the tips. Faults missing substantial parts of the length does not portray the sub surface in a realistic matter and assumptions made based on this strategy could be miss leading. As this is not a very time-consuming methodology and the added details are substantial, we recommend that picking strategies are decreased near fault tips to the resolution of the seismic survey.

A 100 m line spacing will also ensure that when assessing human error that is not possible to avoid due to seismic resolution and the nature of picking line to line is smoothed out, while the general geometry of the fault is still preserved. Faults in this are fund to be close to failure, which indicated that little added pressure by CO_2 could lead to reactivation and increased fluid flow up sections. It is, however, very important to note that changing fault rock properties used in this study will alter the predicted reactivation potential. Values used for cohesion and frictional coefficient are based on previous estimates rather than measurements (Meng et al., 2017). Changing rock properties would alter the predicted stability of the faults. However, this study focuses on how sampling strategy impact reactivation potential and not on the exact values at the Smeaheia site.

The rugosity of a fault planes observed in the field is high, by the nature of seismic surveys, irregularities smaller than the seismic resolution will not be visible in seismic. This means that fault surfaces that honor the seismic data are a lot smoother than that of the real fault

plane. One could argue that the addition of rugosity through human error and triangulation methods with very dense picking strategies could simulate the rugosity found in nature, making seismic fault surfaces more geologically “realistic”. However, the amount of irregularities that should be added to a specific fault would be unknow, and the adding of additional roughness would be plane guessing. Finding sub seismic-scales areas of high reactivation risk would possibly not be very important anyway as the fault is not likely to reactivate at a fraction of the fault size. It is also hard to see how such a small reactivation could contribute to the increased fluid flow up section.

Further research should focus on other areas, other tectonic regimes and if possible investigate how seismic resolution impact calculated reactivation potential.

8.0 Conclusion

To be able to upscale CCS to a level that has an impact on the goals set by the United Nations in the Paris agreement and by the European Commission we are dependent of a very good understanding of the subsurface storage prospects. We need good predictions on how CO2 injected will migrate within the storage unit (and hopefully not out of the storage unit), and to monitor the process we need to understand the predicted pore pressure buildup. When de-risking a CO2 storage prospect, the interpretation of faults is of great importance. Faults greatly impact fluid flow, acting as conduits to flow or it can work as baffles/barriers. Further faults can also be reactivated leading to up section CO_2 flow.

This study show that the picking strategy (sampling interval) used greatly affects throw - distance profiles, impacting fault growth analysis, and the calculated reactivation potential.

- If the picking strategy is to coarse throw – distance profiles was not able to identify all fault segmentation found within the study.
- A picking strategy with 100 m intervals was the coarsest strategy able to identify all fault segments found in the study.
- At fault tips one should opt to use the densest possible picking strategy allowed by the seismic resolution to capture the full resolvable fault length.
- Increased sampling intervals leads to more stable fault surfaces. However, human error causes densely picked fault surfaces to be highly irregular, not honoring the seismic data. 100 m picking intervals are recommended to smooth out irregularities made by human error when assessing fault reactivation potential.

9.0 References

Allan, U. S. (1989). Model for hydrocarbon migration and entrapment within faulted structures. *AAPG bulletin*, *73*(7), 803-811.

Andersen, O., & Sundal, A. (2021). Estimating Caprock Impact on CO2 Migration in the Gassum Formation Using 2D Seismic Line Data. *Transport in Porous Media*, *138*(2), 459-487.

Andersen, T. B., & Jamtveit, B. (1990). Uplift of deep crust during orogenic extensional collapse: A model based on field studies in the Sogn-Sunnfjord region of western Norway. *Tectonics*, *9*(5), 1097-1111.

Andrews, J., Fintland, T., Helstrup, O., Horsrud, P., & Raaen, A. (2016). Use of unique database of good quality stress data to investigate theories of fracture initiation, fracture propagation and the stress state in the subsurface. 50th US Rock Mechanics/Geomechanics Symposium,

Badley, M., Price, J., Dahl, C. R., & Agdestein, T. (1988). The structural evolution of the northern Viking Graben and its bearing upon extensional modes of basin formation. *Journal of the Geological Society*, *145*(3), 455-472.

Badley, M. E. (1985). Practical seismic interpretation.

Bartholomew, I., Peters, J., & Powell, C. (1993). Regional structural evolution of the North Sea: oblique slip and the reactivation of basement lineaments. Geological Society, London, Petroleum Geology Conference Series,

Bell, R. E., Jackson, C. A. L., Whipp, P. S., & Clements, B. (2014). Strain migration during multiphase extension: Observations from the northern North Sea. *Tectonics*, *33*(10), 1936-1963.

Bolle, L. (1992). Troll Field: Norway's Giant Offshore Gas Field: Chapter 28.

Bond, C. E. (2015). Uncertainty in structural interpretation: Lessons to be learnt. *Journal of Structural Geology*, *74*, 185-200.

Bond, C. E., Gibbs, A. D., Shipton, Z. K., & Jones, S. (2007). What do you think this is?``Conceptual uncertainty''in geoscience interpretation. *GSA today*, *17*(11), 4.

Boult, P., & Freeman, B. (2007). Using faults as an aid to horizon mapping in areas of poor 2D seismic: Otway Basin example. *MESA Journal*, *46*, 4-9.

Brown, A. R. (2011). *Interpretation of three-dimensional seismic data*. Society of Exploration Geophysicists and American Association of Petroleum ….

Brudy, M., & Kjørholt, H. (2001). Stress orientation on the Norwegian continental shelf derived from borehole failures observed in high-resolution borehole imaging logs. *Tectonophysics*, *337*(1-2), 65-84.

Cartwright, J. A., Trudgill, B. D., & Mansfield, C. S. (1995). Fault growth by segment linkage: an explanation for scatter in maximum displacement and trace length data from the Canyonlands Grabens of SE Utah. *Journal of Structural Geology*, *17*(9), 1319-1326.

Childs, C., Walsh, J., & Watterson, J. (1997). Complexity in fault zone structure and implications for fault seal prediction. In *Norwegian petroleum society special publications* (Vol. 7, pp. 61-72). Elsevier.

Childs, C., Watterson, J., & Walsh, J. (1995). Fault overlap zones within developing normal fault systems. *Journal of the Geological Society*, *152*(3), 535-549.

Christiansson, P., Faleide, J., & Berge, A. (2000). Crustal structure in the northern North Sea: an integrated geophysical study. *Geological Society, London, Special Publications*, *167*(1), 15-40.

Clausen, J., Gabrielsen, R., Reksnes, P., & Nysaether, E. (1999). Development of intraformational (Oligocene–Miocene) faults in the northern North Sea: influence of remote stresses and doming of Fennoscandia. *Journal of Structural Geology*, *21*(10), 1457-1475.

Commission, E. (2018). *Communication from the commission to the European parliament, the European Council, the Council, the European economic and social committee, the committee of th regions and the European investment Bank. A Clean planet all.* .

Copestake, P., Sims, A., Crittenden, S., Hamar, G., Ineson, J., Rose, P., Tringham, M., Evans, D., Graham, C., & Armour, A. (2003). The Millennium Atlas: petroleum geology of the central and northern North Sea. Geological Society of London,

Coward, M. (1995). Structural and tectonic setting of the Permo-Triassic basins of northwest Europe. *Geological Society, London, Special Publications*, *91*(1), 7-39.

Coward, M., Dewey, J., Hempton, M., Holroyd, J., & Mange, M. (2003). Tectonic evolution. 17-33. *Evans, D., Graham, C., Armour, A. & Bathurst, P.(eds & co-ordinators): The Millennium Atlas: Petroleum geology of the central and northern North Sea. The Geological Society of London, London*.

Cowie, P. (1998). A healing–reloading feedback control on the growth rate of seismogenic faults. *Journal of Structural Geology*, *20*(8), 1075-1087.

Cowie, P. A., & Scholz, C. H. (1992). Displacement-length scaling relationship for faults: data synthesis and discussion. *Journal of Structural Geology*, *14*(10), 1149-1156.

Cowie, P. A., & Shipton, Z. K. (1998). Fault tip displacement gradients and process zone dimensions. *Journal of Structural Geology*, *20*(8), 983-997.

Cowie, P. A., Underhill, J. R., Behn, M. D., Lin, J., & Gill, C. E. (2005). Spatio-temporal evolution of strain accumulation derived from multi-scale observations of Late Jurassic rifting in the northern North Sea: A critical test of models for lithospheric extension. *Earth and Planetary Science Letters*, *234*(3-4), 401-419.

Cunningham, J., Cardozo, N., Townsend, C., & Callow, R. (2020). The impact of seismic interpretation methods on the analysis of faults: A case study from the Snøhvit field, Barents Sea. *Solid Earth Discussions*, *2020*, 1-48.

Davies, R., O'donnell, D., Bentham, P., Gibson, J., Curry, M., Dunay, R., & Maynard, J. (1999). The origin and genesis of major Jurassic unconformities within the triple junction area of the North Sea, UK. Geological Society, London, Petroleum Geology Conference series,

Davies, R. J., Turner, J., & Underhill, J. R. (2001). Sequential dip-slip fault movement during rifting: a new model for the evolution of the Jurassic trilete North Sea rift system. *Petroleum Geoscience*, *7*(4), 371-388.

Davies, R. J., Turner, J., & Underhill, J. R. (2001). Sequential dip-slip fault movement during rifting: a new model for the evolution of the Jurassic trilete North Sea rift system. *Petroleum Geoscience*, *7*(4), 371-388.

Davies, S., Dawers, N. H., McLeod, A., & Underhill, J. R. (2000). The structural and sedimentological evolution of early synrift successions: the Middle Jurassic Tarbert Formation, North Sea. *Basin Research*, *12*(3-4), 343-365.

Deegan, C., & Scull, B. (1977). A standard lithostratigraphic nomenclature for the Central and Northern North Sea.

Deng, C., Fossen, H., Gawthorpe, R. L., Rotevatn, A., Jackson, C. A., & FazliKhani, H. (2017). Influence of fault reactivation during multiphase rifting: The Oseberg area, northern North Sea rift. *Marine and Petroleum Geology*, *86*, 1252-1272.

Dreyer, T., Whitaker, M., Dexter, J., Flesche, H., & Larsen, E. (2005). From spit system to tide-dominated delta: integrated reservoir model of the Upper Jurassic Sognefjord Formation on the Troll West Field. Geological Society, London, Petroleum Geology Conference series,

Eidvin, T., Riis, F., & Rasmussen, E. S. (2014). Oligocene to Lower Pliocene deposits of the Norwegian continental shelf, Norwegian Sea, Svalbard, Denmark and their relation to the uplift of Fennoscandia: A synthesis. *Marine and Petroleum Geology*, *56*, 184-221.

Eidvin, T., & Rundberg, Y. (2007). Post-Eocene strata of the southern Viking Graben, northern North Sea; integrated biostratigraphic, strontium isotopic and lithostratigraphic study. *Norwegian Journal of Geology/Norsk Geologisk Forening*, *87*(4).

Energy, N. M. o. P. a. (2019). *Melding til Stortinger 33, Langskip - Fangst og lagring av CO2*.

Energy, N. M. o. P. a. (2019-2020). *Langskip - fangst og lagring av CO2*. Oslo

Faleide, J. I., Bjørlykke, K., & Gabrielsen, R. H. (2015). Geology of the Norwegian continental shelf. In *Petroleum Geoscience* (pp. 603-637). Springer.

Faleide, J. I., Bjørlykke, K., & Gabrielsen, R. H. (2015). Geology of the Norwegian continental shelf. In *Petroleum Geoscience* (pp. 603-637). Springer.

Ferrill, D. A., Stamatakos, J. A., & Sims, D. (1999). Normal fault corrugation: Implications for growth and seismicity of active normal faults. *Journal of Structural Geology*, *21*(8-9), 1027-1038.

Ferrill, D. A., Stamatakos, J. A., & Sims, D. (1999). Normal fault corrugation: Implications for growth and seismicity of active normal faults. *Journal of Structural Geology*, *21*(8-9), 1027-1038.

Forsberg, C., Plank, S., Tjelta, T., Svano, G., Strout, J., & Svensen, H. (2007). Formation of pockmarks in the Norwegian Channel. Offshore Site Investigation and Geotechnics: Confronting New Challenges and Sharing Knowledge,

Fossen, H. (2016). *Structural geology*. Cambridge university press.

Fossen, H., & Dunlap, W. J. (1999). On the age and tectonic significance of Permo-Triassic dikes in the Bergen-Sunnhordland region, southwestern Norway. *Norsk Geologisk Tidsskrift*, *79*(3), 169-178.

Færseth, R. (1996). Interaction of Permo-Triassic and Jurassic extensional fault-blocks during the development of the northern North Sea. *Journal of the Geological Society*, *153*(6), 931-944.

Færseth, R., & Ravnås, R. (1998). Evolution of the Oseberg fault-block in context of the northern North Sea structural framework. *Marine and Petroleum Geology*, *15*(5), 467-490.

Gabrielsen, R. (1984). Long-lived fault zones and their influence on the tectonic development of the southwestern Barents Sea. *Journal of the Geological Society*, *141*(4), 651-662.

Gabrielsen, R. H. (1989). Reactivation of faults on the Norwegian continental shelf and its implications for earthquake occurrence. In *Earthquakes at North-Atlantic passive margins: neotectonics and postglacial rebound* (pp. 67-90). Springer.

Gabrielsen, R. H., Kyrkjebø, R., Faleide, J. I., Fjeldskaar, W., & Kjennerud, T. (2001). The Cretaceous post-rift basin configuration of the northern North Sea. *Petroleum Geoscience*, *7*(2), 137-154.

Gee, D., & Fossen, H. (2008). Henriksen. N. & Higgins, AK *From the early Paleozoic platforms of Baltica and Laurentia to the Caledonide orogen of Scandinavia and Greenland. Episodes*, *31*(1), 44-51.

Hillis, R., & Nelson, E. (2005). In situ stresses in the North Sea and their applications: Petroleum geomechanics from exploration to development. Geological Society, London, Petroleum Geology Conference series,

Holden, N. (2021). *Structural characterization and across-fault seal assessment of the Aurora CO2 storage site*

Isaksen, D., & Tonstad, K. (1989). *A revised Cretaceous and Tertiary lithostratigraphic nomenclature for the Norwegian North Sea*. Norwegian Petroleum Directorate.

Jackson, C. A.-L., Bell, R. E., Rotevatn, A., & Tvedt, A. B. (2017). Techniques to determine the kinematics of synsedimentary normal faults and implications for fault growth models. *Geological Society, London, Special Publications*, *439*(1), 187-217.

Klemperer, S. L. (1988). Crustal thinning and nature of extension in the northern North Sea from deep seismic reflection profiling. *Tectonics*, *7*(4), 803-821.

Kyrkjebø, R., Gabrielsen, R., & Faleide, J. (2004). Unconformities related to the Jurassic–Cretaceous synrift–post-rift transition of the northern North Sea. *Journal of the Geological Society*, *161*(1), 1-17.

Lervik, K., Spencer, A., & Warrington, G. (1989). Outline of Triassic stratigraphy and structure in the central and northern North Sea. In *Correlation in hydrocarbon exploration* (pp. 173-189). Springer.

Mansfield, C., & Trudgill, B. (1996). The growth of normal faults by segment linkage. *Geol. Soc. Lond. Spec. Publ.*, *99*, 163-177.

Meng, L., Fu, X., Lv, Y., Li, X., Cheng, Y., Li, T., & Jin, Y. (2017). Risking fault reactivation induced by gas injection into depleted reservoirs based on the heterogeneity of geomechanical properties of fault zones. *Petroleum Geoscience*, *23*(1), 29-38.

Michie, E. A., Mulrooney, M. J., & Braathen, A. (2021). Fault interpretation uncertainties using seismic data, and the effects on fault seal analysis: a case study from the Horda Platform, with implications for CO 2 storage. *Solid Earth*, *12*(6), 1259-1286.

Mondol, N. H. (2010). Seismic Exploration. In K.Bjørlykke (Ed.), *Petroleum Geoscience* (Vol. 1, pp. 375-402). Springer-Verlag https://doi.org/10.1007/978-3-642-02332-3_17

Morris, A., Ferrill, D. A., & Henderson, D. B. (1996). Slip-tendency analysis and fault reactivation. *Geology*, *24*(3), 275-278.

Morris, A., Ferrill, D. A., & Henderson, D. B. (1996). Slip-tendency analysis and fault reactivation. *Geology*, *24*(3), 275-278.

Mulrooney, M. J., Osmond, J. L., Skurtveit, E., Faleide, J. I., & Braathen, A. (2020). Structural analysis of the Smeaheia fault block, a potential CO2 storage site, northern Horda Platform, North Sea. *Marine and Petroleum Geology*, *121*, 104598.

Norton, M. G. (1987). The Nordfjord-Sogn Detachment, W. Norway. *Norsk Geologisk Tidsskrift*, *67*(2), 93-106.

Nottvedt, A., Gabrielsen, R., & Steel, R. (1995). Tectonostratigraphy and sedimentary architecture of rift basins, with reference to the northern North Sea. *Marine and Petroleum Geology*, *12*(8), 881-901.

Odinsen, T., Reemst, P., Van Der Beek, P., Faleide, J. I., & Gabrielsen, R. H. (2000). Permo-Triassic and Jurassic extension in the northern North Sea: results from tectonostratigraphic forward modelling. *Geological Society, London, Special Publications*, *167*(1), 83-103.

Ottesen, D., Batchelor, C., Dowdeswell, J., & Løseth, H. (2018). Morphology and pattern of Quaternary sedimentation in the North Sea Basin (52–62 N). *Marine and Petroleum Geology*, *98*, 836-859.

Peacock, D., & Sanderson, D. (1991). Displacements, segment linkage and relay ramps in normal fault zones. *Journal of Structural Geology*, *13*(6), 721-733.

Peacock, D. C., & Sanderson, D. J. (1994). Geometry and development of relay ramps in normal fault systems. *AAPG bulletin*, *78*(2), 147-165.

Peacock, D. C. P., & Xing, Z. (1994). Field examples and numerical modelling of oversteps and bends along normal faults in cross-section. *Tectonophysics*, *234*(1-2), 147-167.

Phillips, T. B., Fazlikhani, H., Gawthorpe, R. L., Fossen, H., Jackson, C. A. L., Bell, R. E., Faleide, J. I., & Rotevatn, A. (2019). The influence of structural inheritance and multiphase extension on rift development, the NorthernNorth Sea. *Tectonics*, *38*(12), 4099-4126.

Reynolds, J. M. (2011). *An Introduction to Applied and Enviromental Geophysics*. Wiley-Blackwell.

Reynolds, J. M. (2011). *An introduction to applied and environmental geophysics*. John Wiley & Sons.

Roberts, A., Yielding, G., Kusznir, N., Walker, I., & Dorn-Lopez, D. (1993). Mesozoic extension in the North Sea: constraints from flexural backstripping, forward modelling and fault populations. Geological Society, London, Petroleum Geology Conference series,

Rotevatn, A., Jackson, C. A.-L., Tvedt, A. B., Bell, R. E., & Blækkan, I. (2019). How do normal faults grow? *Journal of Structural Geology*, *125*, 174-184.

Rotevatn, A., Tveranger, J., Howell, J., & Fossen, H. (2009). Dynamic investigation of the effect of a relay ramp on simulated fluid flow: geocellular modelling of the Delicate Arch Ramp, Utah. *Petroleum Geoscience*, *15*(1), 45-58.

Rundberg, Y., Olaussen, S., & Gradstein, F. (1995). Incision of Oligocene strata; evidence for northern North Sea Miocene uplift and key to the formation of the Utsira sands. *Geonytt*, *22*, 62.

Røe, S. L., & Steel, R. (1985). Sedimentation, sea-level rise and tectonics at the Triassic-Jurassic boundary (Statfjord Formation), Tampen Spur, northern North Sea. *Journal of Petroleum Geology*, *8*(2), 163-186.

Schlische, R. W. (1995). Geometry and origin of fault-related folds in extensional settings. *AAPG bulletin*, *79*(11), 1661-1678.

Schöpfer, M. P., Childs, C., & Walsh, J. J. (2006). Localisation of normal faults in multilayer sequences. *Journal of Structural Geology*, *28*(5), 816-833.

Sejrup, H. P., Aarseth, I., Haflidason, H., & Løvlie, R. (1996). Quaternary of the Norwegian Channel: glaciation history and palaeoceanography. *Oceanographic Literature Review*, *8*(43), 791.

Shipton, Z., Evans, J., & Thompson, L. (2005). The geometry and thickness of deformation-band fault core and its influence on sealing characteristics of deformation-band fault zones.

Shipton, Z. K., Roberts, J. J., Comrie, E., Kremer, Y., Lunn, R., & Caine, J. (2020). Fault fictions: Systematic biases in the conceptualization of fault-zone architecture. *Geological Society, London, Special Publications*, *496*(1), 125-143.

Skurtveit, E., Choi, J. C., Osmond, J., Mulrooney, M., & Braathen, A. (2018). 3D fault integrity screening for Smeaheia CO2 injection site. 14th Greenhouse Gas Control Technologies Conference Melbourne,

Steel, R. (1993). Triassic–Jurassic megasequence stratigraphy in the Northern North Sea: rift to post-rift evolution. Geological Society, London, Petroleum Geology Conference series,

Tao, Z., & Alves, T. M. (2019). Impacts of data sampling on the interpretation of normal fault propagation and segment linkage. *Tectonophysics*, *762*, 79-96.

Ter Voorde, M., Færseth, R., Gabrielsen, R., & Cloetingh, S. (2000). Repeated lithosphere extension in the northern Viking Graben: a coupled or a decoupled rheology? *Geological Society, London, Special Publications*, *167*(1), 59-81.

Tomasso, M., Underhill, J. R., Hodgkinson, R. A., & Young, M. J. (2008). Structural styles and depositional architecture in the Triassic of the Ninian and Alwyn North fields: Implications for basin development and prospectivity in the Northern North Sea. *Marine and Petroleum Geology*, *25*(7), 588-605.

Trudgill, B., & Cartwright, J. (1994). Relay-ramp forms and normal-fault linkages, Canyonlands National Park, Utah. *Geological Society of America Bulletin*, *106*(9), 1143-1157.

Vollset, J., & Doré, A. G. (1984). *A revised Triassic and Jurassic lithostratigraphic nomenclature for the Norwegian North Sea*. Oljedirektoratet.

Walsh, J. J., & Watterson, J. (1988). Analysis of the relationship between displacements and dimensions of faults. *Journal of Structural Geology*, *10*(3), 239-247.

Whipp, P., Jackson, C. L., Gawthorpe, R., Dreyer, T., & Quinn, D. (2014). Normal fault array evolution above a reactivated rift fabric; a subsurface example from the northern Horda Platform, Norwegian North Sea. *Basin Research*, *26*(4), 523-549.

Wrona, T., Magee, C., Jackson, C., Huuse, M., & Taylor, K. (2017). Kinematics of polygonal fault systems: Observations from the northern North Sea: Frontiers of Earth Science, v. 5, 101. In.

Wu, L., Thorsen, R., Ottesen, S., Meneguolo, R., Hartvedt, K., Ringrose, P., & Nazarian, B. (2021). Significance of fault seal in assessing CO2 storage capacity and containment risks–an example from the Horda Platform, northern North Sea. *Petroleum Geoscience*, *27*(3), petgeo2020-2102.

Yielding, G., & Freeman, B. (2016). 3-D seismic-structural workflows–examples using the hat creek fault system.

Ziegler, P. (1975). Geologic evolution of North Sea and its tectonic framework. *AAPG bulletin*, *59*(7), 1073-1097.

Ziegler, P. (1975). NORTH SEA BASIN HISTORY IN THE TECTONIC FRAMEWORK OF NORTH-WESTERN EUROPE.

Ziegler, P. (1982). Triassic rifts and facies patterns in Western and Central Europe. *Geologische Rundschau*, *71*(3), 747-772.

Ziegler, P. (1990). Tectonic and palaeogeographic development of the North Sea rift system. Tectonic evolution of the North Sea rifts,

Appendix A

Variations in Strike, Fault number 1

Picked Every Line, 25 m spacing

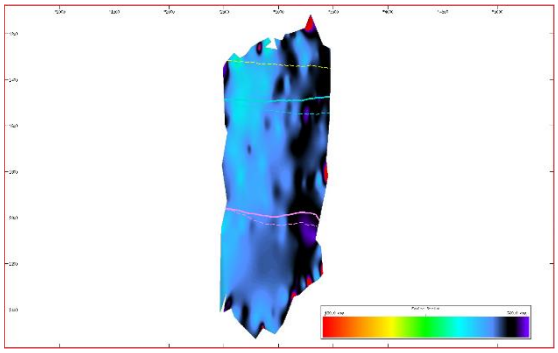

Picked Every 2nd Line, 50 m spacing

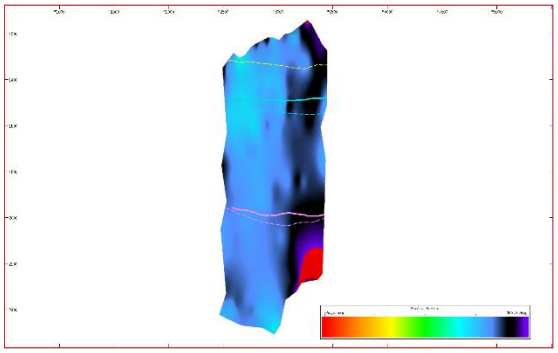

Picked Every 4th Line, 100 m spacing

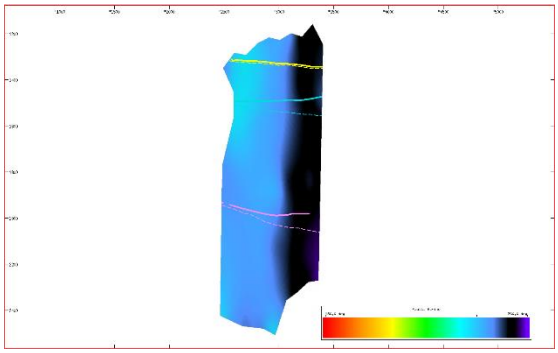

Picked Every 8th Line, 200 m spacing

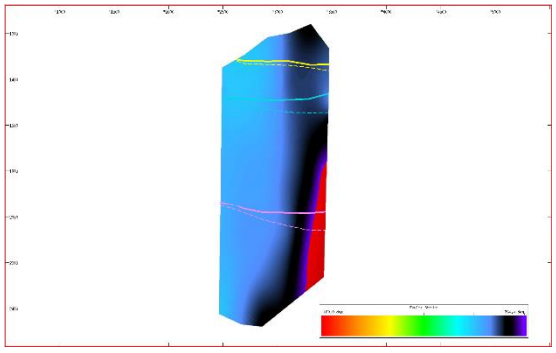

Picked Every 16th Line, 400 m spacing

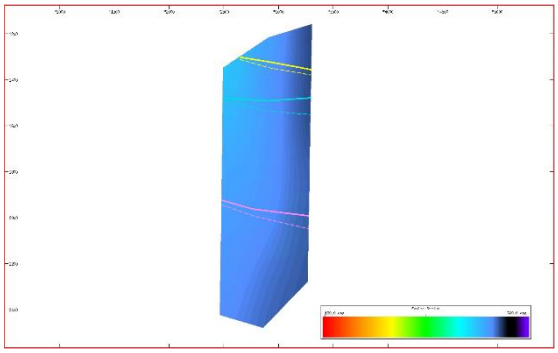

Picked Every 32nd Line, 800 m spacing

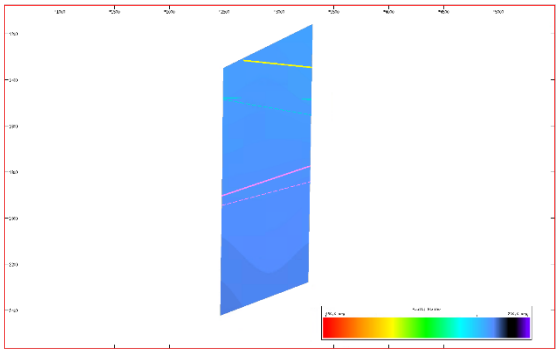

Variations in Throw, Fault number 1

Picked Every Line, 25 m spacing

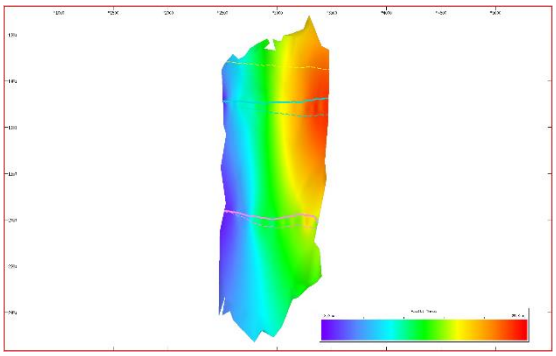

Picked Every 2nd Line, 50 m spacing

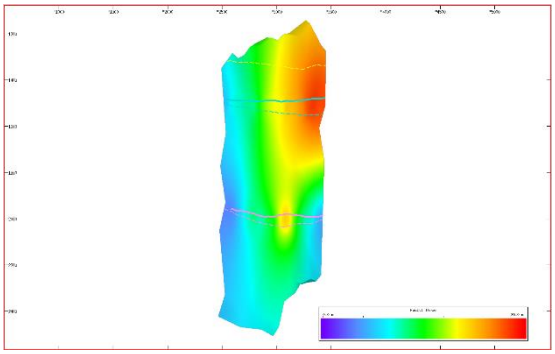

Picked Every 4th Line, 100 m spacing

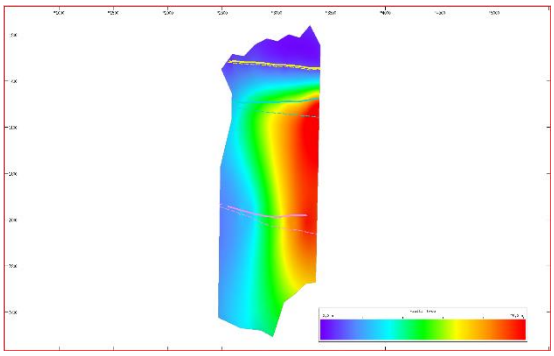

Picked Every 8th Line, 200 m spacing

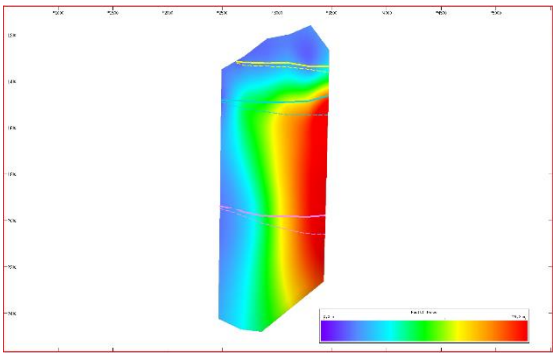

Picked Every 16th Line, 400 m spacing

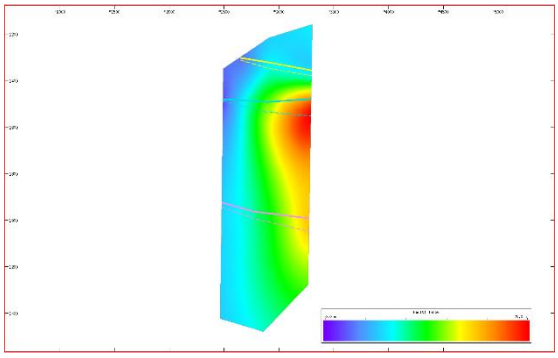

Picked Every 32nd Line, 800 m spacing

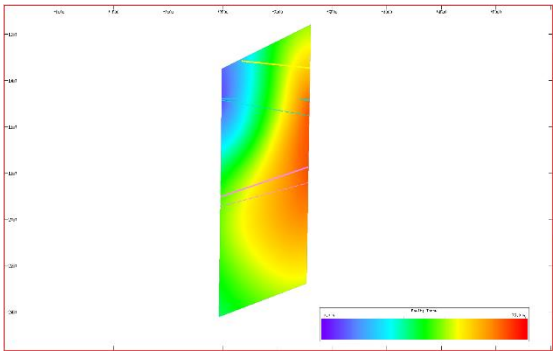

Fault – displacement profiles, Fault number 1

Picked Every Line, 25 m spacing

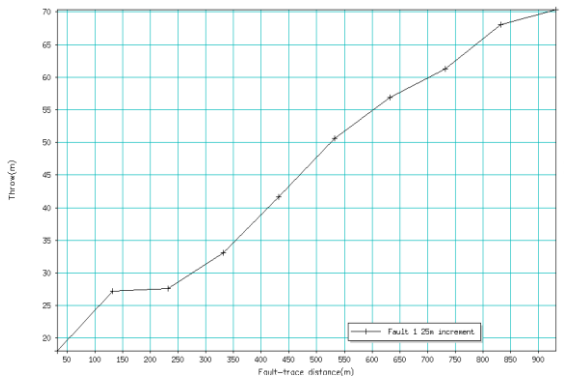

Picked Every 2nd Line, 50 m spacing

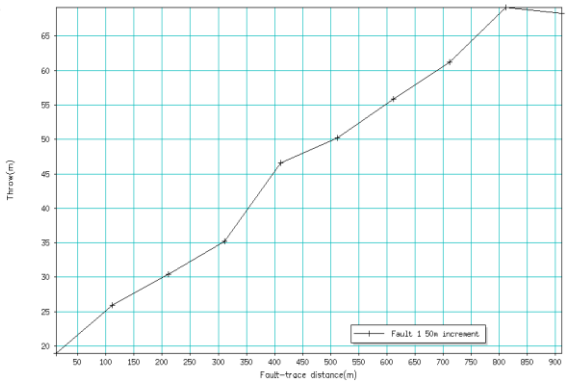

Picked Every 4th Line, 100 m spacing

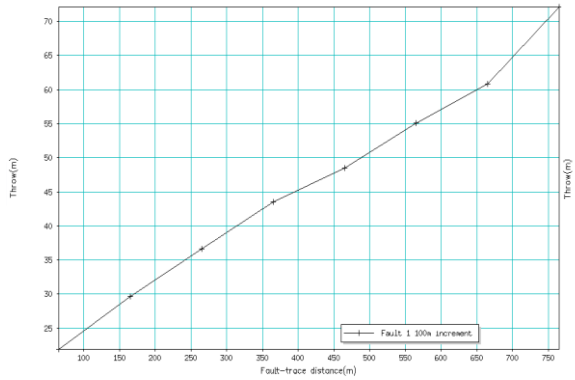

Picked Every 8th Line, 200 m spacing

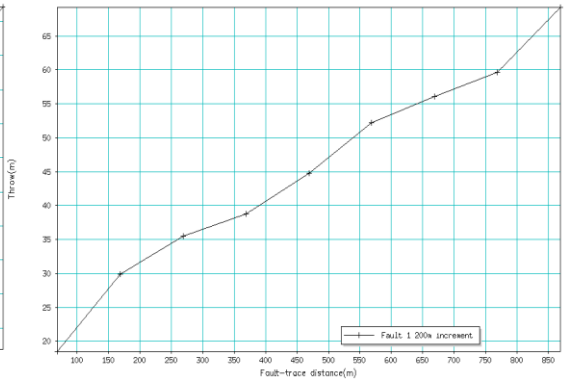

Picked Every 16th Line, 400 m spacing

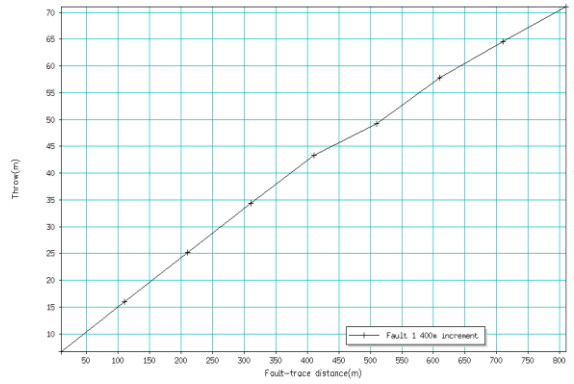

Picked Every 32nd Line, 800 m spacing

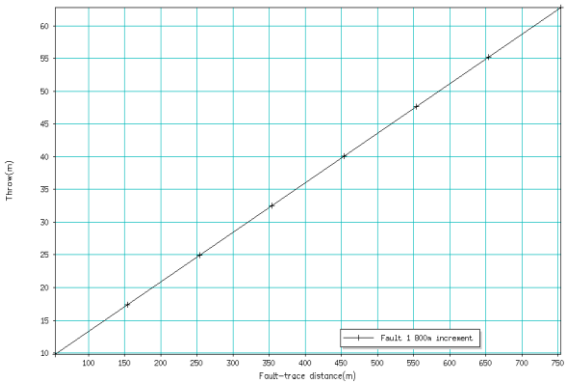

Variations in Dip, Fault number 1

Picked Every Line, 25 m spacing

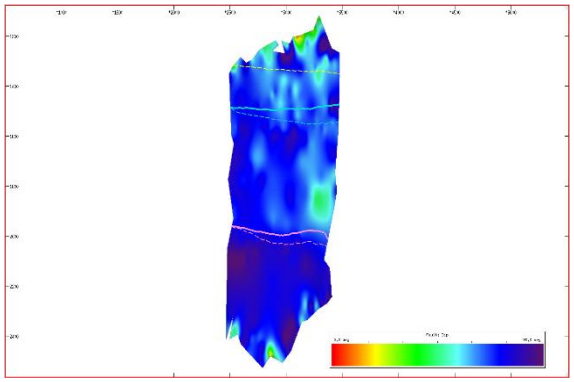

Picked Every 2nd Line, 50 m spacing

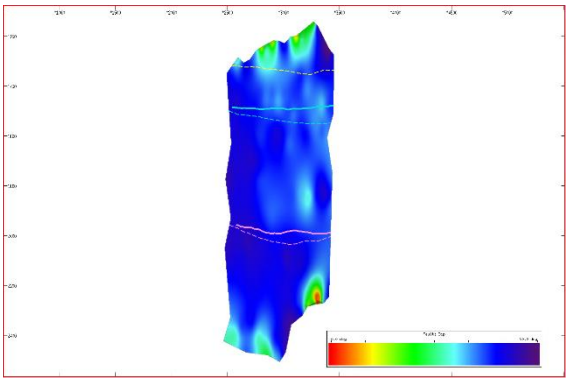

Picked Every 4th Line, 100 m spacing

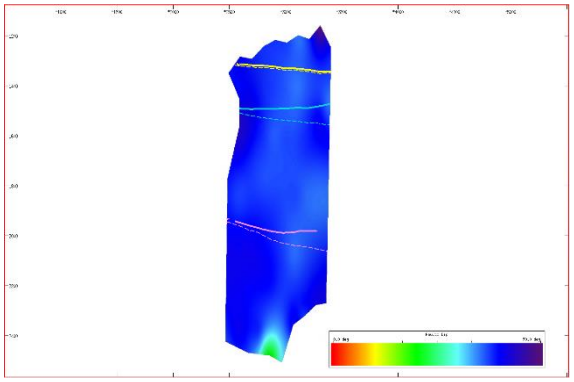

Picked Every 8th Line, 200 m spacing

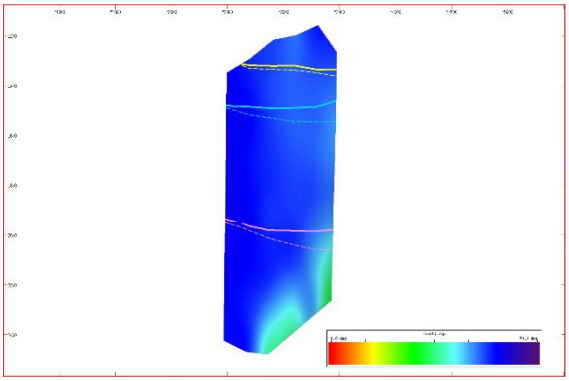

Picked Every 16th Line, 400 m spacing

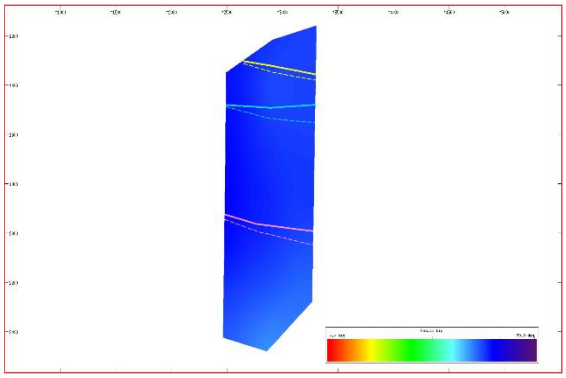

Picked Every 32nd Line, 800 m spacing

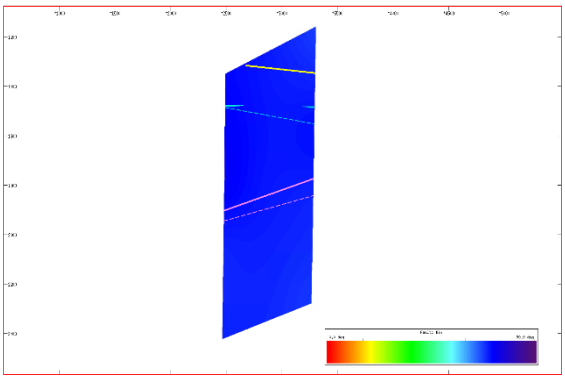

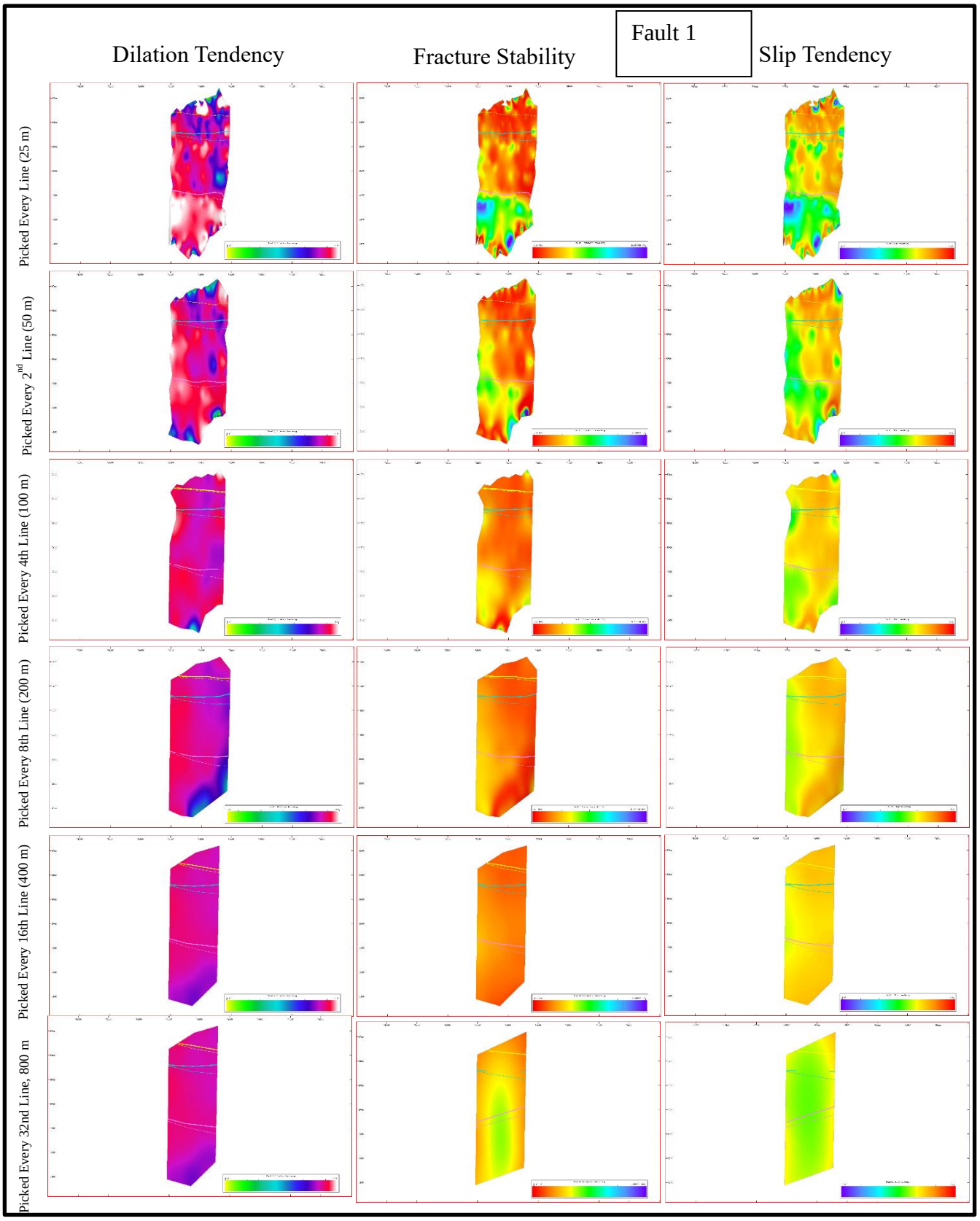
Fault 1
Dilation Tendency
Fracture Stability
Slip Tendency
Picked Every Line (25 m)
Picked Every 2nd Line (50 m)
Picked Every 4th Line (100 m)
Picked Every 8th Line (200 m)
Picked Every 16th Line (400 m)
Picked Every 32nd Line, 800 m

Fault – displacement profiles Fault, number 2

Picked Every Line, 25 m spacing

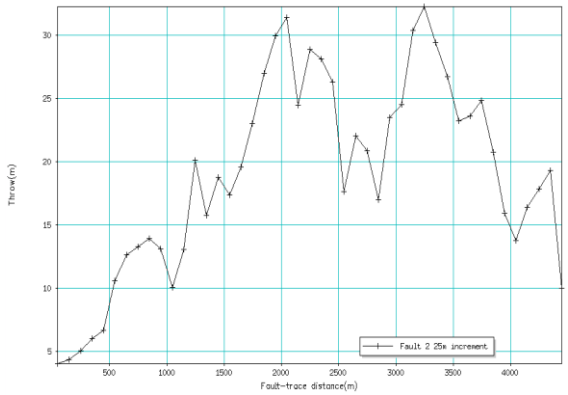

Picked Every 2nd Line, 50 m spacing

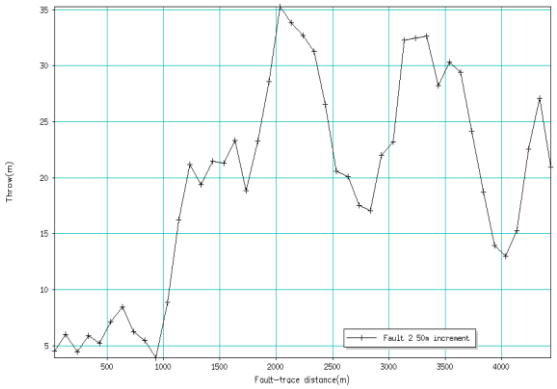

Picked Every 4th Line, 100 m spacing

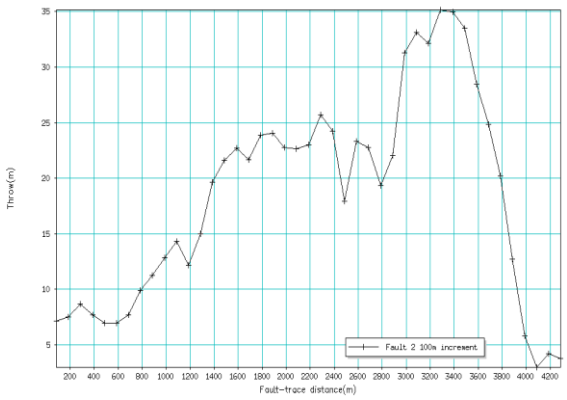

Picked Every 8th Line, 200 m spacing

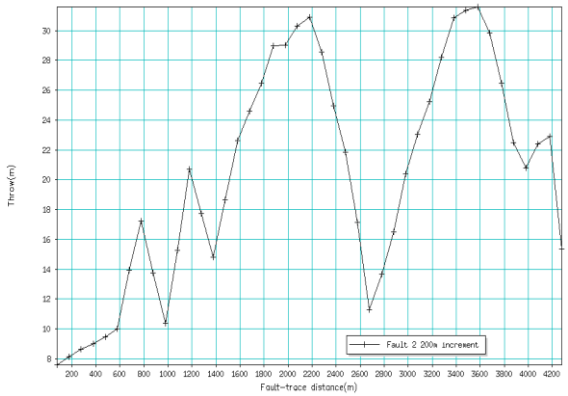

Picked Every 16th Line, 400 m spacing

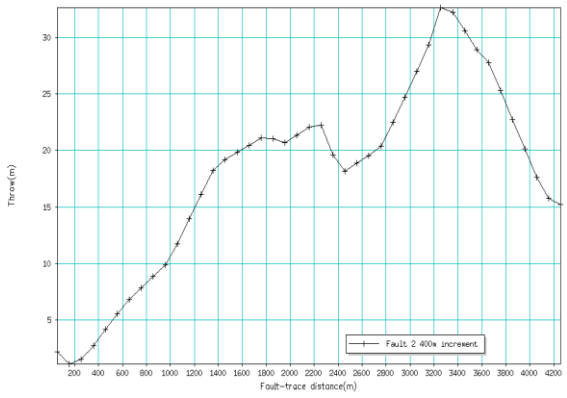

Picked Every 32nd Line, 800 m spacing

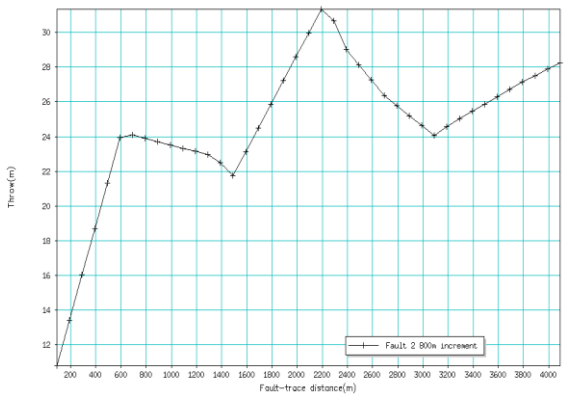

Variations in Throw Fault, number 2

Picked Every Line, 25 m spacing

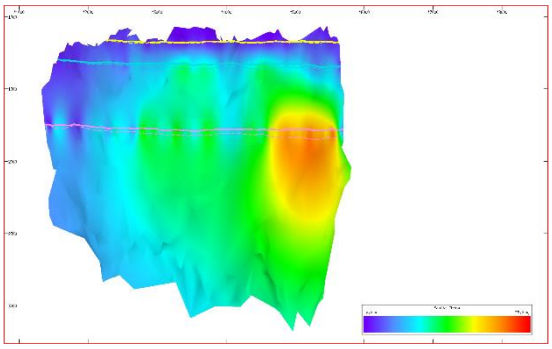

Picked Every 2nd Line, 50 m spacing

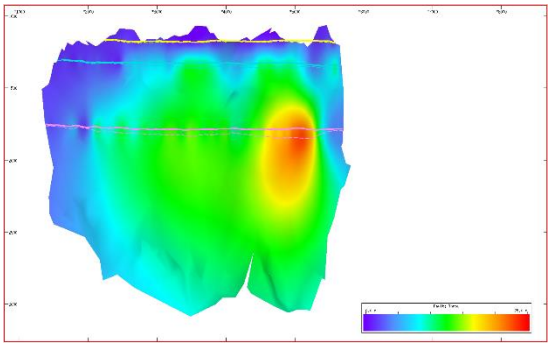

Picked Every 4th Line, 100 m spacing

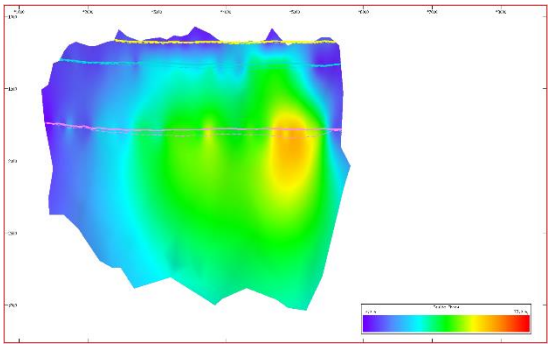

Picked Every 8th Line, 200 m spacing

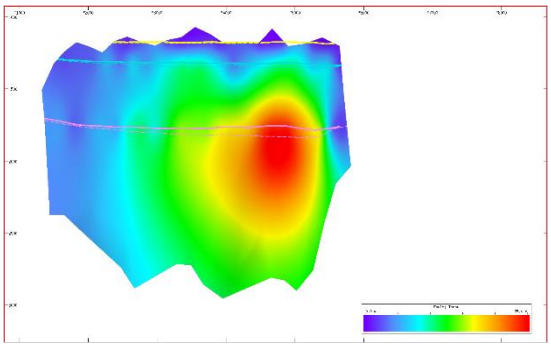

Picked Every 16th Line, 400 m spacing

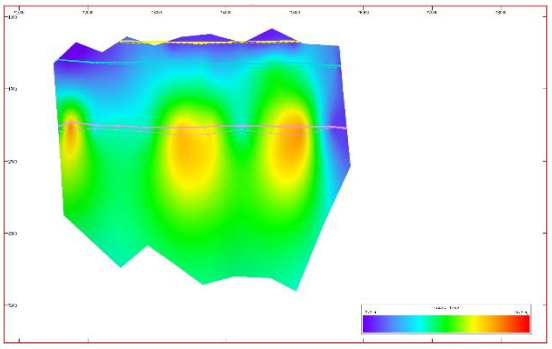

Picked Every 32nd Line, 800 m spacing

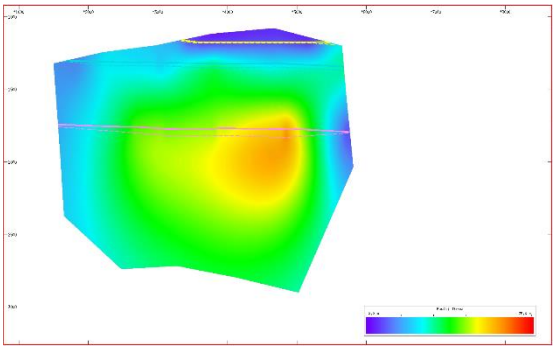

Variations in Dip, Fault number 2

Picked Every Line, 25 m spacing

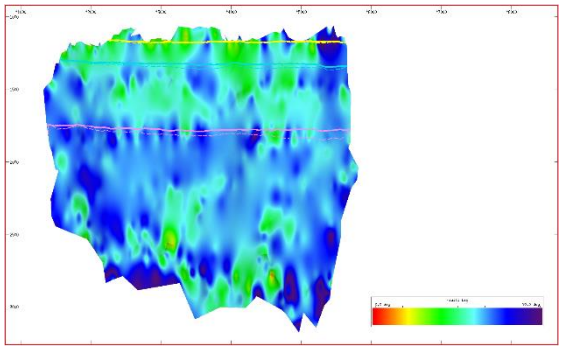

Picked Every 2nd Line, 50 m spacing

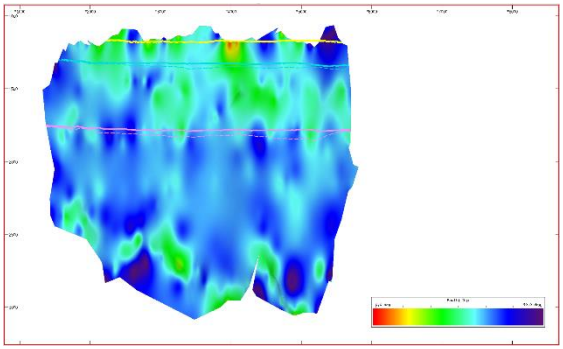

Picked Every 4th Line, 100 m spacing

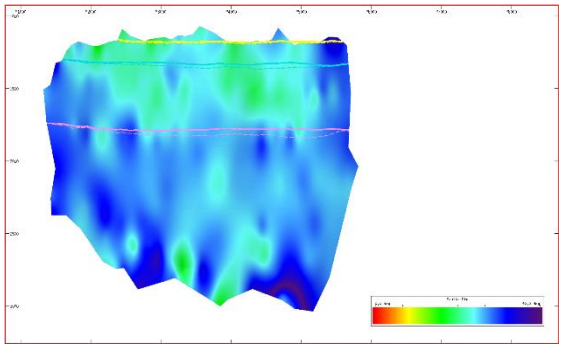

Picked Every 8th Line, 200 m spacing

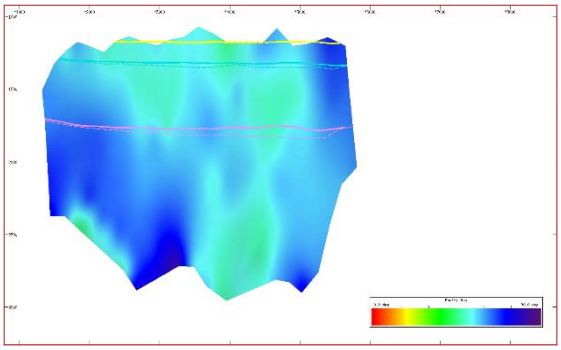

Picked Every 16th Line, 400 m spacing

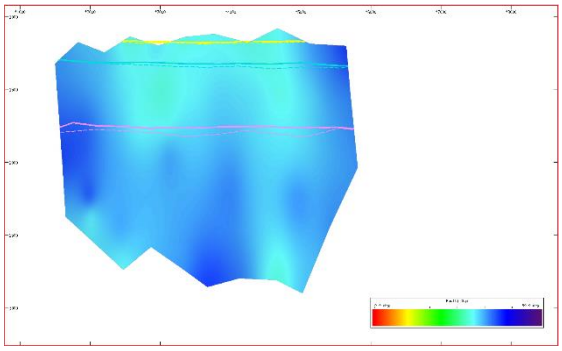

Picked Every 32nd Line, 800 m spacing

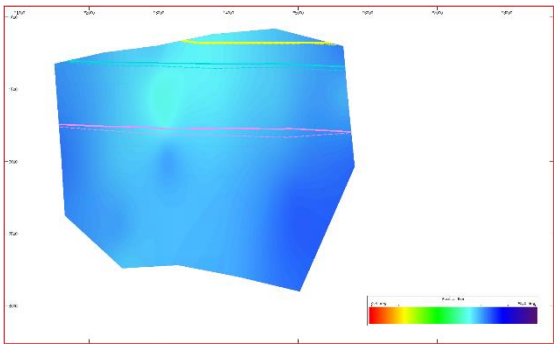

Variations in Strike, Fault number 2

Picked Every Line, 25 m spacing

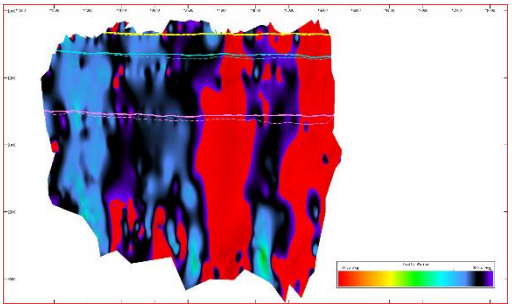

Picked Every 2nd Line, 50 m spacing

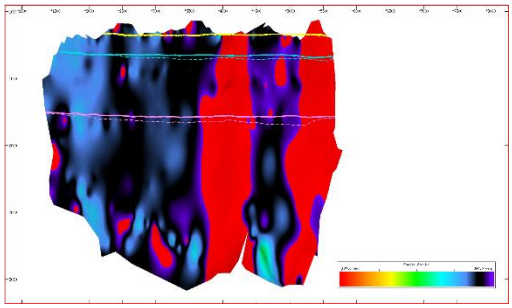

Picked Every 4th Line, 100 m spacing

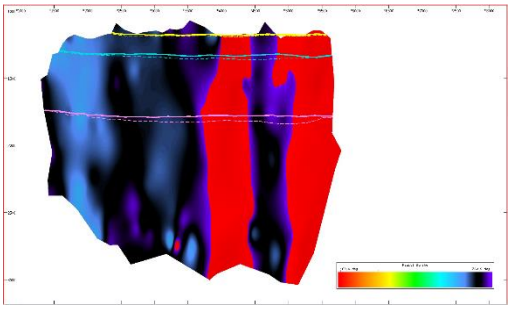

Picked Every 8th Line, 200 m spacing

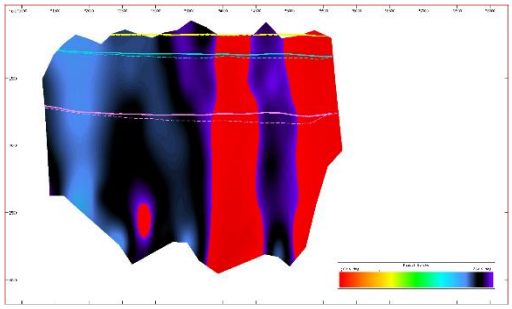

Picked Every 16th Line, 400 m spacing

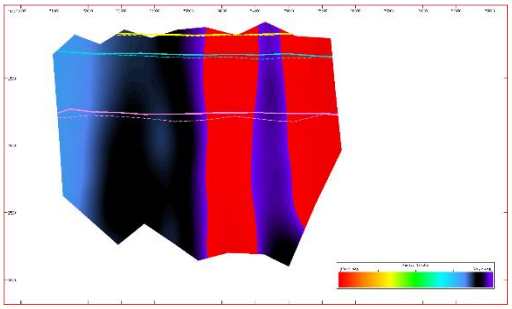

Picked Every 32nd Line, 800 m spacing

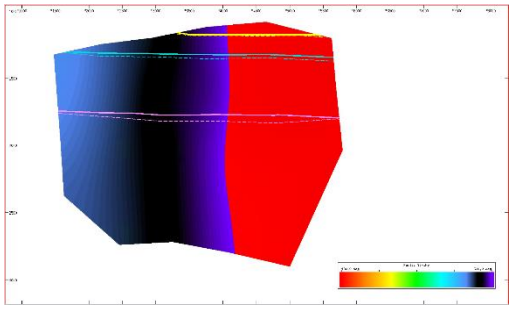

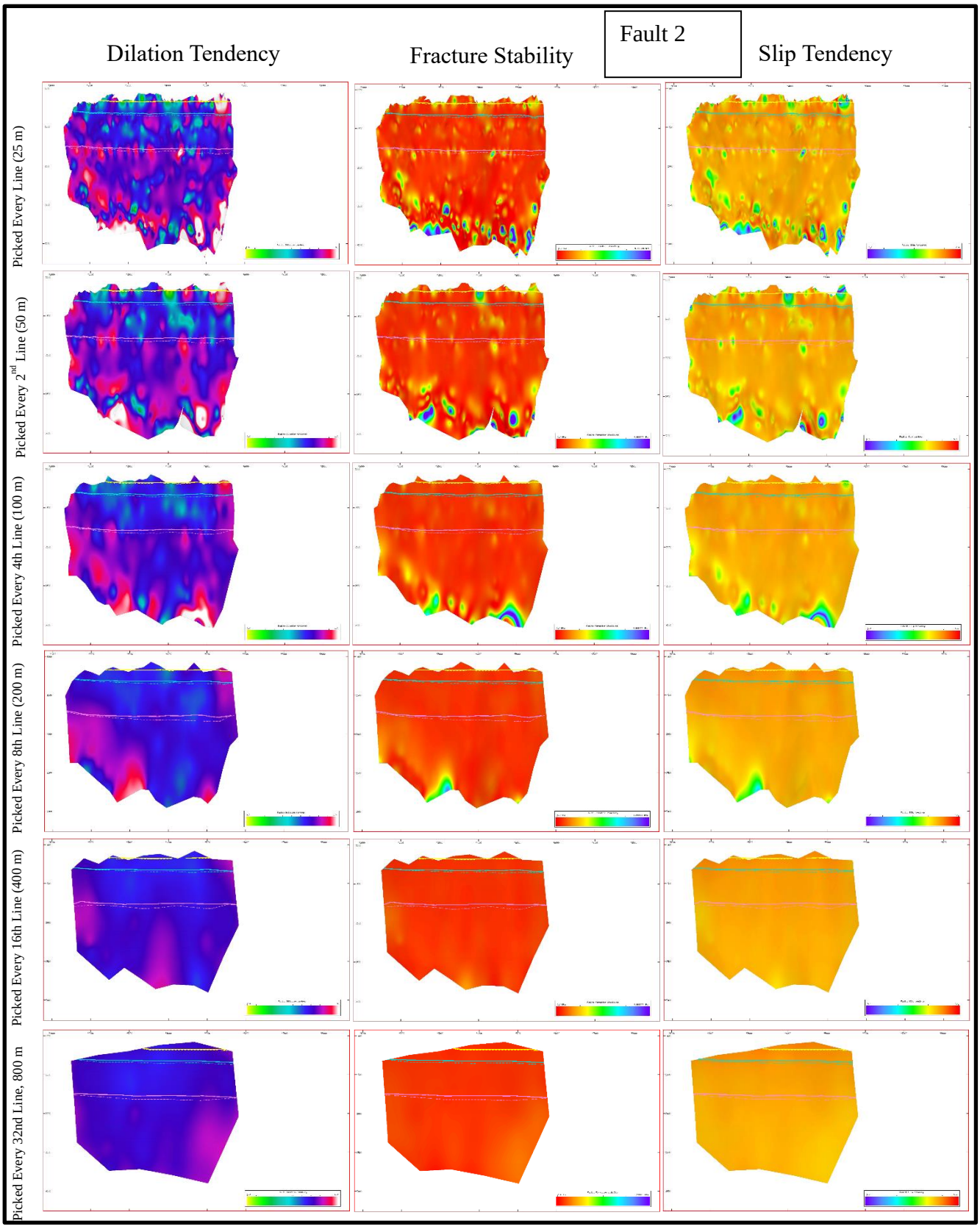
Fault 2
Dilation Tendency
Fracture Stability
Slip Tendency
Picked Every Line (25 m)
Picked Every 2nd Line (50 m)
Picked Every 4th Line (100 m)
Picked Every 8th Line (200 m)
Picked Every 16th Line (400 m)
Picked Every 32nd Line, 800 m

Fault – displacement profiles Fault, number 3

Picked Every Line, 25 m spacing

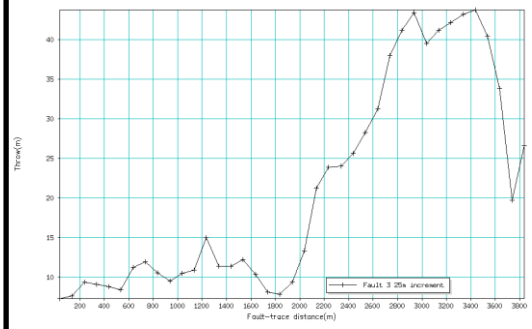

Picked Every 2nd Line, 50 m spacing

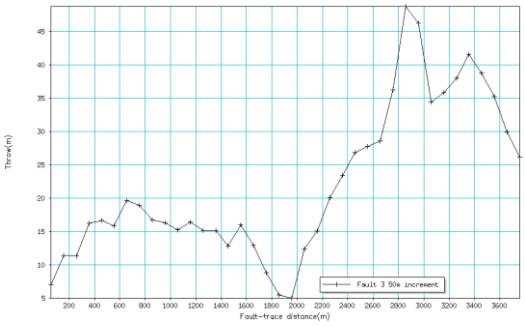

Picked Every 4th Line, 100 m spacing

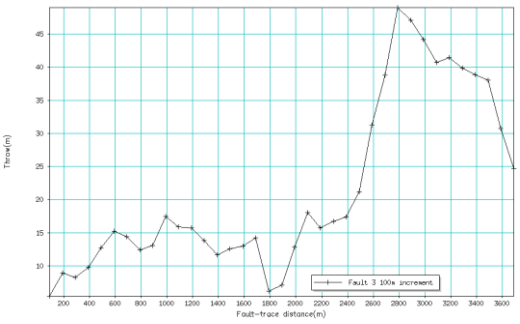

Picked Every 8th Line, 200 m spacing

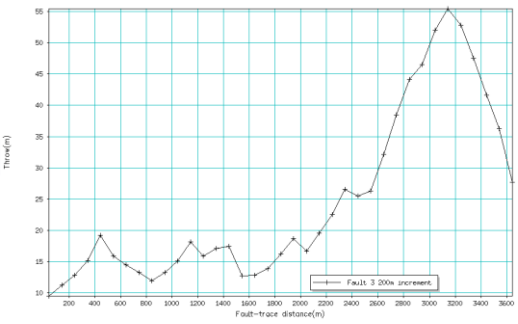

Picked Every 16th Line, 400 m spacing

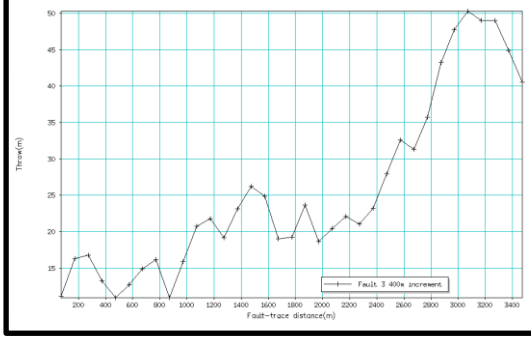

Picked Every 32nd Line, 800 m spacing

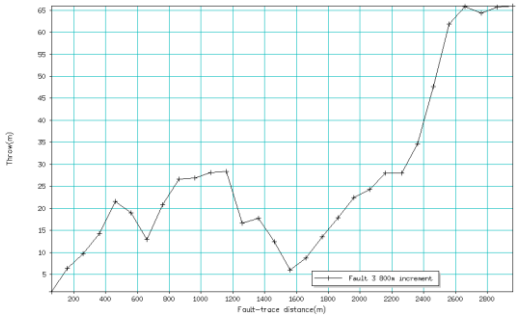

Variations in Throw Fault, number 3

Picked Every Line, 25 m spacing

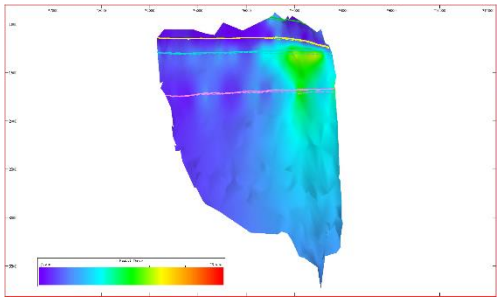

Picked Every 2nd Line, 50 m spacing

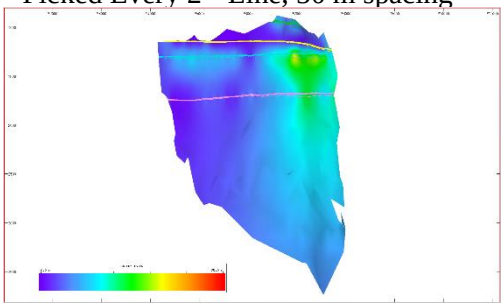

Picked Every 4th Line, 100 m spacing

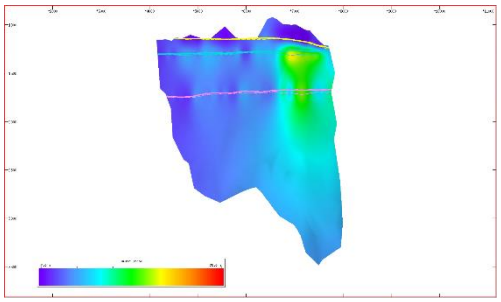

Picked Every 8th Line, 200 m spacing

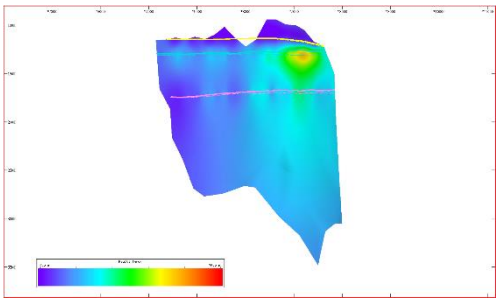

Picked Every 16th Line, 400 m spacing

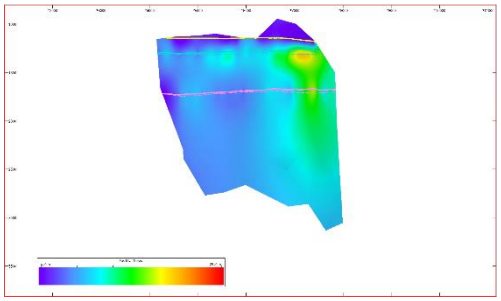

Picked Every 32nd Line, 800 m spacing

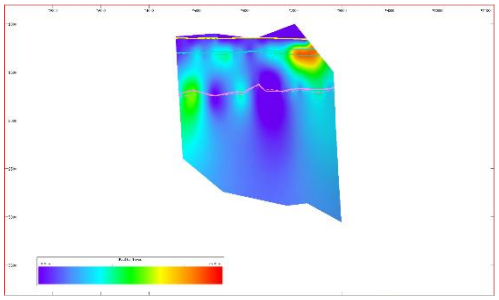

Variations in Dip, Fault number 3

Picked Every Line, 25 m spacing

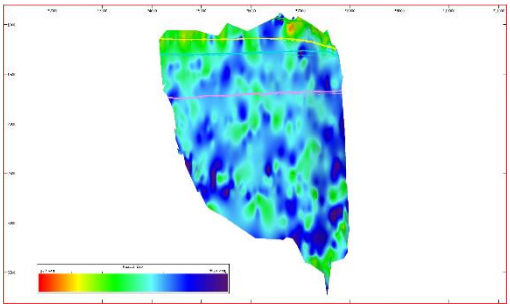

Picked Every 2nd Line, 50 m spacing

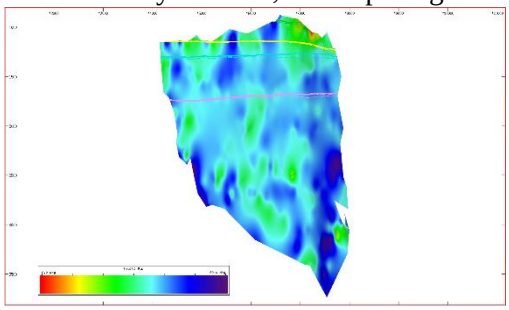

Picked Every 4th Line, 100 m spacing

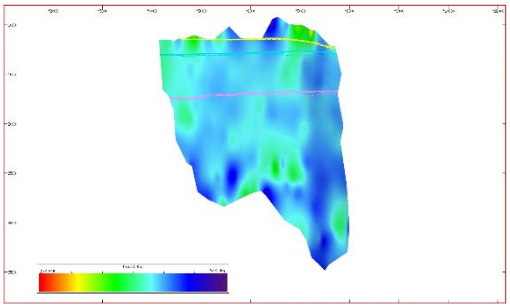

Picked Every 8th Line, 200 m spacing

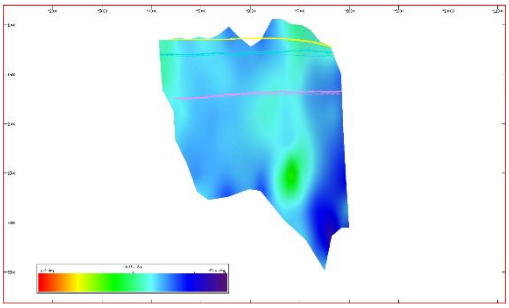

Picked Every 16th Line, 400 m spacing

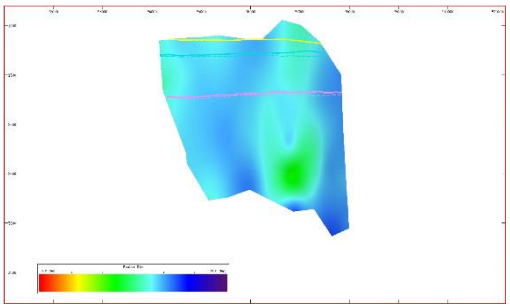

Picked Every 32nd Line, 800 m spacing

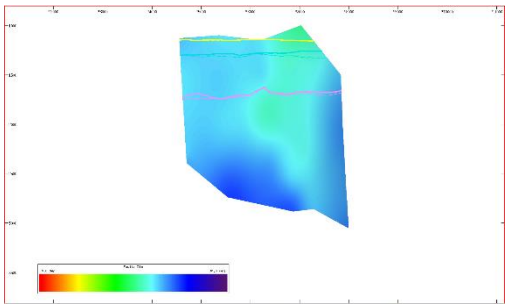

Variations in Strike, Fault number 3

Picked Every Line, 25 m spacing

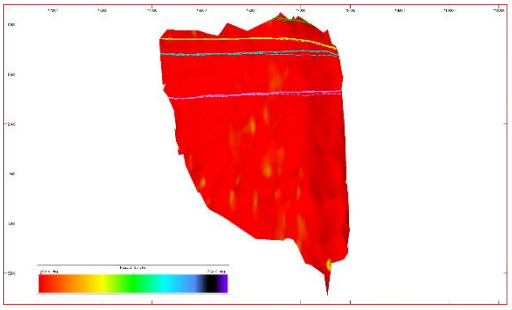

Picked Every 2nd Line, 50 m spacing

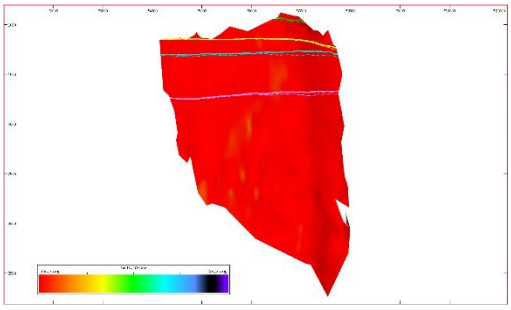

Picked Every 4th Line, 100 m spacing

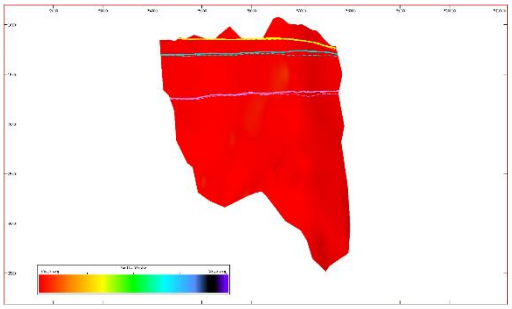

Picked Every 8th Line, 200 m spacing

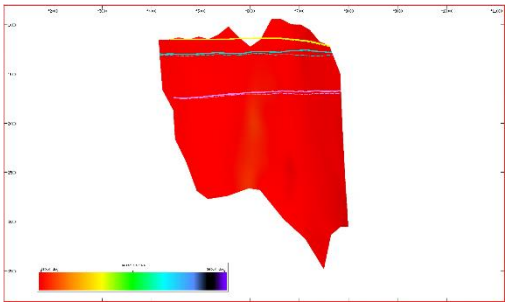

Picked Every 16th Line, 400 m spacing

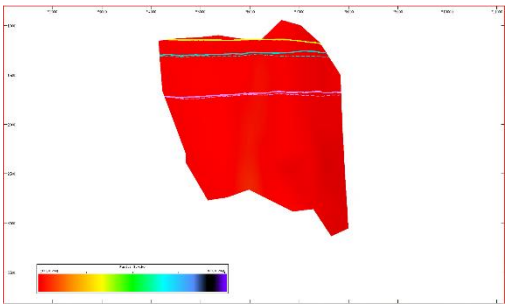

Picked Every 32nd Line, 800 m spacing

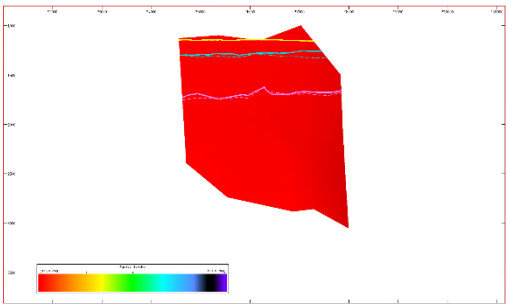

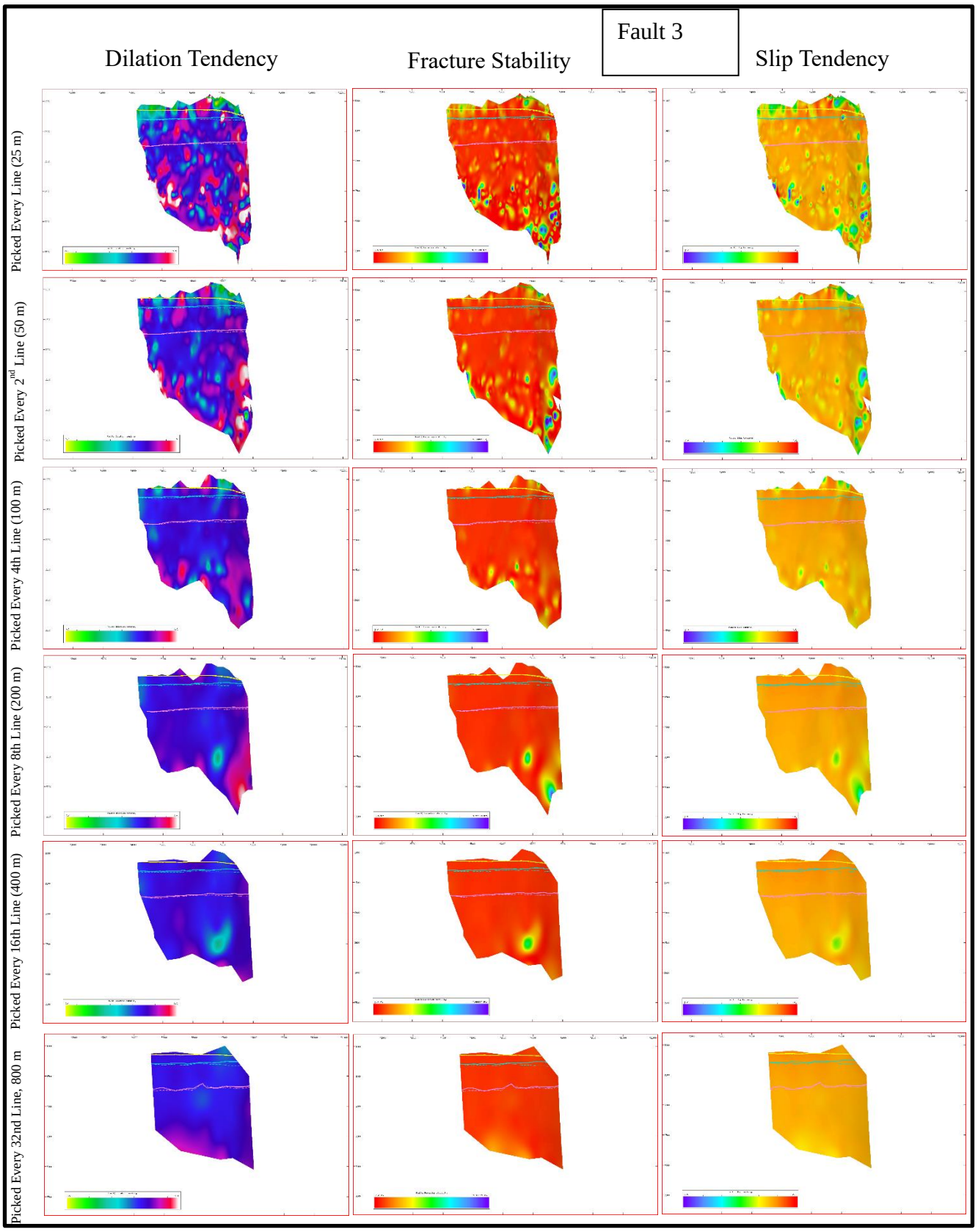
Fault 3
Dilation Tendency
Fracture Stability
Slip Tendency
Picked Every Line (25 m)
Picked Every 2nd Line (50 m)
Picked Every 4th Line (100 m)
Picked Every 8th Line (200 m)
Picked Every 16th Line (400 m)
Picked Every 32nd Line, 800 m

Fault – displacement profiles Fault, number 4

Picked Every Line, 25 m spacing

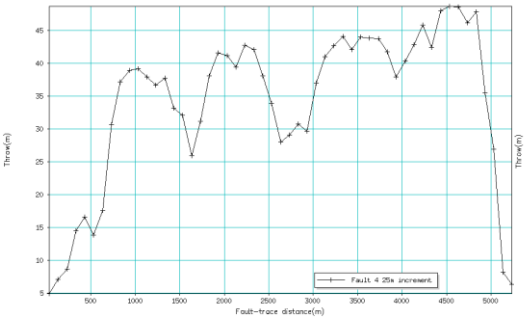

Picked Every 2nd Line, 50 m spacing

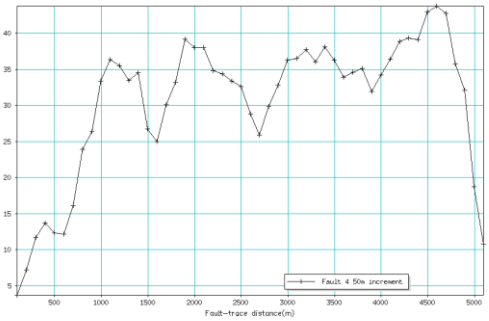

Picked Every 4th Line, 100 m spacing

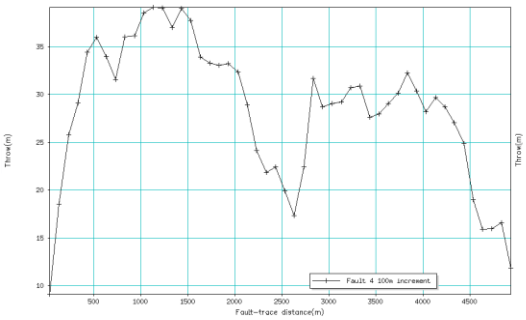

Picked Every 8th Line, 200 m spacing

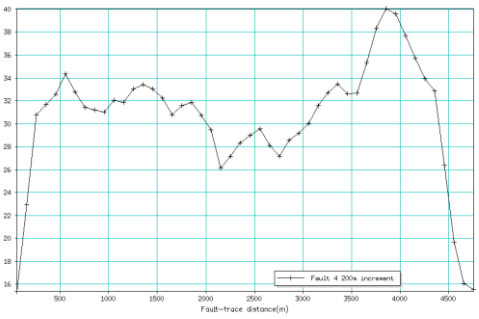

Picked Every 16th Line, 400 m spacing

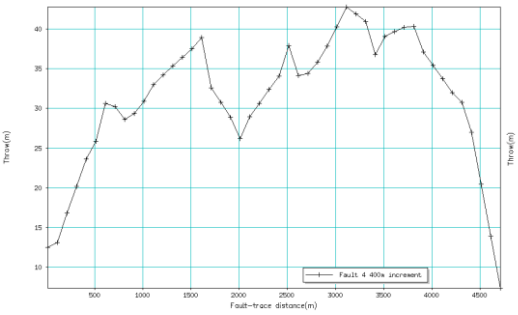

Picked Every 32nd Line, 800 m spacing

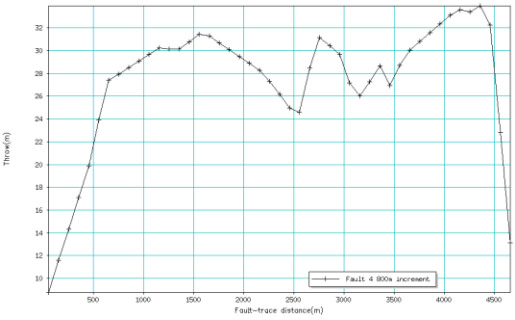

Variations in Throw Fault, number 4

Picked Every Line, 25 m spacing

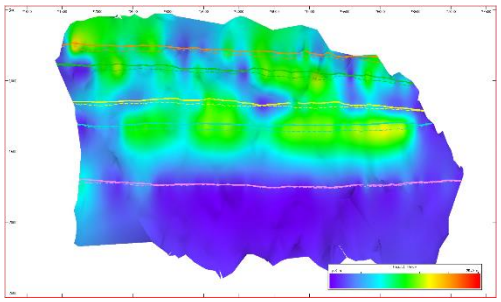

Picked Every 2nd Line, 50 m spacing

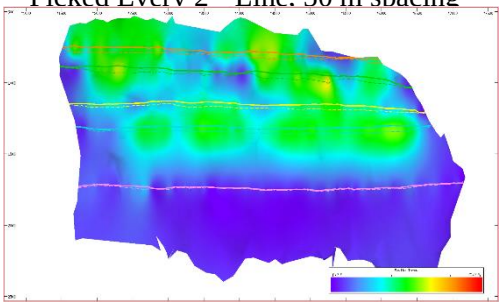

Picked Every 4th Line, 100 m spacing

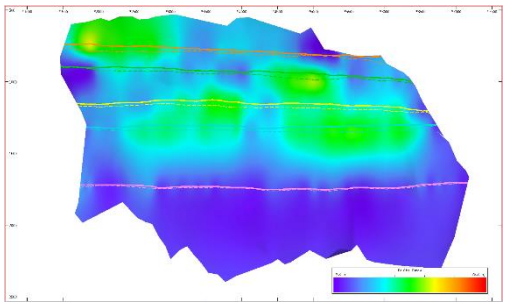

Picked Every 8th Line, 200 m spacing

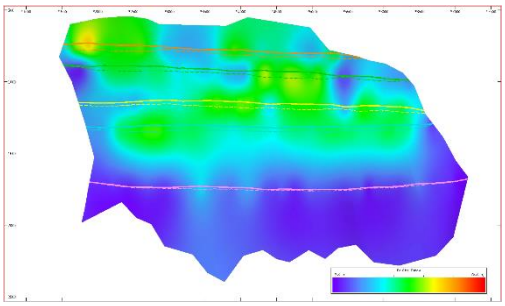

Picked Every 16th Line, 400 m spacing

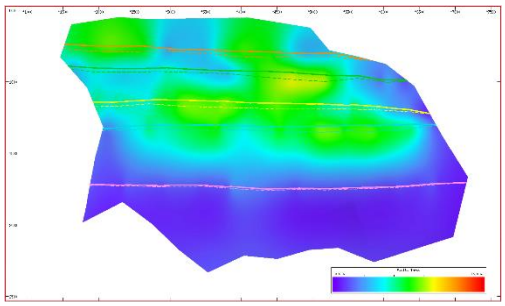

Picked Every 32nd Line, 800 m spacing

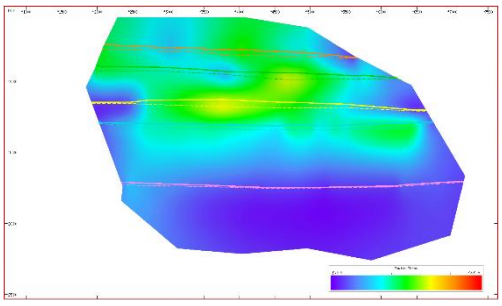

Variations in Dip, Fault number 4

Picked Every Line, 25 m spacing

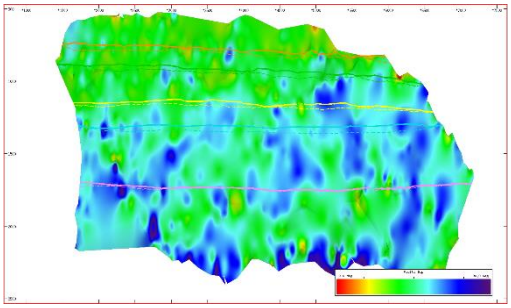

Picked Every 2nd Line, 50 m spacing

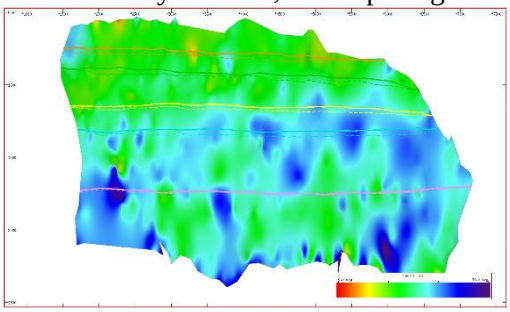

Picked Every 4th Line, 100 m spacing

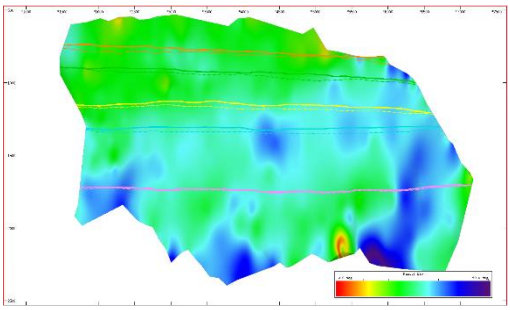

Picked Every 8th Line, 200 m spacing

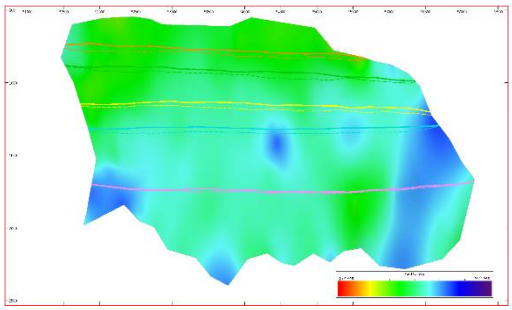

Picked Every 16th Line, 400 m spacing

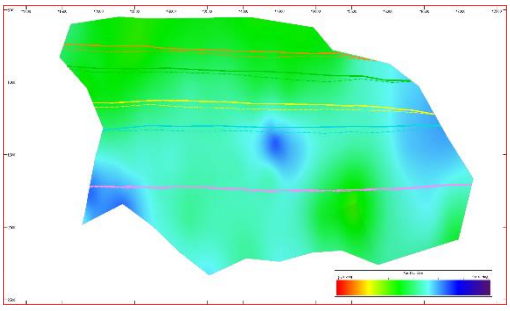

Picked Every 32nd Line, 800 m spacing

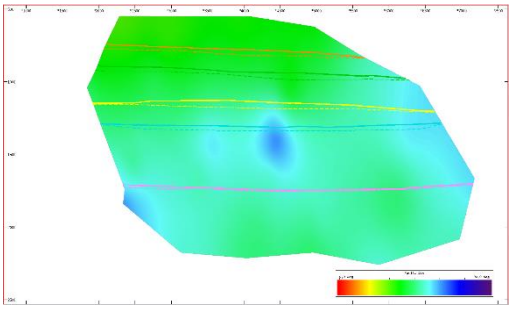

Variations in Strike, Fault number 4

Picked Every Line, 25 m spacing

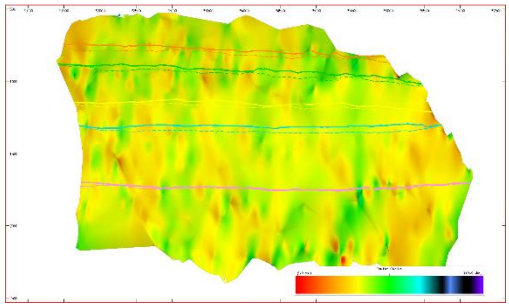

Picked Every 2nd Line, 50 m spacing

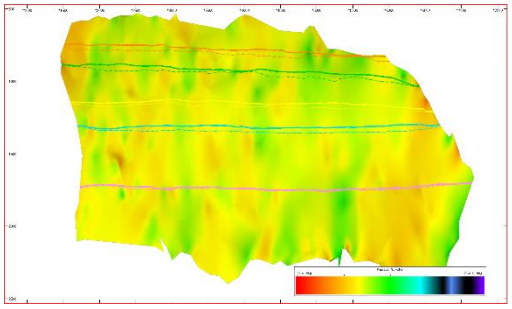

Picked Every 4th Line, 100 m spacing

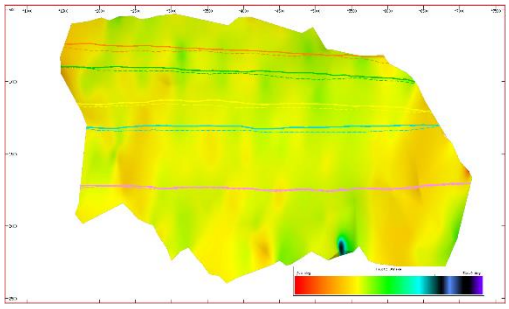

Picked Every 8th Line, 200 m spacing

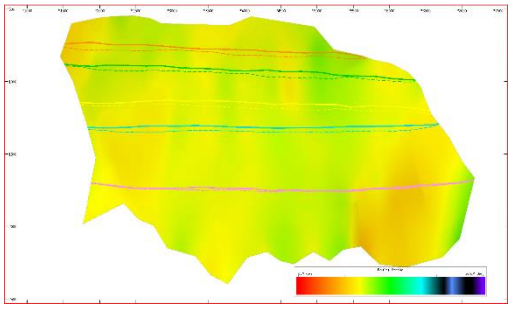

Picked Every 16th Line, 400 m spacing

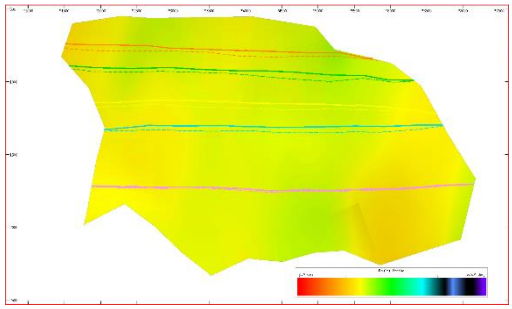

Picked Every 32nd Line, 800 m spacing

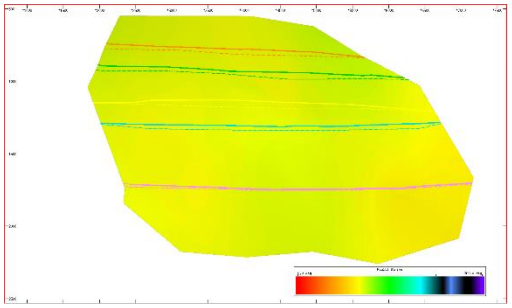

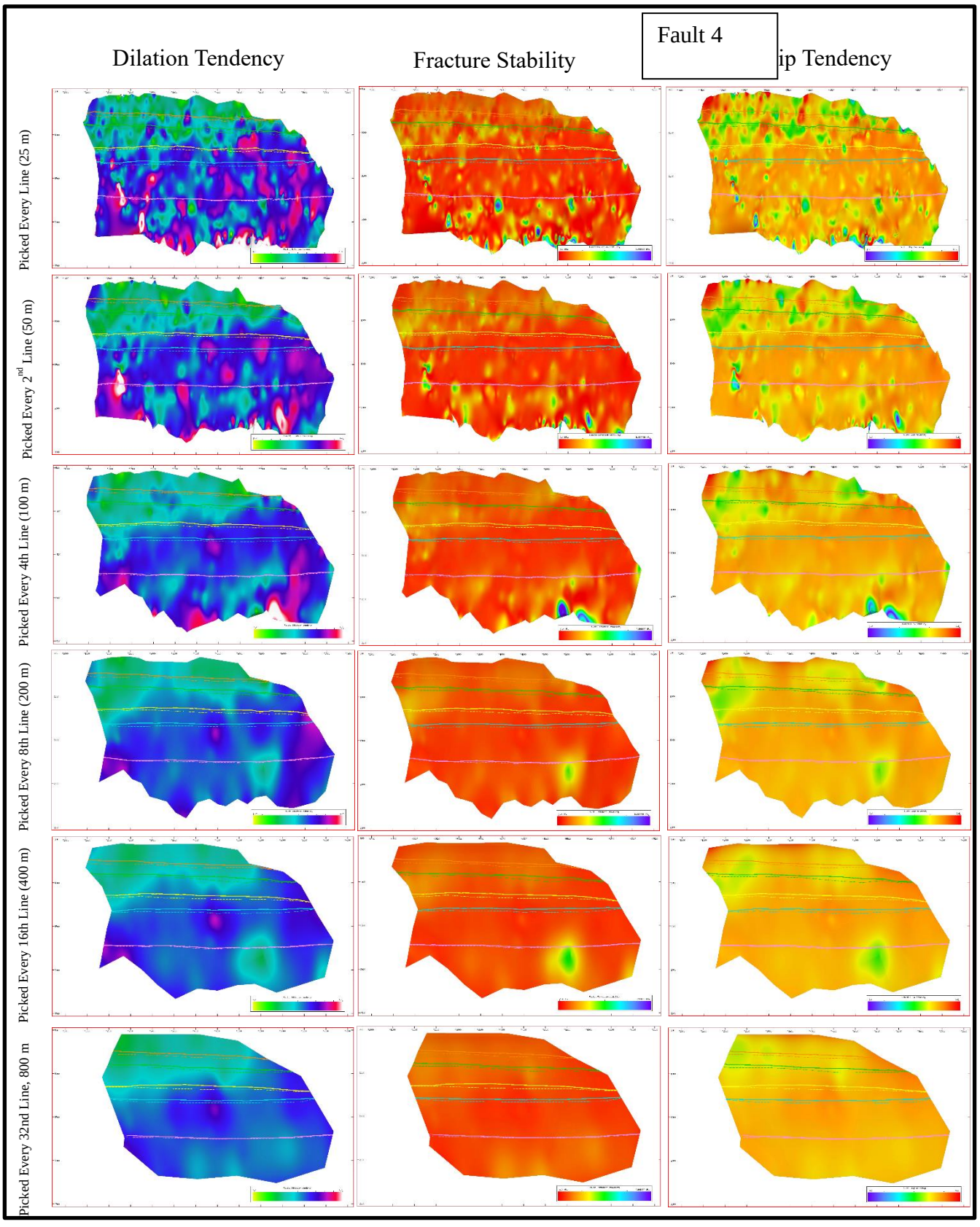
Fault 4
Dilation Tendency
Fracture Stability
ip Tendency
Picked Every Line (25 m)
Picked Every 2nd Line (50 m)
Picked Every 4th Line (100 m)
Picked Every 8th Line (200 m)
Picked Every 16th Line (400 m)
Picked Every 32nd Line, 800 m

Fault – displacement profiles Fault, number 5

Picked Every Line, 25 m spacing

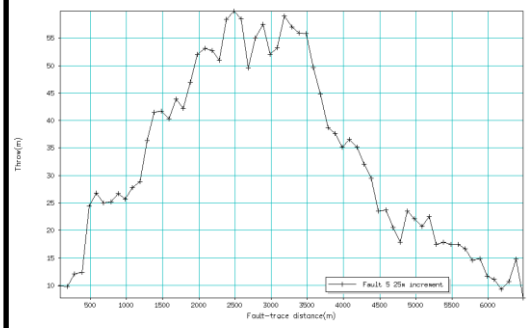

Picked Every 2nd Line, 50 m spacing

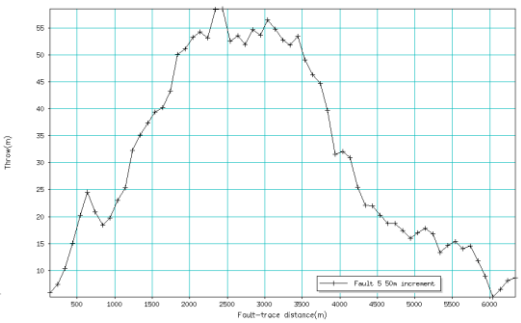

Picked Every 4th Line, 100 m spacing

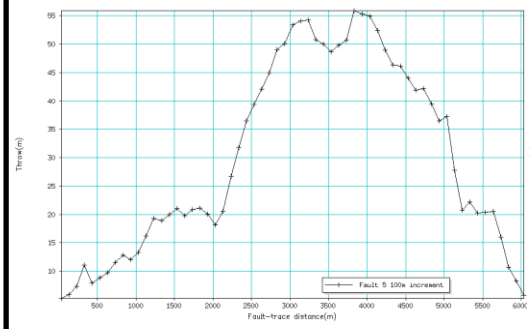

Picked Every 8th Line, 200 m spacing

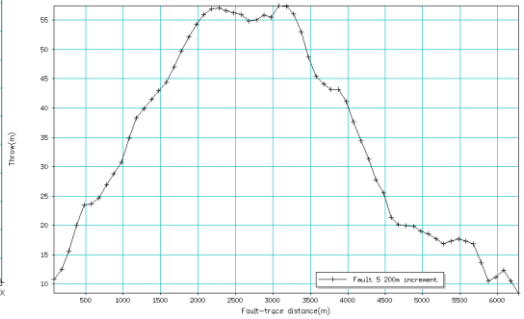

Picked Every 16th Line, 400 m spacing

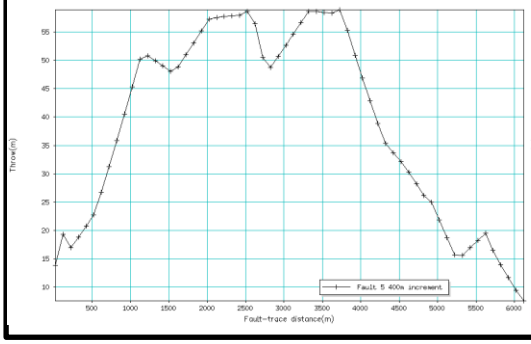

Picked Every 32nd Line, 800 m spacing

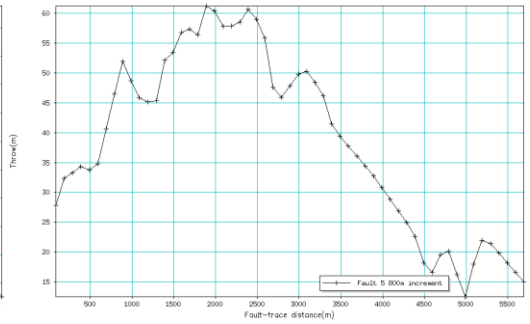

Variations in Throw Fault, number 5

Picked Every Line, 25 m spacing

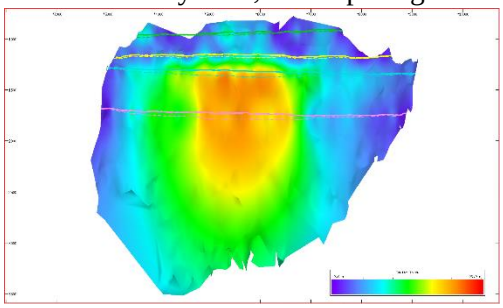

Picked Every 2nd Line, 50 m spacing

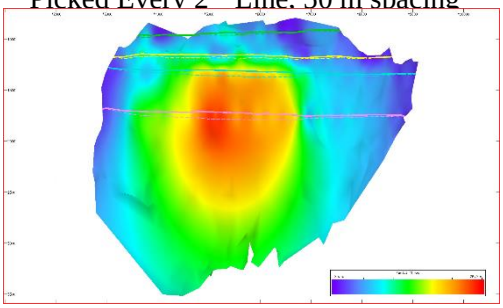

Picked Every 4th Line, 100 m spacing

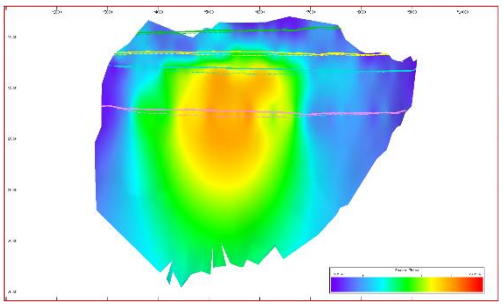

Picked Every 8th Line, 200 m spacing

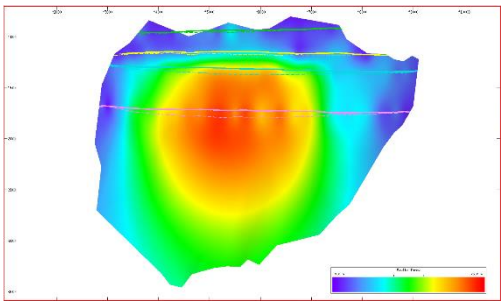

Picked Every 16th Line, 400 m spacing

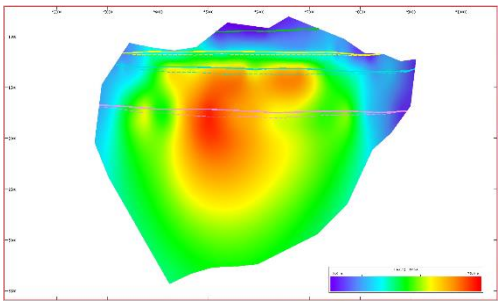

Picked Every 32nd Line, 800 m spacing

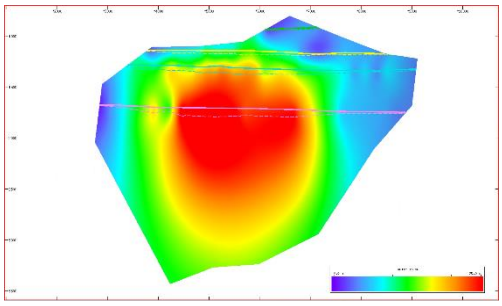

Variations in Dip, Fault number 5

Picked Every Line, 25 m spacing

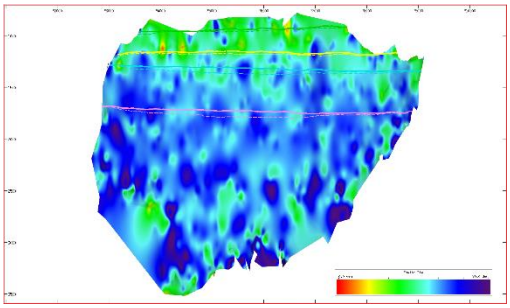

Picked Every 2nd Line, 50 m spacing

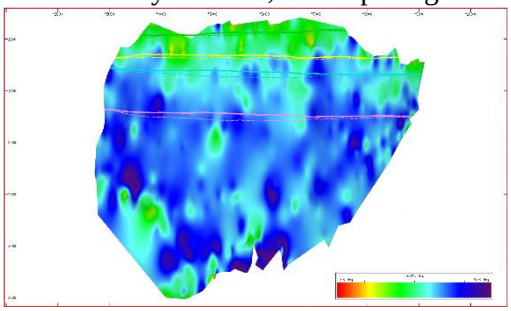

Picked Every 4th Line, 100 m spacing

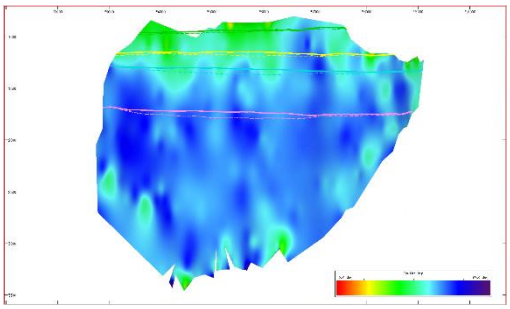

Picked Every 8th Line, 200 m spacing

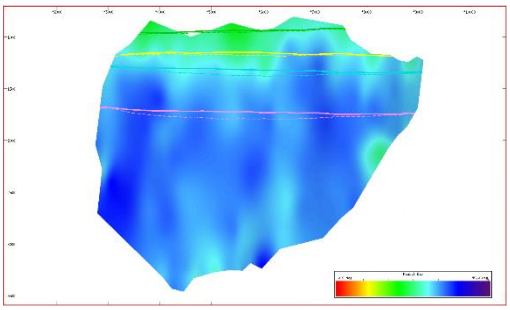

Picked Every 16th Line, 400 m spacing

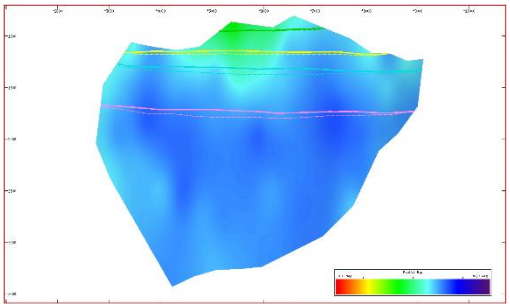

Picked Every 32nd Line, 800 m spacing

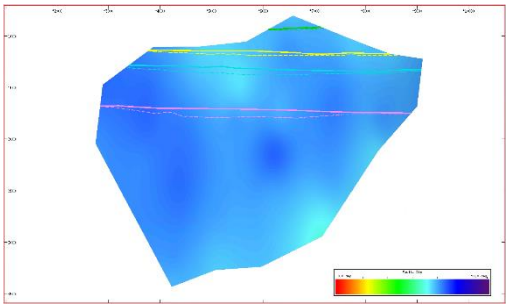

Variations in Strike, Fault number 5

Picked Every Line, 25 m spacing

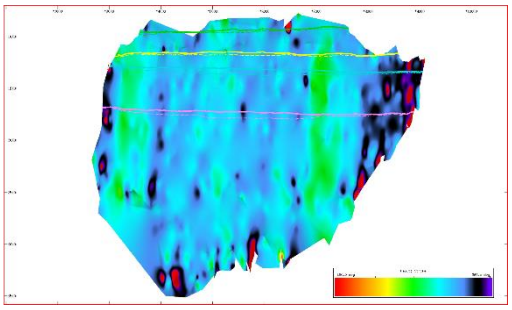

Picked Every 2nd Line, 50 m spacing

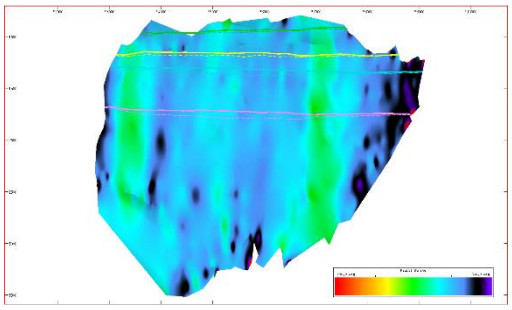

Picked Every 4th Line, 100 m spacing

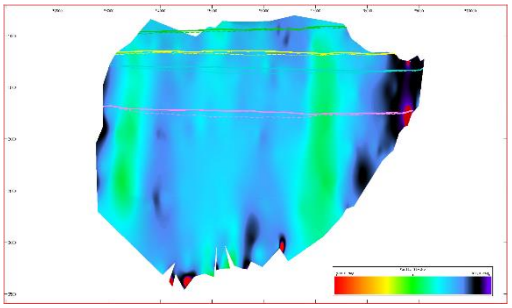

Picked Every 8th Line, 200 m spacing

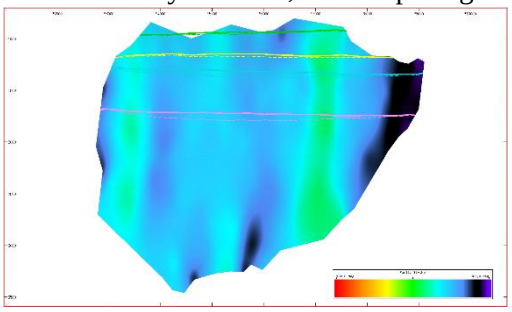

Picked Every 16th Line, 400 m spacing

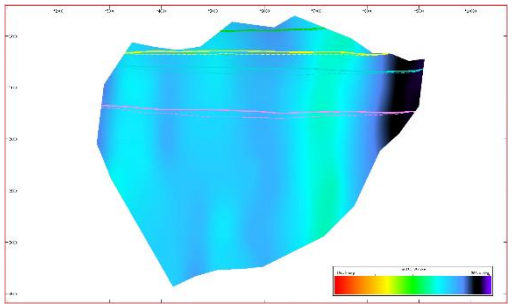

Picked Every 32nd Line, 800 m spacing

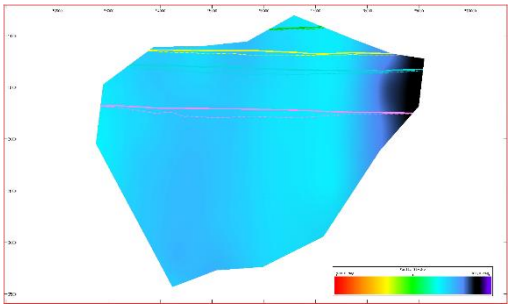

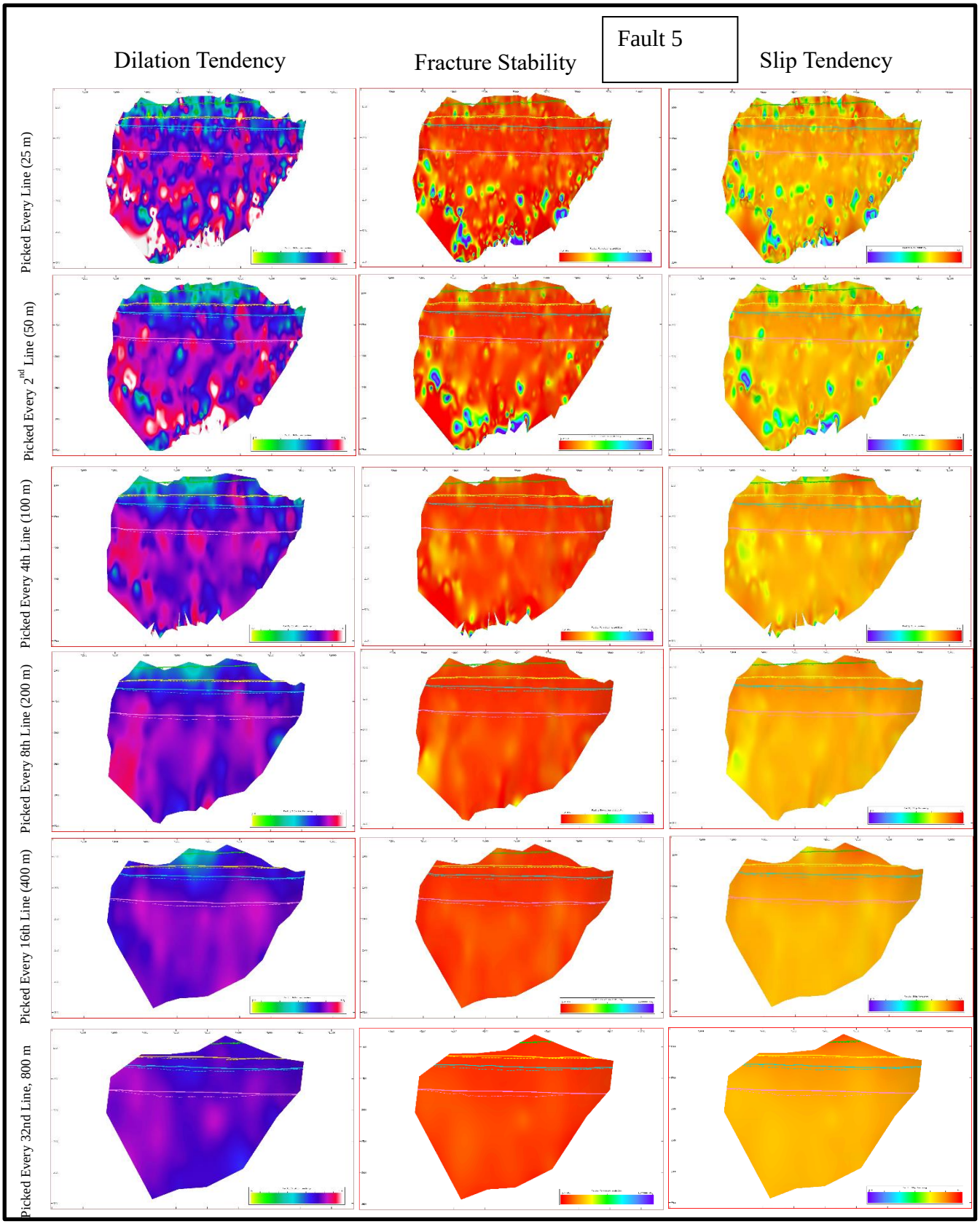
Fault 5
Dilation Tendency
Fracture Stability
Slip Tendency
Picked Every Line (25 m)
Picked Every 2nd Line (50 m)
Picked Every 4th Line (100 m)
Picked Every 8th Line (200 m)
Picked Every 16th Line (400 m)
Picked Every 32nd Line, 800 m

Variations in Strike Fault number 6

Picked Every Line, 25 m spacing

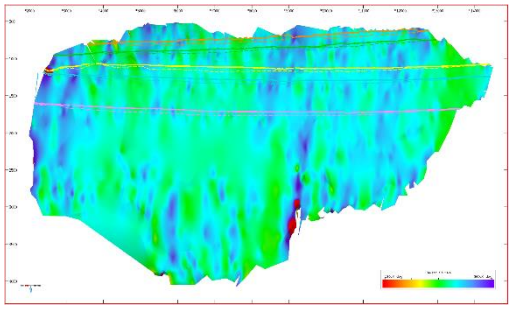

Picked Every 2nd Line, 50 m spacing

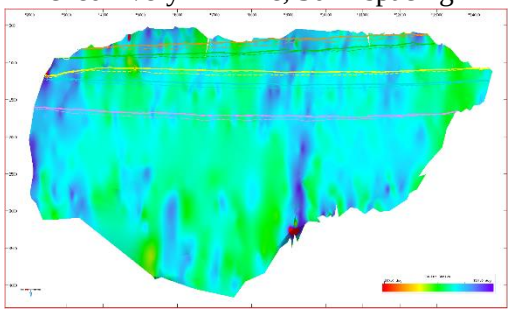

Picked Every 4th Line, 100 m spacing

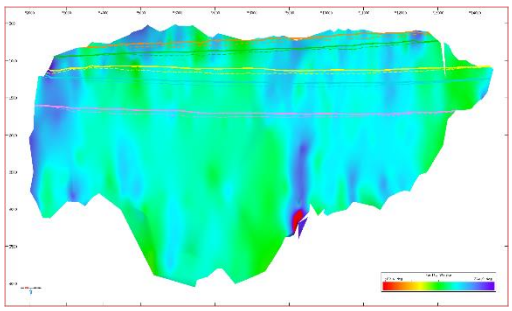

Picked Every 8th Line, 200 m spacing

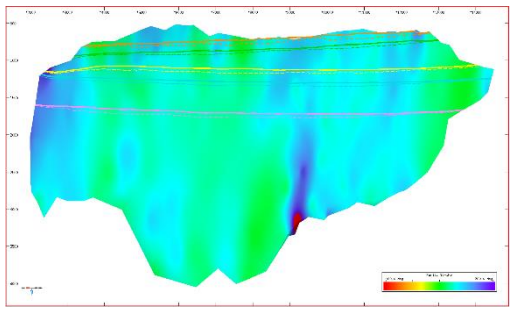

Picked Every 16th Line, 400 m spacing

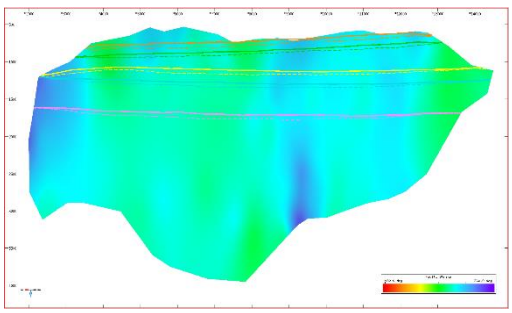

Picked Every 32nd Line, 800 m spacing

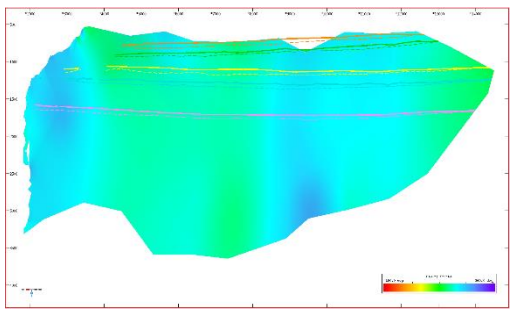

Variations in Throw Fault number 6

Picked Every Line, 25 m spacing

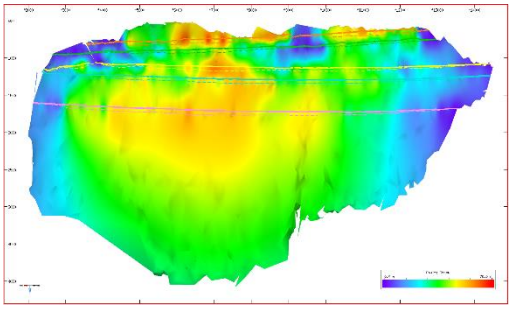

Picked Every 2nd Line, 50 m spacing

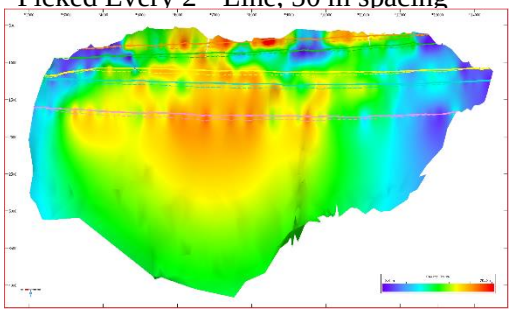

Picked Every 4th Line, 100 m spacing

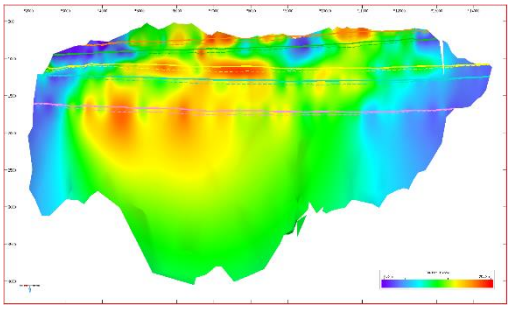

Picked Every 8th Line, 200 m spacing

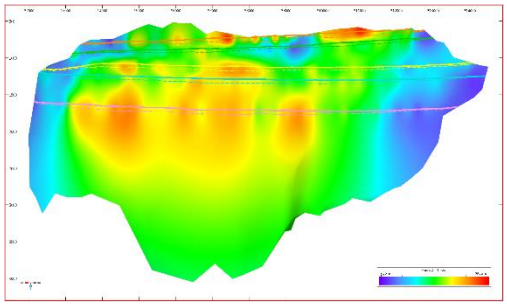

Picked Every 16th Line, 400 m spacing

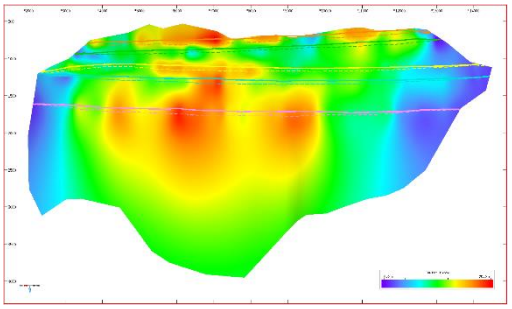

Picked Every 32nd Line, 800 m spacing

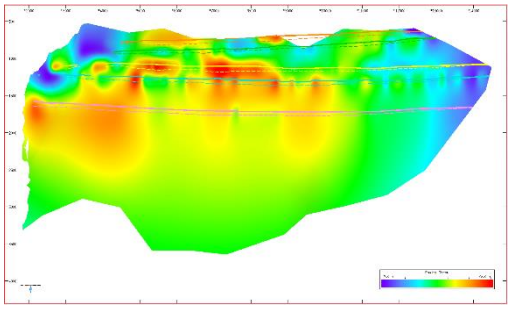

Fault – displacement profiles Fault number 6

Picked Every Line, 25 m spacing

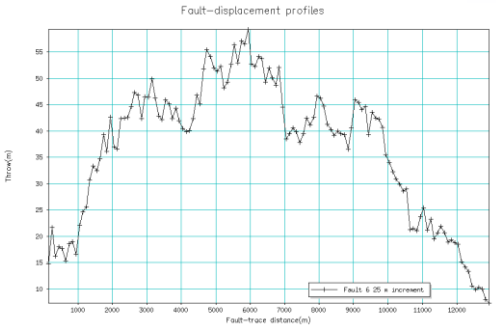

Picked Every 2nd Line, 50 m spacing

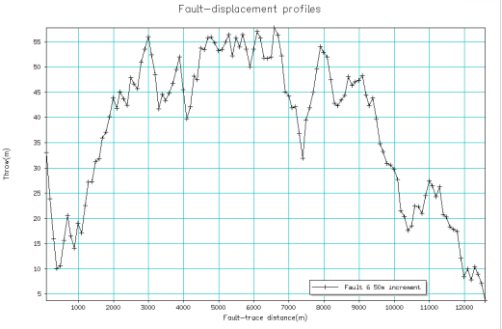

Picked Every 4th Line, 100 m spacing

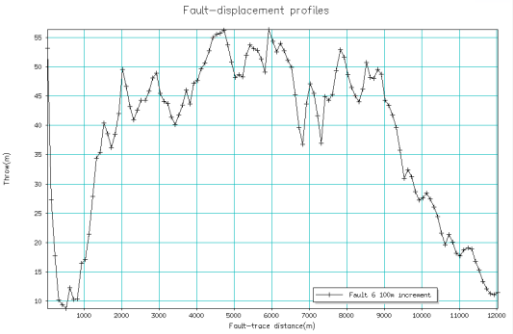

Picked Every 8th Line, 200 m spacing

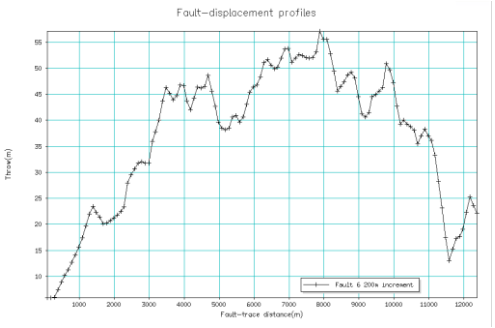

Picked Every 16th Line, 400 m spacing

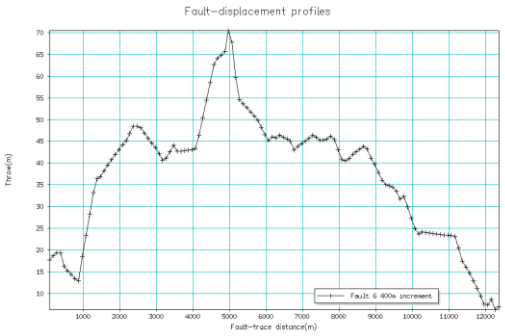

Picked Every 32nd Line, 800 m spacing

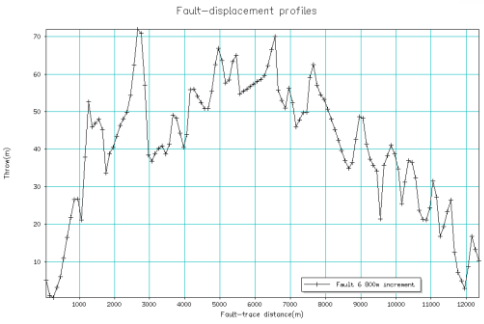

Variations in Dip Fault number 6

Picked Every Line, 25 m spacing

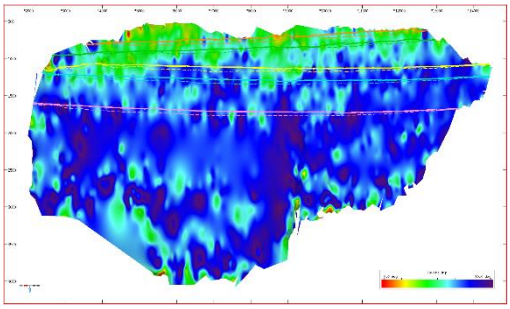

Picked Every 2nd Line, 50 m spacing

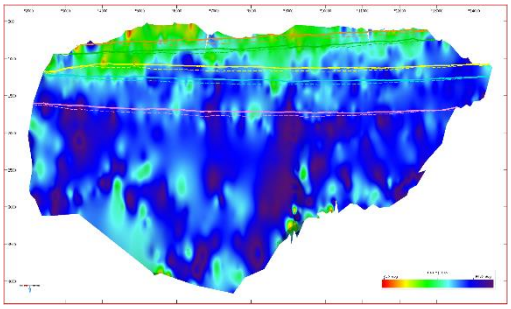

Picked Every 4th Line, 100 m spacing

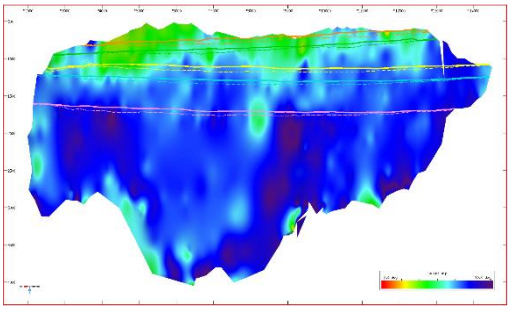

Picked Every 8th Line, 200 m spacing

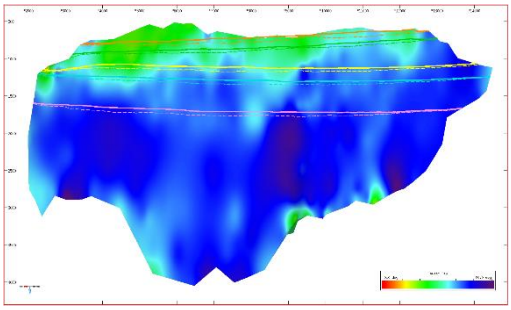

Picked Every 16th Line, 400 m spacing

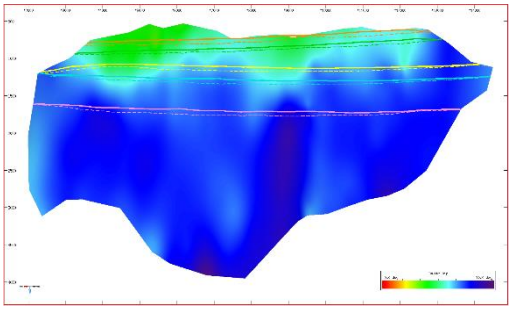

Picked Every 32nd Line, 800 m spacing

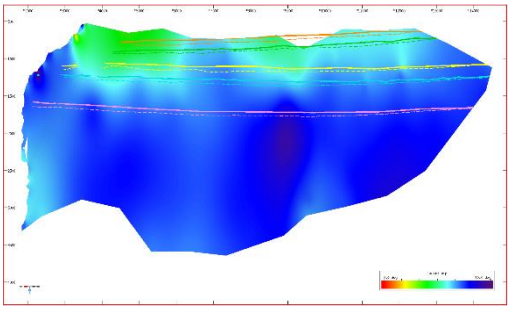

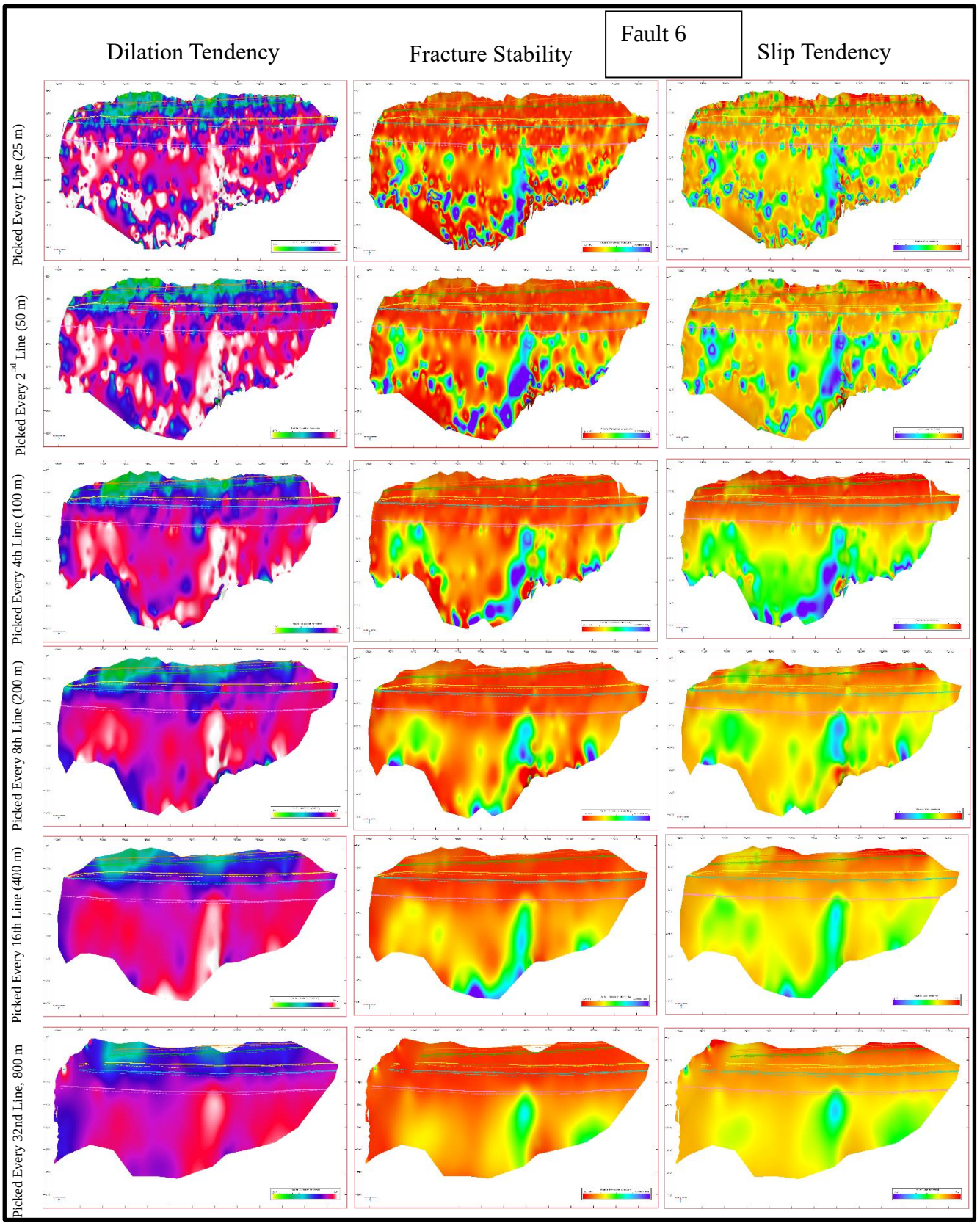
Fault 6
Dilation Tendency
Fracture Stability
Slip Tendency
Picked Every Line (25 m)
Picked Every 2nd Line (50 m)
Picked Every 4th Line (100 m)
Picked Every 8th Line (200 m)
Picked Every 16th Line (400 m)
Picked Every 32nd Line, 800 m